CBETA PROJECT REPORT

A Review of the Project and Milestones

Prepared for: New York State Energy Research and Development Authority

Project Manager: Scott Larsen

Prepared by: Brookhaven National Laboratory and Cornell University

Authors: D. Trbojevic[1], G. Hoffstaetter[2], R. Michnoff[1], N. Banerjee[2], J. Barley[2], A. Bartnik[2], I. Bazarov[2], J.S. Berg[1], L. Borak[1], S. Brooks[1], D. Burke[1], J. Crittenden[2], J. Crone[3], L. Cultrera[2], K. Deitrick[2], J. Dobbins[2], C. Franck[2], R. Gallagher[2], C. Gulliford[2], B. Heltsley[2], R. Hulsart[1], J. Jones[3], D. Jusic[2], R. Kaplan[2], D. J. Kelliher[3], G. Mahler[1], F. Meot[1], V. Kostroun[2], B. Kuske[4], Y. Li[2], M. Liepe[2], W. Lou[2], M. McAteer[4], T. Miyajima[5], K. Ming[5], B. Muratori[3], S. Peggs[1], P. Quigley[2],J. Renta[1], T. Roser[1], D. Sabol[2], D. Sagan[2], J. Sears[2], C. Shore[2], E. Smith[2], K. Smolenski[2], C. Stoll[1], S. Thomas[1], S. Trabocchi[1], N. Tsoupas[1], J. Tuozzollo[1], V. Veshcherevich[2], J. Völker[4], D. Widger[2], H. Witte[1]

(1) Brookhaven National Laboratory/NY (BNL), (2) Cornell University/NY (CU), (3) STFC/UK, (4) HZB/FRG, (5) KEK/J

NYSERDA contract number: 102192

Primary contractor: Brookhaven National Laboratory (BNL), Upton, NY

Primary collaborator: Cornell University (CU), Ithaca, NY

Table of Contents

Table of Figures

Acronyms and Abbreviations

ft	feet
kWh	kilowatt hours
m/s	meters per second
MW	megawatts
nm	10^{-9} m
μm	10^{-6} m
ps	10^{-12} s
ns	10^{-9} s
NYS	New York State
NYSERDA	New York State Energy Research and Development Authority
W	watts
BNL	Brookhaven National Laboratory
BSA	Brookhaven Science Associates, contracted by t DOE to operate BNL
C-AD	Collider-Accelerator Department, BNL
CBETA	Cornell-Brookhaven ERL Test Accelerator
CHESS	Cornell High Energy Synchrotron Source
CLASSE	Cornell Laboratory for Accelerator-Based Sciences and Education
DOE	U.S. Department of Energy
EIC	Electron-Ion Collider
ERL	Energy Recovery Linac
FAT	Fractional Arc Test
FEL	Free Electron Laser
FFA	Fixed Field Alternating
KPP	Key Performance Parameters
Linac	Linear Accelerator
MLC	Main Linac Cryomodule
NAS	National Academy of Sciences
NSAC	Nuclear Science Advisory Committee
PI	Principal Investigator
PM	Project Manager
QCD	Quantum Chromo Dynamics
RF	Radio Frequency
SRF	Superconducting Radio Frequency

Executive Summary

This report describes the world's first multi-turn particle accelerator that captures the accelerated particles and reuses the energy to accelerate new particles. Electrons are accelerated and decelerated in a linear accelerator (Linac) and transported through multiple turns in a single beamline return loop. This multi-turn Energy Recovery Linac (ERL), referred to as the Cornell-BNL ERL Test Accelerator (CBETA), was constructed by the U.S. Department of Energy's (DOE) Brookhaven National Laboratory (BNL) and Cornell University and is located on the Cornell campus in Ithaca, NY. This project paves the way for ultra-bright particle accelerators that use far less energy than today's technology and is referred to as a "green accelerator."

Applications include medical isotope production, cancer therapy, x-ray sources, and industrial applications such as micro-chip production, as well as more energy-efficient machines for basic research in physics, materials science, and many other fields. One application will be especially highlighted in this report: Scientists may use such energy-recovery accelerator technology to efficiently generate electrons for "cooling" ions at the Electron-Ion Collider, a groundbreaking nuclear physics research facility that will be located at Brookhaven Lab. Currently only ERLs appear capable of producing electron beams of the power needed for this application.

Additionally, energy is saved by using permanent magnets in the beamline that steers the particles through the accelerator; these require no electricity to operate. CBETA therefore introduces what is expected to become the most energy-efficient technologies for high-performance accelerators of the future, enabling brighter beams.

The energy of the beam is recovered in Superconducting Radio Frequency (SRF) cavities, which can store electro-magnetic fields with minimal losses. These SRF cavities accelerate electrons in the first 4 pass through the linac. In 4 subsequent passes, the electrons are decelerated, pumping their energy back into the cavities' fields where it is available to accelerate new particles. This makes CBETA the world's first 8-pass ERL with SRF cavities. This ERL concept was first proposed in 1965 by Maury Tigner, professor emeritus at Cornell University, but it took decades of work at Cornell and elsewhere to develop the necessary technology.

The single common beam pipe return loop that takes the electrons back to the linac to be accelerated 4 times, and later decelerated 4 times, has a novel feature never realized before. While there is an independent "lane" for each electron energy, all 4 energy beams travel through the same chain of magnets, referred to as Fixed-Field-Alternating-gradient (FFA) arrangement. The permanent magnets of

this FFA were designed, developed, and precisely tuned at BNL. Because the different beam energies traverse the same magnet chain, the number of accelerator rings is reduced to only one, resulting in additionally fabrication cost savings.

CBETA's construction and commissioning was funded by the New York State Energy Research and Development Authority (NYSERDA) as a 42-month contract that began on November 1, 2016 and used components that were previously developed with funds from the National Science Foundation (NSF) and from industrial partners. This report describes how all 11 technical milestones of this contract have been achieved. The CBETA team reached the final technical milestone of full 4-turn energy recovery in the early hours of December 24, 2019, one week ahead of schedule.

This 4-turn ERL operation was the final of a set of 11 technical project milestone; milestone #1, the engineering design, was completed by February 2017 and technical developments lead to milestone #4, the first beam in the ERL's main SRF accelerator by September 2017; first article magnets allowed milestone #6, the fractional arc test, which brought the beam through every magnet type by May 2018; construction of the one-turn configuration lead to the first energy recovered beam in CBETA by July 2019; and finally, after completing the 4-turn configuration, milestone #11, four turn energy recovery for low current beams, was reached with only 11 weeks of beam commissioning.

With the successful completion of milestone #11, the CBETA team realized two concepts for the first time: a multi-turn ERL that accelerates particle beams and subsequently recovers the energy in SRF accelerating structures, and a FFA accelerator that uses a single beamline with permanent magnets to transport seven different accelerated and decelerated beams. The success of this new "green" technology and the impact it has on many accelerator applications has been highlighted in press releases [84, 89], which were referenced in many news outlets, e.g. [90, 91, 92, 93, 94] and lead to further articles in physics, engineering, and popular news [95, 96, 97, 98, 99, 100].

Subsequent sections of this report describe the project, and include illustrations of the design, highlights of the construction, and details about the commissioning process, in order to demonstrate the satisfaction of all project milestones per the contract with NYSERDA. The importance of CBETA for the Electron Ion Collider at BNL is also described, and extensive references are provided.

1 Overview

1.1 Purpose of the document

The Cornell-BNL ERL Test Accelerator (CBETA), is a new particle accelerator financed by the New York State Energy Research and Development Authority (NYSERDA) through a contract with Brookhaven National Laboratory (BNL), with a start date of November 1, 2016 and extending for a period of 42 months. BNL and Cornell University formed a collaboration to fulfill all the requirements of the contract. The details provided in this closeout report, along with supporting documents listed in the references section of this report, is intended to document that all of the NYSERDA project milestones have been satisfied as defined in this 2016 contract, and that the project was successfully completed.

1.2 Background of the CBETA project

In 2014, BNL and Cornell University collaborated to design a multi-turn Energy Recovery Linear-accelerator (ERL) using SRF acceleration and a single beam line made of Fixed Field Alternating-gradient (FFA) permanent magnets [1]. The motivation for this work was to test new concepts being considered for a future Electron Ion Collider (EIC), the next large particle accelerator in the US. It recently has been decided that this accelerator will be located in New York State, at BNL.

Cornell University had previously constructed and commissioned an electron source, a high-power SRF injector linac, and a high-current SRF linac for ERL operation with funds from the National Science Foundation (NSF) and from industry. With a funding start in 2005, Cornell University designed a hard-X-ray ERL and prototyped these main components, culminating in the Project Design Definition Report in 2013 [2].

Meanwhile, FFA magnets were envisioned at BNL for the EIC; and in 2012, construction began on a single beam line made of FFA permanent magnets to demonstrate that beams with a wide range of energies could be transported in a single beamline [1] using strong magnets that do not require an external power source. Typical electro-magnets used in accelerators require substantial power to operate.

Experts from BNL teamed with experts from Cornell and in 2014 began to design a proof of principle accelerator that combines the ERL and FFA concepts [4]. A 4-pass ERL was to be constructed, in which 7 beams with 4 widely varying energies are returned to the linac through a single FFA beamline. A unified CBETA team with constituents of two renowned accelerator institutions, BNL and Cornell, worked diligently together to efficiently design a new groundbreaking accelerator, the multi-pass ERL with FFA return loop and superconducting RF cavities, CBETA.

The ERL, SRF, and FFA concepts all provide enormous energy savings. ERLs reuse energy from decelerated beam to accelerate new beam, SRF accelerating structures absorb minimal energy in their walls, and the permanent magnets used in the FFA do not use power at all. Since NYSERDA has great interest in developing new technologies that provide energy savings, the partnership between NYSERDA as the funding agency and CBETA seemed like a natural fit.

Every project milestone was achieved, and the final most challenging technical milestone, demonstration of four-pass energy recovery, was satisfied on December 24, 2019, one week ahead of the schedule that was developed in 2016. Figure 1.2-1 shows plots of all 7 beams as measured around the accelerator and the beam spot after the 8th and final path through the linac.

As mentioned in the joint BNL/Cornell press release for 4-turn energy recovery in CBETA: "This accomplishment makes CBETA the first multi-turn ERL to recover the energy of accelerated particle beams in SRF accelerating structures, and the first accelerator to use a single beamline with fixed magnetic fields to transport seven different accelerating and decelerating energy beams" [84].

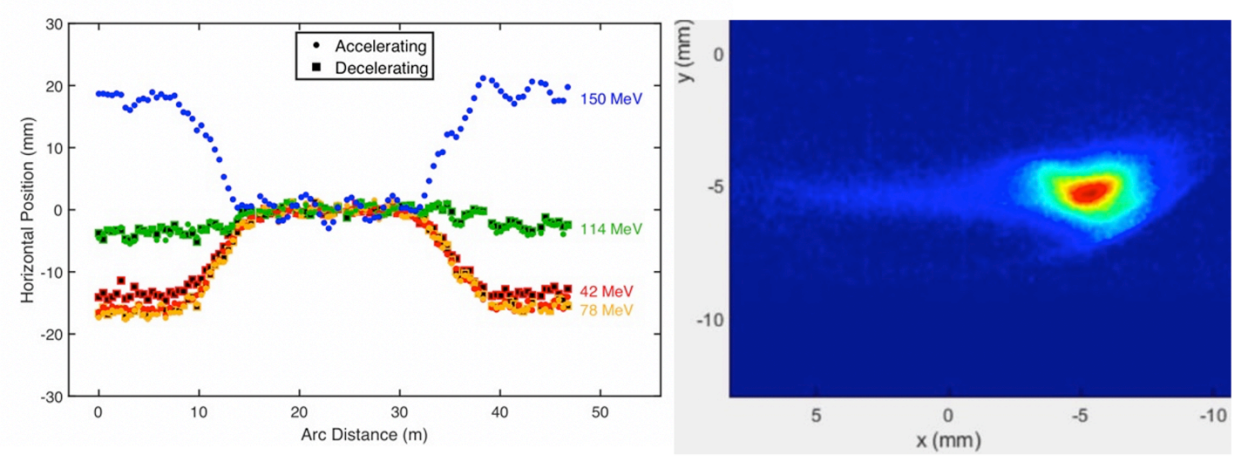

Figure 1.2-1: All 7 orbits in CBETA, 4 being accelerated and 3 being decelerated (left) and the beam spot after the 8th and final path through the main linac (right).

1.3 Description of the CBETA Accelerator

The layout of the CBETA machine is shown in Fig. 1.3-1. The path of the beam from injection to beam stop is as follows: Electron beam is generated by the 400 kV electron source and then accelerated to 6 MeV through the Injector Cryomodule (ICM) (labeled IN in the figure). The beam is then accelerated by 36 MeV to 42 MeV through the Main Linac Cryomodule (MLC) (labeled LA in the figure).

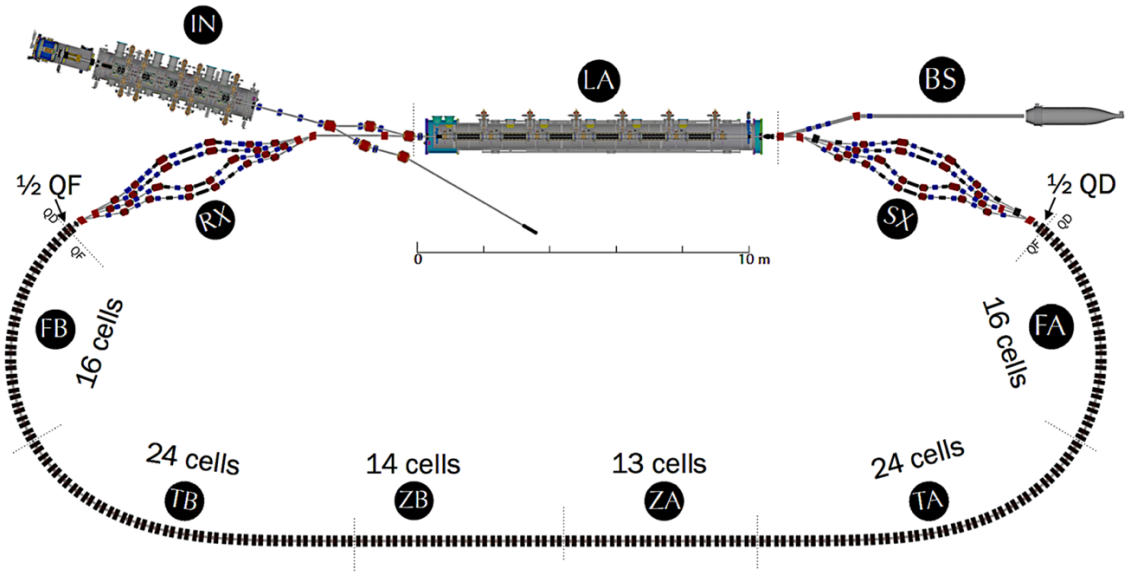

Figure 1.3-1: The major components of CBETA are the injector (IN), the Main Linac Cryomodule (MLC) (LA), the beam stop (BS), the four splitter lines (SX), the Fixed Field Alternating-gradient arc (FFA) consisting of the first arc (FA), transition from the arc to the straight (TA), straight section (ZA and ZB), transition from the straight to the arc (TB), second arc (FB), and finally the four splitter beamlines (RX).

The 42 MeV beam travels through the innermost SX line, S1, then into the FFA permanent magnet loop (FA, TA, ZA, ZB, TB, and FB), through the inner most RX line R1, then back into the MLC (LA) for the second pass, adding another 36 MeV. This process continues until the beam is accelerated to 150 MeV after the fourth MLC pass at which time the beam travels through the outer most SX line S4, into the FFA loop, through the outer most RX line R4, and back to the entrance of the MLC. The beam path length for this fourth turn through S4 and R4 is different from the others by one half an RF period, which makes the beam 180 degrees out of RF phase with respect to the other passes, thus causing the beam to decelerate henceforth by 36 MeV (from 150 MeV to 142 MeV) as it passes through the MLC. For the remaining MLC passes, the beam travels through S3, the FFA, R3, the MLC, S2, the FFA, R2, the MLC, S1, the FFA, R1, and the MLC. At this point the beam is decelerated from 42 MeV back to the original 6 MeV and it travels through the beam stop line (labeled BS in the figure) and into the beam stop itself.

The path that the beam travels and the energy evolution is as follows:

- From the source: 400 keV (operated at 300 kV)
- Through the ICM: 400 keV to 6 MeV
- 1st pass through the MLC: 6 MeV to 42 MeV (+36 MeV)
- S1, FFA, R1: 42 MeV
- 2nd pass through the MLC: 42 MeV to 78 MeV (+36 MeV)

- S2, FFA, R2: 78 MeV
- 3rd pass through the MLC: 78 MeV to 114 MeV (+36 MeV)
- S3, FFA, R3: 114 MeV
- 4th pass through the MLC: 114 MeV to 150 MeV (+36 MeV)
- S4, FFA, R4: 150 MeV
- 5th pass through the MLC: 150 MeV to 114 MeV (-36 MeV)
- S3, FFA, R3: 114 MeV
- 6th pass through the MLC: 114 MeV to 78 MeV (-36 MeV)
- S2, FFA, R2: 78 MeV
- 7th pass through the MLC: 78 MeV to 42 MeV (-36 MeV)
- S1, FFA, R1: 42 MeV
- 8th pass through the MLC: 42 MeV to 6 MeV (-36 MeV)
- Beam stop line to the beam stop: 6 MeV

The 400 kV electron source, the ICM and the MLC were previously constructed by Cornell with NFS and industry funding before the CBETA project began. Having this equipment available along with the system experts significantly decreased the overall CBETA project cost and risk. The source and ICM had been previously commissioned with excellent performance results. The MLC had been previously tested without beam, and CBETA provided an opportunity to test this state-of-the-art superconducting RF system with beam.

The ICM is composed of 5 RF cavities; and for CBETA 4 of the 5 cavities were used to provide a total of 5.6 MeV acceleration. The MLC is composed of 6 RF cavities, with each operated at about 6 MeV to provide a total of 36 MeV acceleration or deceleration.

Within the collaboration, Cornell University was responsible for the electron source, the MLC, the SX and RX splitter lines with electromagnets, power supplies, and the complete vacuum system; while BNL was responsible for the FFA permanent magnet loop with corrector coils, and the beam position monitor system. Both institutions shared responsibility for beam commissioning activities, beam physics analysis, control system development and additional instrumentation systems.

The primary functions of the SX and RX splitter lines are:

- To match electron properties from and to the linac towards and from the single FFA beamline.
- To provide the correct path length for each energy such that electrons arrive at the MLC either at the top of the sinusoidal RF wave for acceleration or at the bottom of the RF sinusoidal function (180^o degrees opposite voltage) for deceleration.
- To provide an isochronous condition for each energy during the energy recovery mode, so that the path length hardly depends on energy. The ERL acceleration is typically done at the crest of the sinusoidal function, rarely off the crest as in synchrotrons.

The FFA loop is a single beam line that transports seven different beams at the same time, 4 after being accelerated and 3 after being decelerated. This is a novel approach that has never been done in an accelerator, and significantly reduces cost since one common beam line is used instead of four.

The primary functions of the FFA section are:

- To transport 7 beams back to the linac, either for acceleration or deceleration. This utilizes the unique FFA property to transport beams with nearly a factor of 4 different energies in one beamline.
- To provide orbit corrections for all 7 beams simultaneously.

1.4 Project Goals

The CBETA project was initiated to perform proof of principle experiments for unproven innovative cost-saving accelerator concepts planned to be used in the future EIC. Performing these tests with successful results prior to the EIC construction would reduce the EIC project risk by learning early that these complex ideas are viable solutions. An accelerator was to be constructed with the capability to test the following specific concepts:

- Using a superconducting RF (SRF) system for multiple pass Energy Recovery Linacs (ERL) applications
- Using an FFA with permanent magnets for multiple pass ERL applications
- Merging of multiple energy electron beam orbits in an FFA into the same orbit in the straight section.
- Orbit correction algorithms that could be used to correct magnet imperfections (misalignments, magnetic field errors etc.) for multiple simultaneous beam with different energies.
- Multiple pass recirculation and energy recovery for high beam currents.

Based on these requirements, the following primary goals for the CBETA project funded by NYSERDA were defined:

- Design and construct an SRF linac for 8 total passes – 4 accelerating and 4 decelerating, with the capability of 36 MeV acceleration change with each pass through the linac.
- Design and construct a return loop beam line using the FFA concept and permanent magnets, capable of transporting 7 electron beams simultaneously spanning nearly factor of four in energy range. (42 MeV to 150 MeV)
- Design, develop and test multiple splitter/combiner beamlines on either side of the SRF linac as the interface between the linac and the FFA return loop, where each splitter/combiner beamline is dedicated to one specific energy. The primary purpose of each individual splitter/combiner line is to match the phase of the beam as it reenters the linac after each turn through the FFA section.

- Demonstrate energy recovery in a single pass through an SRF linac, where some RF cavities accelerate while others decelerate, such that the entrance energy into the linac is the same as the exit energy. (6 MeV in, 6 MeV out, with each of the 6 RF cavities either accelerating or decelerating by 6 MeV)
- Perform energy scan tests to confirm that a wide range of energies can be transported through the FFA beam line. (38.6 to 60 MeV)
- Demonstrate energy recovery for a single-pass machine configuration, with 1 acceleration pass and 1 deceleration pass through an SRF linac. (inject at 6 MeV, accelerate to 42 Mev, decelerate back to 6 MeV)
- Demonstrate energy recovery for a four-pass machine configuration, with 4 accelerating and 4 decelerating passes through an SRF cavity, where beam from seven of these passes traverses the FFA permanent magnet return loop. (four energies: 42, 78, 114, 150 MeV)
- Demonstrate successful transport of 7 electron beams spanning nearly a factor of 4 in energy through the common FFA beam line. (energy range: 42 to 150 MeV)
- Study the effects of temperature dependence, magnetic errors, misalignments, chromatic effects with vibrations, etc., and methods for correcting these errors.

These goals were subsequently used to develop the specific milestones as defined in the contract and reported in section 2 herein. CBETA has successfully achieved all of these goals within the timeline defined in the project. The specific details of the results will be discussed in section 2.

2 Fulfillment of the NYSERDA contract milestones

The contract milestones

Table 2-1 provides a list of the 12 CBETA NYSERDA milestones per the contract. The column labeled "Contract Date" is the date for each milestone per the contract, and the column labeled "Actual" is the date that the milestone was claimed achieved. Two Go/no go milestones (#4 and #6) were defined to ensure that each of these major accomplishments was completed prior to continuing execution of the project. If either of these milestones was not satisfactorily achieved, then NYSERDA could have optionally discontinued funding the project. That option was fortunately not necessary as all milestones were achieved as expected.

Note that milestone #8 – Final assembly and pre-beam commissioning complete, is the only milestone that was not completed on time. However, it is very important to also note that this delay did not impact completion of the final most challenging technical milestone #11 – commissioning of the complete four pass machine with energy recovery.

Table 2-1: The NYSERDA contract milestones

#	Technical milestone	Month Contract Date			Actual
	NYSERDA funding start date		11/01/2016		
1	Engineering design documentation complete	3	01/31/2017		01/31/2017
2	Engineering design documentation complete	6	04/30/2017		04/30/2017
3	Magnet production approved	8	06/30/2017		06/23/2017
4	**Beam through Main Linac Cryomodule**	**10**	**08/31/2017**	**Go-no-go**	**06/16/2017**
5	First production hybrid magnet tested	14	12/31/2017		12/21/2017
6	**Fractional Arc Test: Beam through MLC & prototype girder**	**18**	**04/30/2017**	**Go-no-go**	**04/20/2018**
7	Girder production run complete	25	11/30/2018		11/21/2018
8	Final assembly and pre-beam commissioning complete	28	02/28/2019		03/13/2019
9	Single pass beam energy scan	32	06/30/2019		06/03/2019
10	Single pass beam with energy recovery	36	10/31/2019		06/24/2019
11	Four pass beams with energy recovery (low current)	32	12/31/2019		12/24/2019
12	Project complete	36	04/30/2020		03/31/2020

This report is part of the 12th and final milestone.

These 12 milestones characterize critical phases of the project and are used to structure this section of the report. The wording of these milestones is taken directly from the Statement of Work in the contract

with NYSERDA. However, please note that the final design used Halbach permanent magnets instead of the "hybrid magnets" referenced in the milestone details below. After detailed analysis, the Halbach magnet option was found to be lower cost, simpler to construct, and easier to commission.

Milestone 1: Complete Engineering Design Documentation

Goal: Complete documentation of the engineering design of the project.

- Drawings and specifications of the overall system as well as all technical sub-systems.
- Baseline lattice layout of the accelerator and the baseline parameters.

Milestone 2: Assemble Prototype Girder

Goal: Assemble and test the prototype girder using 8 hybrid magnets.

- An assembled prototype girder to be used in the accelerator circumference made of 8 hybrid magnets blocks embedded into iron poles and back-legs.
- Perform rigorous magnetic, mechanical, alignment and thermal tests on the prototype and document the results of the tests.

Milestone 3: Approve Magnet Production

Goal: Successful approval of the production of all magnets to be used in the accelerator.

- Assemble conventional electromagnets in the two combiner-separator regions of the accelerator.
- Assemble relatively weak electromagnet corrector magnets with hybrid magnets on the arc girders and assemble the strong electromagnets on the combiner-separator tables.
- Perform rigorous magnetic, mechanical, alignment and thermal tests on the full assembly.
- Analyze the test results and if successful approve the production of all magnets.

Milestone 4: Beam through Main Linac Cryomodule

Goal: Successfully pass a small beam current through Main Linac Cryomodule

- Move the Main Linac Cryomodule (MLC) unit which accelerates the beam to the test site.
- Move the supported infrastructure including RF power and cryogenics to the test site.
- Integrate the MLC and the supporting infrastructure for beam testing.
- Pass the small beam current once through the MLC and capture it by a beam stop. The return arc will not be in place at this time.

Milestone 5: Test Production Hybrid Magnets

Goal: Successfully test first production hybrid magnet.

- Select a single vendor for the production of hybrid magnets.
- Transfer production technology and assembly skills from the project team to the vendor.
- Monitor the production throughout the process.
- Test every magnet before assembly onto magnet girders.

Milestone 6: Perform Fractional Arc Test: Beam through Main Linac Cryomodule and Prototype girder

Goal: Successfully perform fractional arc test.

- Pass the beam through the MLC, through one channel of one of the separator-combines, and through an arc girder.
- Carry out performance testing of the identified sub-systems with and without the beam.
- Document all trouble shooting incidents, performance issues and rectify them.

Milestone 7: Complete Girder Production Run

Goal: Complete the girder production run.

- Complete construction of all hybrid magnets.
- Complete performance testing of all hybrid magnets.
- Complete girder assembly and carry out the production run.

Milestone 8: Complete Final Assembly and Pre-Beam Commissioning

Goal: Complete final assembly and pre-beam commissioning

- Ship pre-aligned girders to Cornell University.
- Assemble, install and align the girders in the LOE hall, along with the other components including the vacuum system, beam instrumentation, shielding, control system and safety system.
- Complete the final assembly for pre-beam commissioning through system integration.
- Carryout detailed systems checks to ensure accurate functioning of the system and have the system pre-beam commissioning ready.

Milestone 9: Single Pass Beam Energy Scan

Goal: Successfully complete single pass beam energy scan

- Pass the beam through the MLC and around the arc once during this first phase of beam commissioning.
- Test the ability of the hybrid arc magnets to pass a broad range of beam energies during this test.

- Perform energy scan by adjusting the accelerating voltage of the MLC by activating the beam diagnostic systems. Document all results.

Milestone 10: Single Pass Beam with Energy Recovery

Goal: Successfully complete single pass beam with energy recovery.

- Pass the beam through the MLC and decelerate it during the second time.
- Measure the efficiency of the energy recovery of the accelerator at low currents.
- Perform design of experiments on energy recovery variation with beam current and with other accelerator parameters.

Milestone 11: Four Pass Beam with Energy Recovery (Low Current)

Goal: Successfully complete energy recovery during 4 passes.

- Pass the beam through the MLC 8 times in full operation.
- Accelerate the beam to higher energies during 4 passes and then decelerating during remaining 4 passes.
- Measure the multi-turn energy recovery in the superconducting accelerator during the 4 decelerating passes.

2.1 Engineering design documentation complete - Milestone #1

The CBETA Design Report [5] is the primary document that defines the machine design details and was used to demonstrate that the design was complete per milestone #1.

General papers and tech notes are available in the reference section of this report [17, 25, 42, 51, 52, 53, 54, 55, 60, 72, 74, 115, 133]. Additional technical details and analyses are available in other documents listed in the references section of this report [18, 28, 29, 31, 32, 34, 39, 41, 43, 44, 45, 46, 49, 50, 54, 56, 60, 61, 70, 72, 109, 113, 114, 107, 125, 144, 129] and multiple technical drawings and documents for different systems have been developed and are available on the Cornell computer systems.

CAD layouts of the CBETA accelerator hall are provided in Fig. 2.1-1. Figure 2.1-2 shows the layout of the FFA loop and shielding layout for personnel protection. Note that the shielding wall is installed only on the left side and the bottom left. This is because ground soil is present on the remaining perimeter on the outside of the building. A photo of the fully assembled CBETA accelerator is shown in Fig. 2.1-3.

Additional supporting documents related to each sub-system are available on the CBETA Supporting Documents web page [83].

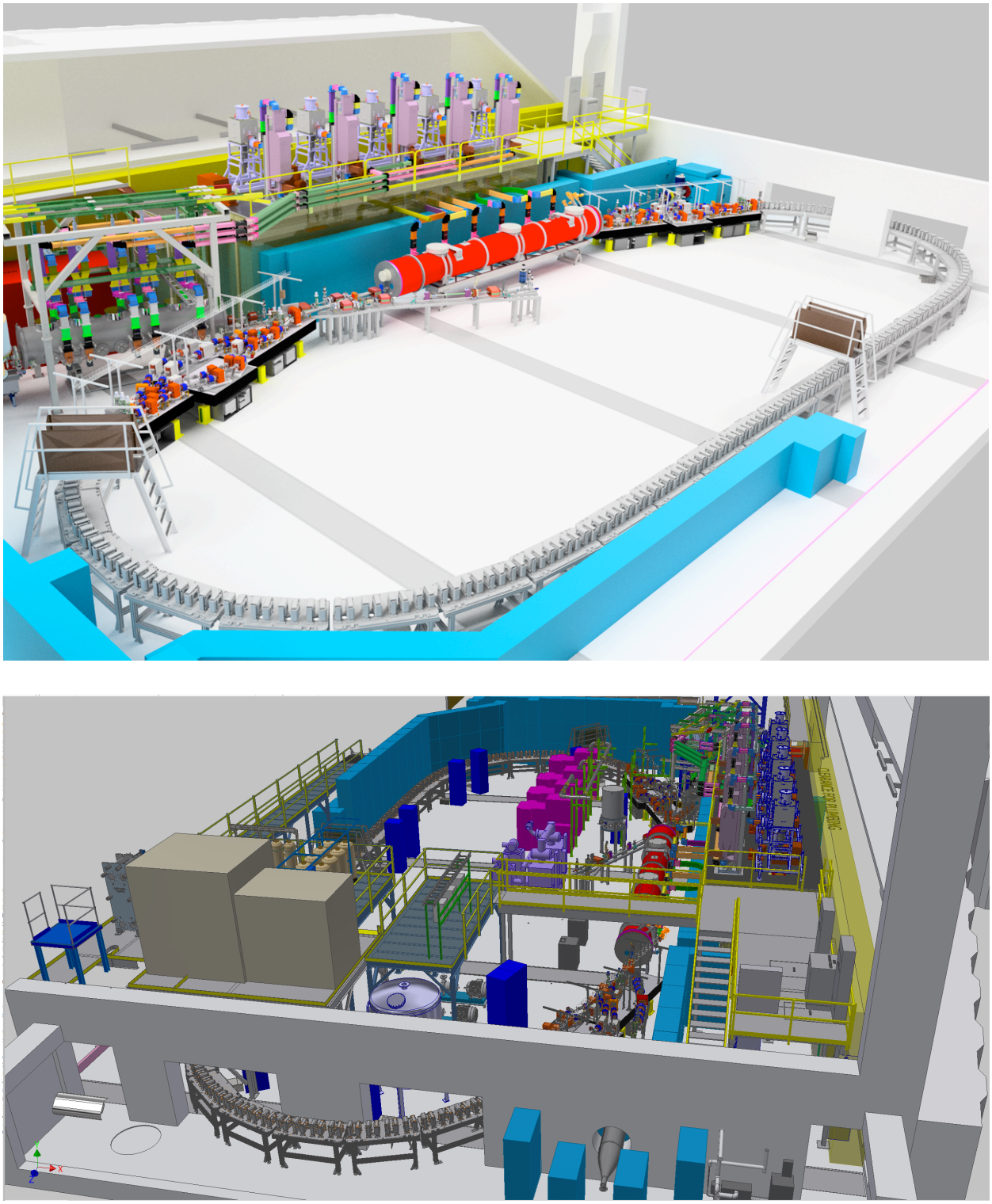

Figure 2.1-1:Layout of the CBETA accelerator in the Wilson Hall at Cornell University.

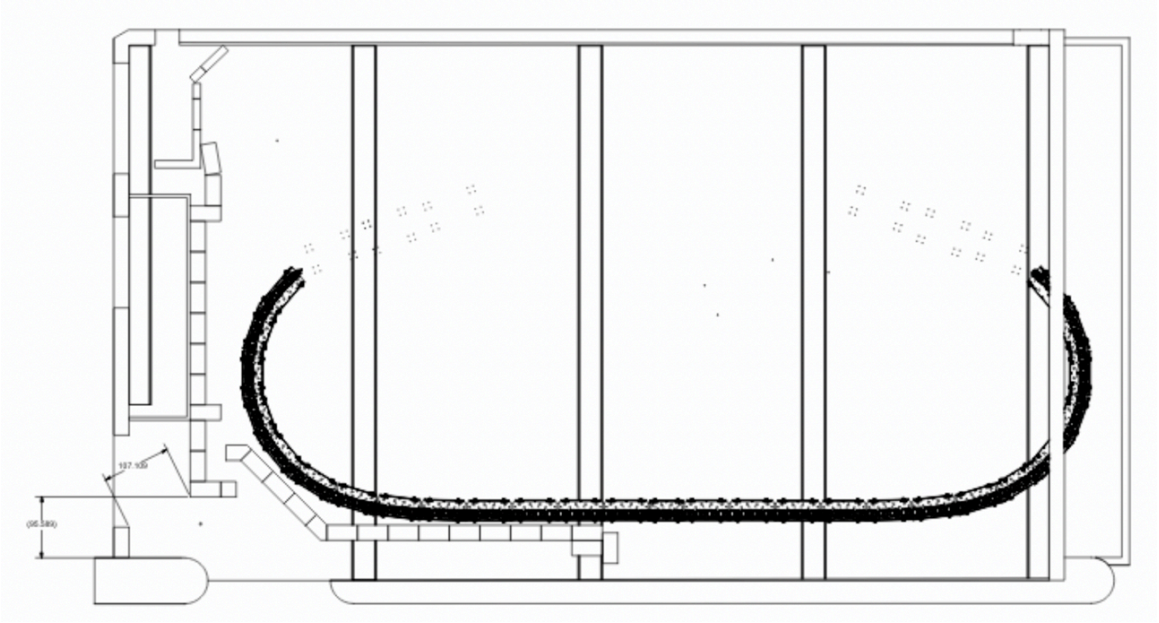

Figure 2.1-2: CBETA shielding wall for the personal protection system.

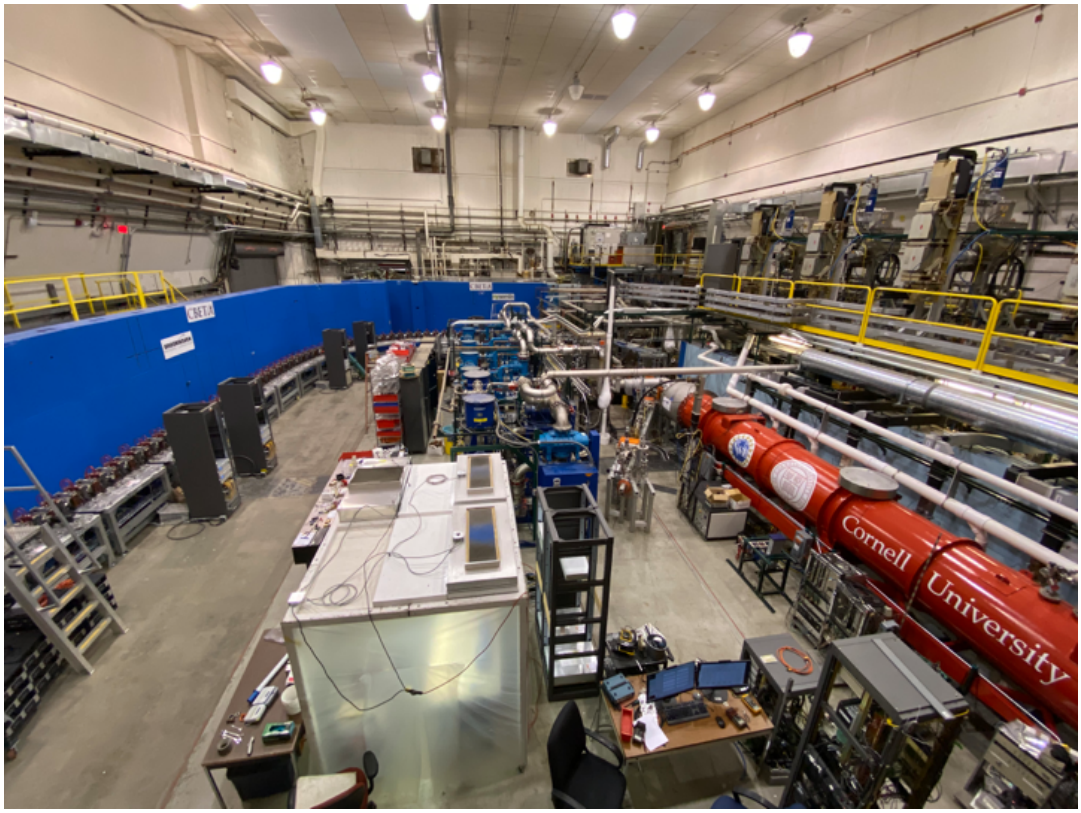

Figure 2.1-3: Photo of the fully assembled CBETA accelerator. The MLC is the red device on the right side. The blue wall is the concrete shielding wall. The FFA permanent magnet loop is visible along the blue shielding wall. The splitter sections on either side of the MLC are not visible in this photo.

The major subsystems for the CBETA accelerator include:

- 400 kV DC electron source
- Injector Cryo-Module (ICM)
- Main Linac Cryomodule (MLC)
- Vacuum system
- SX and RX splitter electromagnets
- SX and RX splitter power supplies
- FFA Halbach permanent magnets
- FFA corrector magnets
- FFA corrector magnet power supplies
- Control system and software applications
- Beam instrumentation systems
    - Beam position monitor system
    - Bunch arrival monitor system
    - Slow loss monitor system
    - Fast loss monitor system
- Equipment protection system with fast beam shutdown
- Personnel protection system
- Infrastructure systems – power, water, building air conditioning, mezzanine, etc.

2.2 Prototype girder assembled - Milestone #2

Most of the accelerator circumference is composed of Halbach permanent combined function magnets. Eight permanent magnets are assembled together onto different girder configurations. A prototype girder (Fig. 2.2-1) was constructed per Milestone #2 and subjected to rigorous magnetic, mechanical, alignment, and thermal tests [112].

Lessons learned and technology developed from the prototype girder were directly used in the contract to construct 220 production magnets. Techniques developed during the prototype development resulted in a new technology for producing high quality combined function magnets.

Figure 2.2-1: First Girder with eight Fixed Field Alternating-gradient (FFA) magnets fully assembled.

Multiple options were considered for the magnet construction, with the final design consisting of aluminum blocks for aligning and supporting the permanent magnet wedges. To ease installation of the magnets on the beam pipe, each magnet was assembled in two halves.

This created an additional manufacturing complication because special tooling was needed to hold the magnets in place while the adhesive dried. In addition, the aluminum blocks include water channels to provide temperature stabilization with 85F water flow. The permanent magnets produce very strong magnetic forces, attracting or repelling, depending on the polarity configuration. During this development the BNL CBETA team found that the West System epoxy, usually used for marine applications, provided very good adhesive force. This epoxy provided a very firm adhesion between the aluminum blocks and the permanent magnet wedges made of $Nd_2Fe_{14}B$. The magnetic material wedges were of superb quality and property consistency. They were procured from the Canadian Chinese enterprise All-Star Magnetics. The permanent magnet wedge properties and dimensions were measured with Helmholtz coil measurement systems at the BNL Light Source magnet facility and at the magnet fabrication vender, KYMA.

After assembling the magnet wedges into the aluminum blocks, the final step was to tune the magnetic field of each magnet using a harmonic wire correction system developed by Stephen Brooks at BNL [119]. A wire holder with channels is installed on the inner radius of the permanent magnet to hold the iron tuning wires in place [118]. The radial position and lengths of each iron tuning wire are determined using the rotating coil measurements and custom developed analysis software.

This technology is ready to be used in future applications like proton cancer therapy gantries.

2.3 Magnet production approved – Milestone #3

2.3.1 Permanent magnets for the FFA return loop

BNL was responsible for the design and manufacture of the FFA permanent magnets and corrector magnets installed around each permanent magnet.

Two types of permanent magnet designs were considered for the FFA. The first consisted of iron dominated hybrid magnets where permanent magnet blocks are placed behind quadrupolar iron poles. The properties of the magnetic field are defined by the shape of the iron poles. The second design consisted of Halbach type permanent magnets where the magnetic field is defined by permanent magnet wedges that are placed around a circular aperture. After detailed studies, the Halbach magnet design was selected. Their advantages are smaller size, larger fields, less field leakage, and less field coupling to neighboring magnets.

Beam simulation studies for CBETA were performed using a variety of assumptions for magnet qualities. Misalignment errors were introduced with rms between 20-50 μm, 50-100 μm, 100-200 μm. In addition, the weighted sum of the harmonic multipoles in the FFA magnets was studied by requiring such that the emittance of the beam does not get larger than $\delta\varepsilon/\varepsilon<10$ %. Table 2.3-1 shows the calculated allowable multipole and misalignment error limits.

The prototype girder magnet tests proved very successful, with all magnets being within the required multipole range and within the required limits between +-0.1% the integral quadrupole field. After these extensive tests confirmed that the Halbach permanent magnet design would satisfy the machine requirements, magnet production was approved. Milestone #3 was achieved on time, and the fully assembled first girder with eight high quality magnets provided enough information and allowed us to develop a new permanent magnet technology. This opened the door to engage high-level competition with worldwide companies with experience in permanent magnet developments.

Transporting electron beams with 4 different energies simultaneously through the FFA permanent magnets required specifically designed and precisely modeled fields. Excellent experimental results were obtained when electrons finally traversed these permanent FFA magnets simultaneously at 42, 78, 114, and 150 MeV. Success in the agreement between the theoretical predictions and measurements was a consequence of:

- detailed magnet and lattice simulations
- accurately constructed permanent magnets. The required precision in dimension and field quality was achieved for all 220 permanent magnets. To finetune the field quality, a new technique of harmonic iron wire corrections was developed

The permanent magnet assembly contract was awarded to KYMA, located in Italy and Slovenia [78]. Their previous expertise included designing, manufacturing, characterizing and commissioning insertion devices: undulators and wigglers using permanent magnets, primarily for light sources. KYMA proved quite competent, producing high quality magnets, and completing the magnet assembly on time and within their estimated cost.

Table 2.3-1: Limits on allowed magnetic multipoles and misalignment

To keep increase in either X/Y emit/beam_size to be < 10%

Individual limits

b2	37	a2	140
b3	30	a3	90
b4	26	a4	80
b5	21	a5	65
b6	21	a6	63
b7	19	a7	58
b8	21	a8	56
b9	18	a9	53

$$B_x + iB_y = \frac{b_n + ia_n}{L}(x+iy)^n \qquad b_n = \left[10^{-4}\frac{GL}{r_0^{n-1}}\right]u_0$$

Multipole limits

$$\sqrt{\Sigma_n(\frac{b_n}{lim\_b_n})^2 + (\frac{a_n}{lim\_a_n})^2} < 0.75$$

The corrector magnets [16] installed around each permanent magnet assembly were designed by BNL, and the contract to fabricate the magnets was awarded to Sag Harbor Industries in Sag Harbor, Long Island, NY.

Several papers and tech notes were written related to the design, fabrication and testing of the FFA permanent magnets [30, 33, 35, 36, 37, 63, 68, 101, 102, 103, 105, 106, 108, 100, 111, 117, 123, 124, 126, 137, 138, 142].

2.3.2 Electromagnets for the eight splitter/combiner beamlines

Cornell University was responsible for the design and manufacture of the electro-magnets used in the SX and RX splitter lines. Following extensive modeling studies [24, 48, 104, 120, 121, 128, 148], a Request for Proposals was issued in December 2016. The seven responses received from reputable magnet design and fabrication firms varied greatly in engineering detail and cost. The contract to fabricate the magnets was awarded in May 2017, to Elytt Energy in Spain [79]. Their proposal was not only the most detailed in terms of engineering; it was also the lowest cost.

The cost was kept within budget partly because Elytt adopted the design work at Cornell with only minor modifications. The result was satisfactory. While there were significant delivery delays, these did not cause any delays in the Fractional Arc Test, the Single-pass Test or the final commissioning of the full machine in October 2019.

The final order included 40 dipole magnets, 64 quadrupole magnets (see Fig. 2.3-1) and 32 vertical corrector magnets. The quality of the magnet fabrication and field measurements was very high. These are described in extensive documentation [149] provided by Elytt Energy. In addition to the ten Hall-probe-based field map measurements provided by Elytt for nine of the air-cooled quadrupole magnets, BNL provided two precise rotating-coil measurements for one of them.

Figure 2.3-1: Shipment of 32 quadrupole magnets in preparation at Elytt Energy.

The results (Fig. 2.3-2) show the uniformity in integrated gradient to be 0.5% RMS. The average value for the integrated gradient of 0.4188 T is 2.5% lower than the design value of 0.430 T, a difference easily compensated with excitation current, since these magnets operate far below saturation.

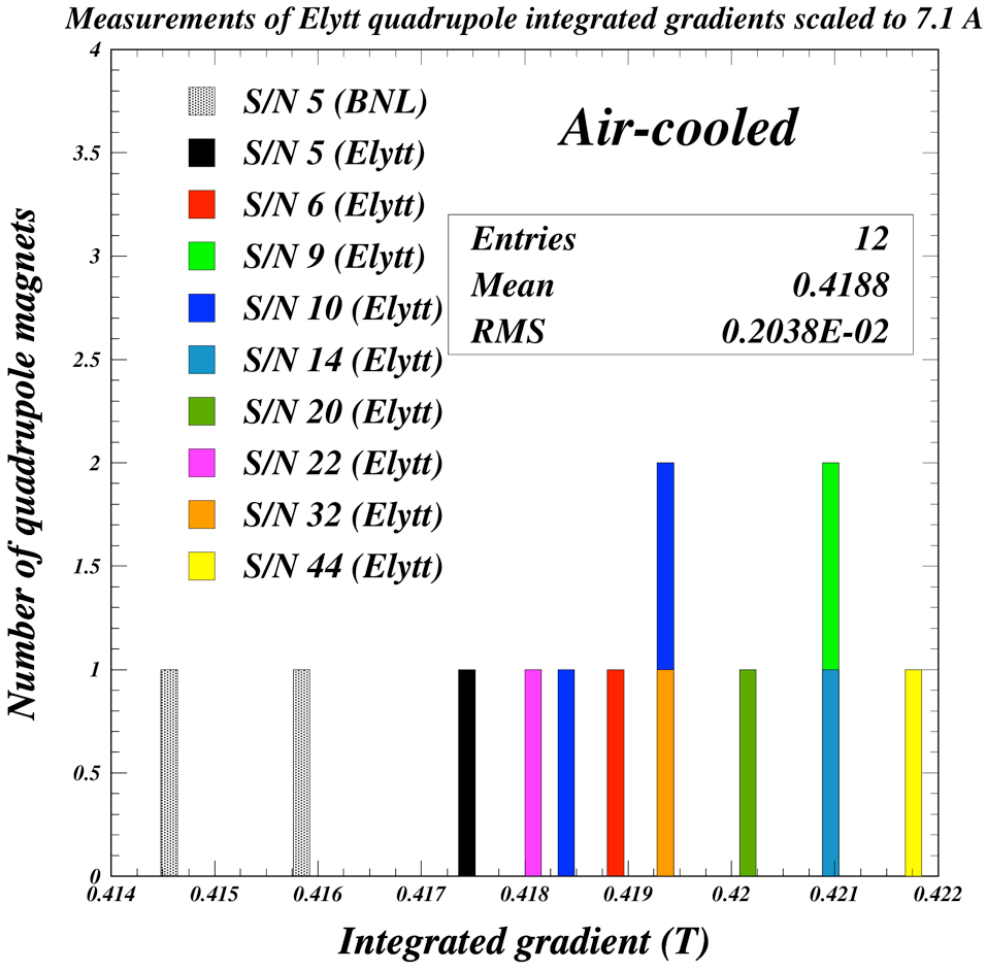

Figure 2.3-2: Twelve measurements of the integrated gradient performed by Elytt Energy and BNL on ten of the air-cooled splitter quadrupole magnets, exhibiting a uniformity of 0.5%.

The severe transverse space constraints presented an uncommon challenge in the design of the splitter dipole magnets, requiring an unorthodox design approach. The solution was found as a collaborative effort of Cornell physicists and engineers with the Elytt engineers. An innovation was the narrow "waist" visible in Fig. 2.3-3, which lowers the maximum field value of the magnet but accommodates elements in the neighboring beamlines, in some cases at the level of a few millimeters. The design parameters were chosen on the basis of electron tracking through the modeled field maps, rather than on straight-line field integrals. A bend angle uniformity of 0.1% over +-15 mm was specified and achieved. Consequentially,

the straight-line integrals, the measurements of which serve as fabrication quality control, exhibit greater non-uniformity than the bend angles.

The construction accuracy which successfully met this challenge is shown in Fig. 2.3-4 for a 24-cm-long dipole magnet. The agreement between the magnets as constructed and the two finite-element models used by Cornell (Opera) and Elytt Energy (ANSYS) is observed to be better than 0.1% over +-15 mm, where the nonuniformity in the straight-line integral is about +-0.3%. In terms of field strength as a function of excitation current, all dipole magnets designs were found to agree with the models to within 3%.

Figure 2.3-3: Splitter dipole magnet on the measurement system at Elytt Energy. The narrowed “waist” and the shaped chamfer on the end of the bottom pole face are in evidence.

Eighteen special-purpose magnets were designed at Cornell University in consultation with BNL magnet experts and fabricated in a joint effort by Cornell and BNL. These consisted of six 10-cm-long dipoles, four 11-cm-long dipoles, four 18-cm-long septum magnets and four 32-cm-long septum magnets with a curved geometry for the 150-MeV lines. In addition, BNL provided two quadrupole magnets of the highest integrated gradient for use in the 150-MeV lines.

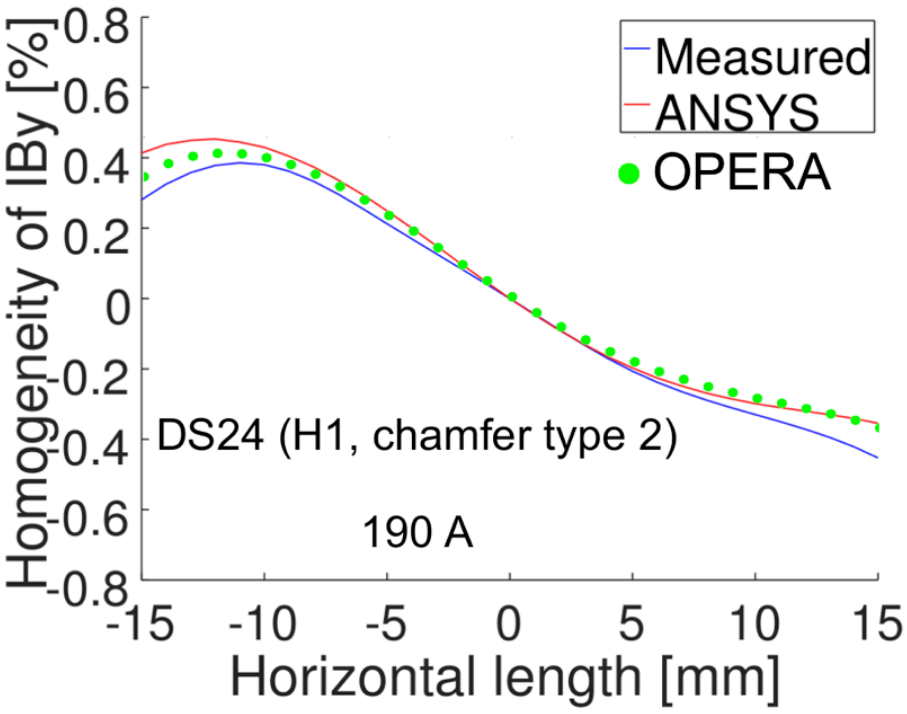

Figure 2.3-4: Transverse dependence of the magnetic field integral in a 24-cm-long DS24 dipole magnet. The measured values are compared to results from the ANSYS and Opera finite-element models.

2.4 Beam through the Main Linac Cryomodule (MLC) – Go/No Go Milestone #4

Beam through the Main Linac Cryomodule was established on May 15th, 2017, reaching the CBETA project major funding milestone #4 - Beam through the MLC [116], three months ahead of schedule. For this test, the team had to successfully accelerate the electron beam from 6 MeV from the Injector Cryomodule (ICM) to a final energy of 12 MeV in the Main Linac Cryomodule (MLC). This test was conducted by systematically testing each of the six superconducting accelerating cavities one at a time. All six cavities were confirmed to successfully accelerate the beam by a minimum of 6 MeV as required.

Initial work focused on preparing the RF in MLC cavity #2 (this is the 2nd closest to the beam stop) for the beam test. The MLC was turned on and cavity #2 was tuned in the klystron loop at 3 MeV without microphonics compensation. The cavity voltage was raised to a peak of 10 MeV (without electron beam) with the compensation on. The target setpoint for CBETA operation is only 6 MeV, so the microphonics compensation allowed for a significant improvement beyond that target. Following the ICM, the buncher, and source, were turned on. The magnet and RF settings were set to their baseline setpoints previously determined and used.

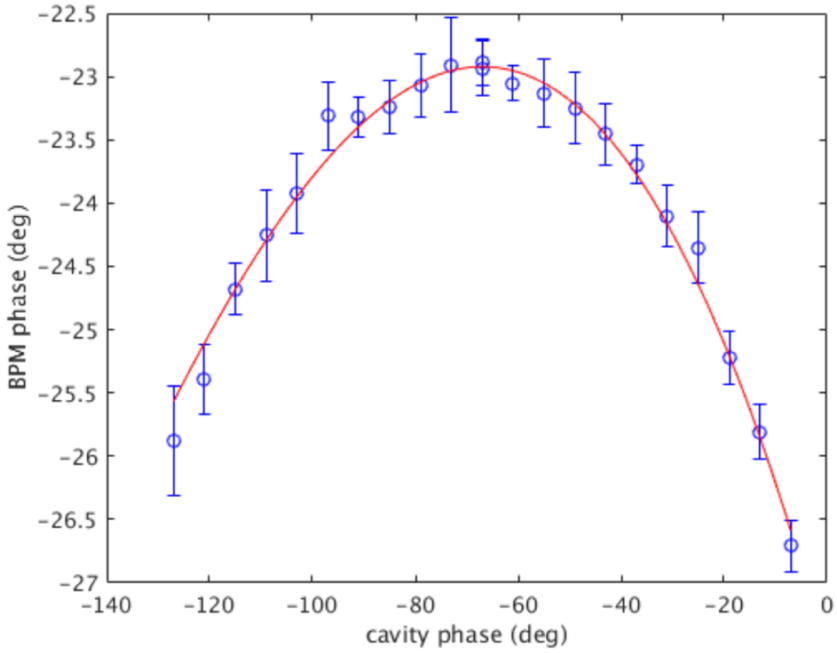

Figure 2.4-1: The beam arrival phase as a function of the cavity phase. At the peak of the plot the beam had reached the full energy of 12 MeV.

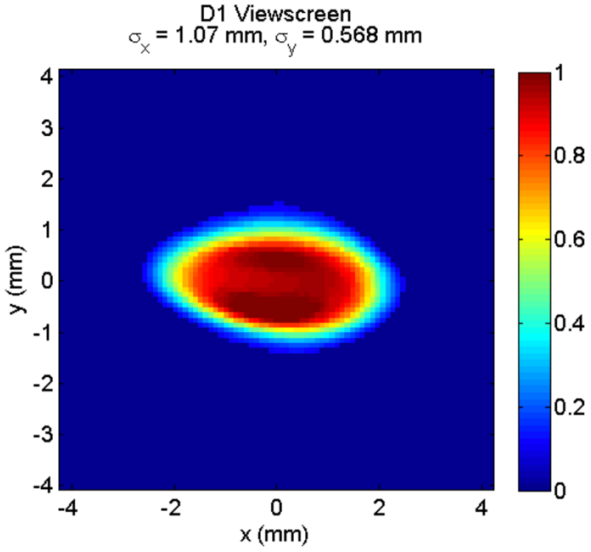

Figure 2.4-2: View screen image of the 12 MeV electron beam on the screen right before the beam stop after MLC.

After the laser was turned on, no additional machine tuning was required as the electron beam was already getting through to the beam stop view screen. The MLC was tuned on to the target 6 MeV energy gain setpoint, and the cavity was phased on the MLC on-crest, as shown in Fig. 2.4-1, ensuring that the

full acceleration was delivered to the electron beam. As expected, the total BPM arrival phase change is only 3 degrees, due to the short distance between the RF cavity and BPM. The resolution of the BPM system was sufficient to adequately phase the cavity.

The verification that the electron beam was being accelerated to the full 12 MeV was confirmed by the recorded position of the beam on the beam stop view screen as shown in Fig. 2.4-2). The view screen was removed after the measurements with the electron current increased to 1 μA for a radiation survey of the perimeter of the CBETA area. During the survey the beam loss monitoring fiber was tested, and the results recorded for later analysis.

Radiation levels slightly above ideal were detected within a 6-foot radius of the east entrance. In order to allow daytime operation, this was remedied with a simple modification to extend the perimeter near the east entrance. There were no levels above the normal background outside this perimeter; therefore, no additional precautions were necessary.

Though many tests of the MLC were previously performed, this milestone is both the first test of the MLC with an electron beam, and also the first test of the LLRF system's ability to regulate and stabilize the cavity field.

A major challenge was the very high Q of the cavity and the presence of microphonics from the helium vessel. It is also the first time all Cornell-BNL ERL Test Accelerator accelerating systems from the electron source to the Main Linac Cryomodule have been operated together and with beam. Despite these challenges, and the aggressive schedule of the CBETA project, this test was completed more than 3 months ahead of schedule.

Many papers and tech notes have been written regarding the design, construction and testing of the MLC [6-14, 19-22, 26, 27, 38, 47, 57, 59, 62, 64, 65, 73, 76, 145].

2.5 First girder tested – milestone #5

The Halbach permanent magnet assembly was designed by BNL personnel, and as previously mentioned the contract for fabrication was awarded to KYMA [78]. The technology and assembly skills developed at BNL during construction of the prototype magnets were directly transferred to the vendor via written documents and web meetings.

The performance by KYMA was exceptional. First articles of each magnet type were fabricated at KYMA and tested at BNL. The start of production was approved in July 2017, after BNL tested and confirmed that the first articles were acceptable. KYMA completed fabrication of all the magnets on a

tight time schedule, with excellent quality. Multiple tests were performed at KYMA, including water-cooling pressure tests as shown in Fig. 2.5-2. Photos of the KYMA magnet assembly line together with the first production girder are shown in Fig. 2.5-3.

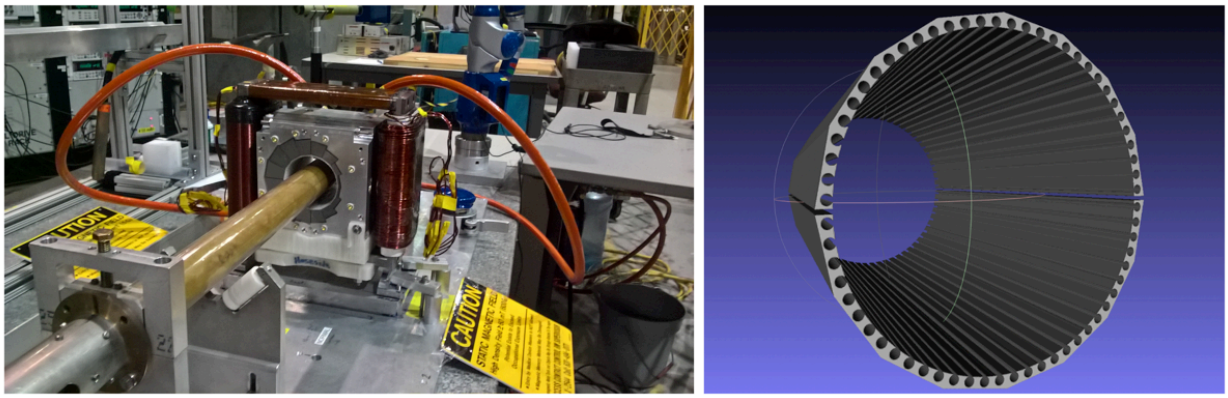

Figure 2.5-1: The Harmonic coil magnetic measurements and the tuning wire holder.

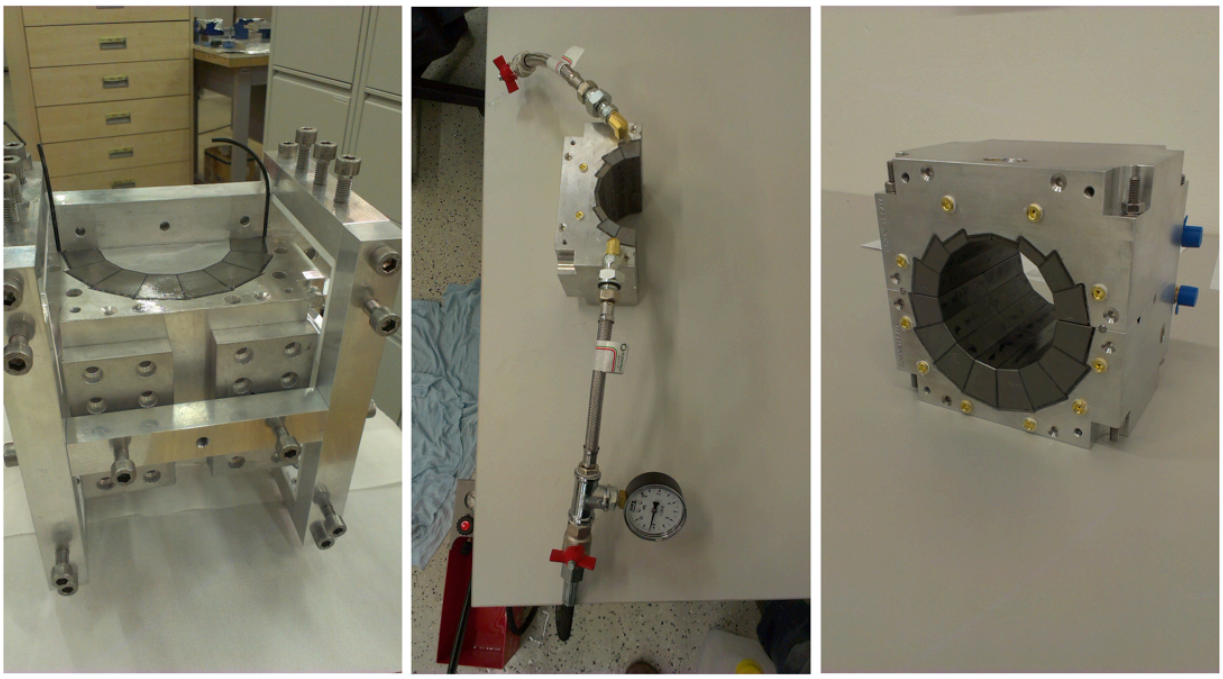

Figure 2.5-2: One of the KYMA magnet assembly rigs, water-cooling pressure testing, and a completed magnet.

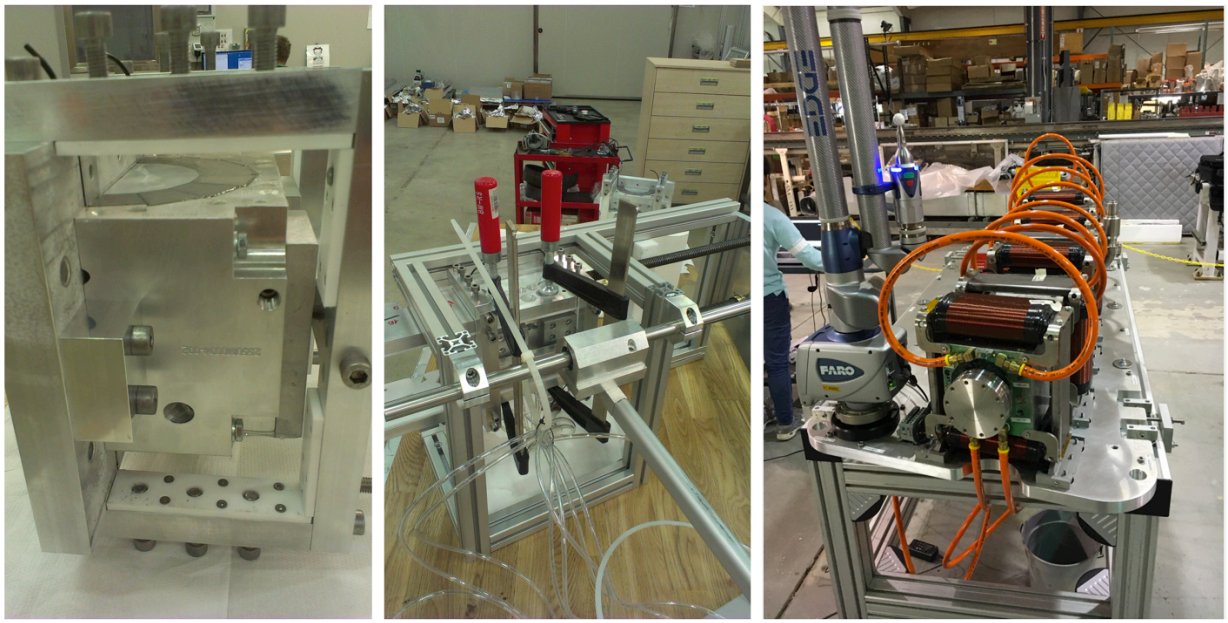

Figure 2.5-3: KYMA assembly line for the FFA magnets and the first prototype girder tested at the BNL.

The BNL team monitored the KYMA magnet production via weekly web meetings with the head of the assembly team and the president of the company. The sequence of magnet production was defined by BNL in order to follow the desired girder assembly sequence.

All permanent magnet assemblies included tests with multiple harmonic coil magnetic measurements [119]. After the first measurement with the permanent magnet assembly, with the 85 F water system connected to the magnet and with the harmonic coil system set precisely by the surveyors, multipole field errors were determined. The wire harmonic correction was then calculated, and the wires placed into the circular holder (Fig. 2.5-1) [118].

2.6 Fractional Arc Test (FAT): Beam through MLC and prototype girder – Milestone #6

The Fractional Arc Test consisted of accelerating the 6 MeV electron beam from the source and ICM to 42 MeV through the MLC, and passing the beam through one channel of one of the separator-combiners (S1), and through the first FFA arc girder.

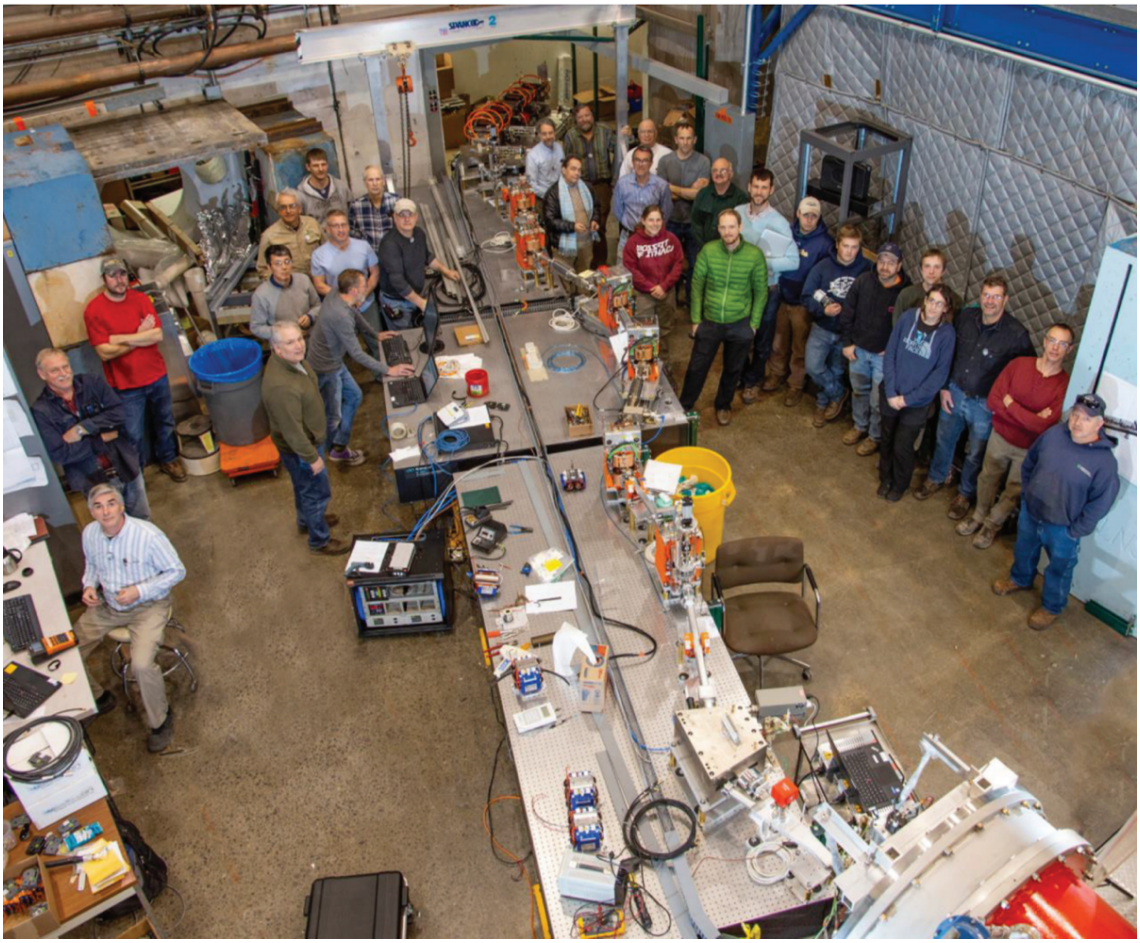

Figure 2.6-1: CBETA Fractional Arc Test Celebration.

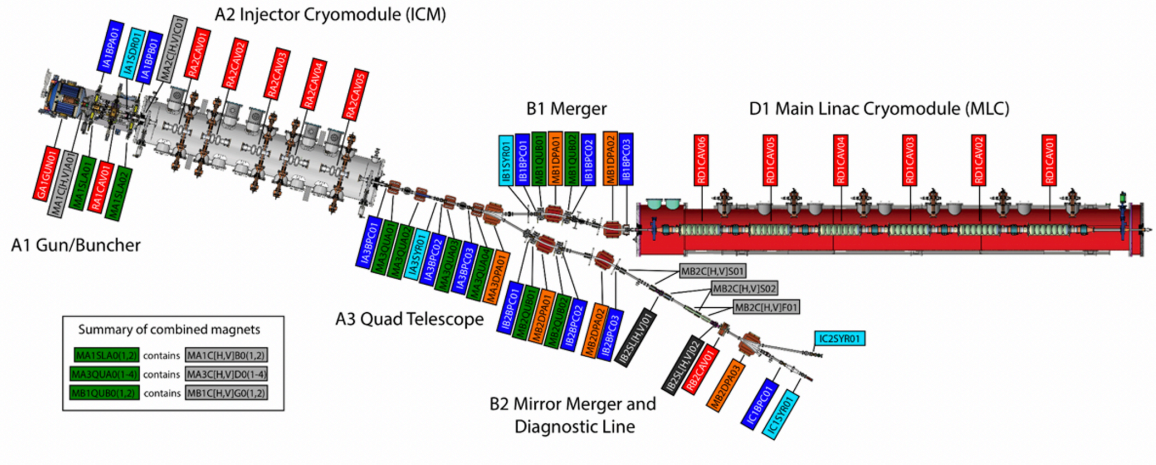

Figure 2.6-2: Layout of the post linac section of the FAT experiment. Beam exits the linac and enters the S1 splitter line at the bottom right and proceeds to the fractional FA arc (top right).

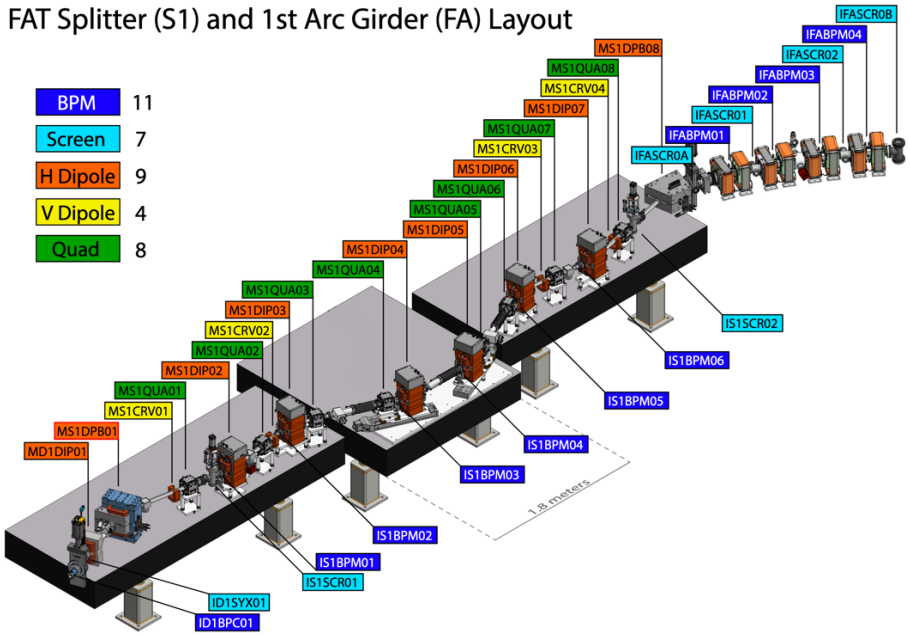

Figure 2.6-3: Layout of the post linac section of the FAT experiment. Beam exits the linac and enters the S1 splitter line at the bottom right and proceeds to the fractional FA arc (top right).

This was a very successful test as not only was the electron beam sent through both the splitter beam line and the FFA first girder, but the entire control system was also successfully tested, including remote magnet control, the timing system, beam position monitors system, beam profile viewers, software scripts, and the superconducting MLC. The photo in Fig. 2.6-1 was taken after successfully satisfying Milestone #6: Fractional Arc Test (FAT). The experimental results from the FAT have been published as papers and internal tech notes [40, 66, 75, 127, 130, 134, 141]. The layouts used in the FAT are shown in Figs. 2.6-2 and 2.6-3.

2.6.1 Injector Tuning

The beam parameters at the entrance to the MLC were measured and adjusted using the Emittance Measurement System (EMS) in the diagnostic line. This position of the diagnostic line corresponds to the beam position in front of the MLC used as an initial condition for further beam matching in CBETA.

To obtain the required beam properties, the source, solenoid, quadrupoles, and other beam line elements were used. This is a necessary first step in all CBETA conditions as it defines the initial condition before the MLC. The results from the measurements of the electron beam properties after the injector tuning are shown in Fig. 2.6-4 and are compared with simulation.

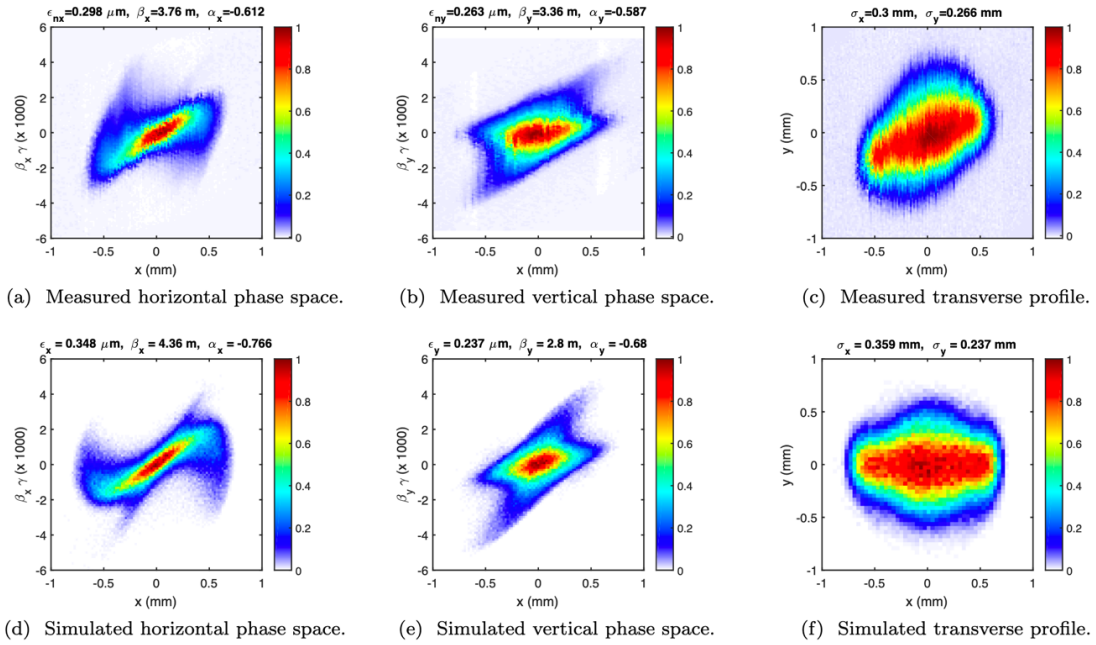

(a) Measured horizontal phase space. (b) Measured vertical phase space. (c) Measured transverse profile.

(d) Simulated horizontal phase space. (e) Simulated vertical phase space. (f) Simulated transverse profile.

Figure 2.6-4: Beam properties: horizontal and vertical phase space and transverse profiles at the B2 mirror merger obtained experimentally (upper part) and by simulation (lower part).

2.6.2 MLC commissioning

Each MLC cavity was calibrated by first setting the voltage to a fixed value of roughly 2-4 MeV, and then slowly changing the cavity phase from 0-360°.

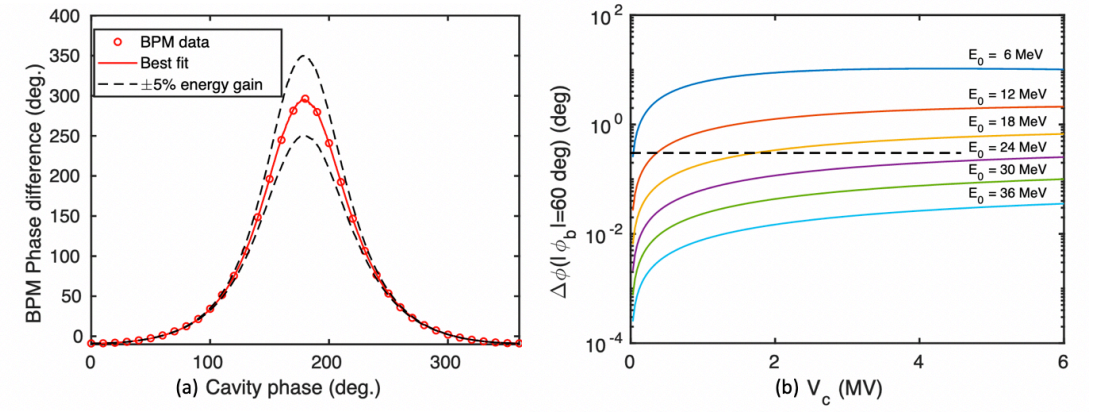

Figure 2.6-5: Left, (a): Change of the arrival time of the beam (shown as a phase change with respect to the RF clock) as a function of MLC cavity 6 phase set-point at a constant cavity gradient. Measured points are shown compared to the best-fit model, and models that have ±5% energy gain. Right, (b): Change of the arrival time of the beam (shown as a phase change with respect to the RF clock) for each MLC cavity voltage turned on sequentially. For each cavity turn-on, the reference time is set to 0.

An example set of data for the first MLC cavity is shown in Fig. 2.6-5(a). In the figure, the trend for the best-fit energy calibration is shown, along with energy gains 5% higher and lower, to give a sense of the measurement sensitivity. From the random error in the BPM phases, the estimated error is approximately 0.4% for the final cavity calibrations. Assuming this represents the most significant source of error, this implies an overall error in the total MLC energy gain of roughly $\sqrt{6}\cdot 0.4\% \approx 1\%$ for any given machine setting.

2.6.3 S1 beam line commissioning

After steering the 42 MeV electron beam from the MLC to the end of the line, difference orbit measurements were taken for each magnet and compared to a model. In general, very good agreement was obtained to the simulation, and a representative set of the data is shown in Fig. 2.6-6. The establishment of single or multi-pass energy recovery requires precise control of the time of flight – the return phase(s) of the beam(s) at the MLC. To achieve this, the CBETA design makes use of two adjustable path length chicanes in for each beam energy. Each chicane features a pair of remotely controlled translation stages for online control of the path length. In particular, the low energy S1 splitter line path length adjustment system provides up to 9.6 mm (or 15^{o} at the speed of light) total path length adjustment during beam operation.

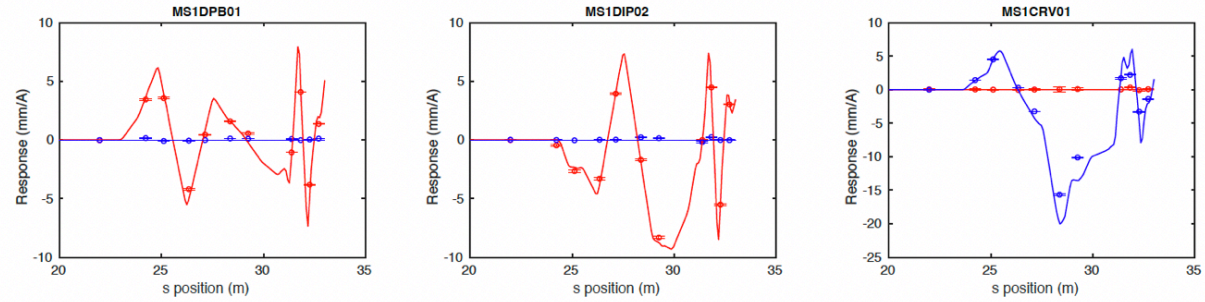

Figure 2.6-6: Measured orbit response to dipole magnet kicks (points) compared to prediction from simulation (lines). Horizontal response is shown in red, and vertical in blue. An example magnet is shown for each type of dipole encountered after the injector merger.

Synchronous movement of the two stages ensures that minimal stress is placed on the bellows connecting the chicane vacuum chambers. In the S1 splitter line these two stages are located directly under S1 dipoles MS1DIP04 and MS1DIP05, as shown in Fig. 2.6-3. A change in translation stage position of Δl results in a path length change Δs experienced by the beam given by:

$$\Delta s = 2\,(1 - \cos\,\theta_{bend})\,\Delta l, \quad \ldots(1)$$

where $\theta_{bend} = 23.3^o$ is the bend angle of the inner splitter chicane. The sixth BPM in the S1 line is capable of reporting both position and beam arrival phase. With all cavities in the MLC turned off, the 6 MeV electron beam was steered through the splitter line, and the reported BPM arrival phase was zeroed. The stage was then moved by Δl= +1 cm and then back -1 cm, and the measured BPM phase during the movement was recorded, as shown in Fig. 2.6-8. Eq. (1) implies a Δl= +1 cm stage movement results in a 1.63 mm path length change seen by the beam. The measured BPM phase data in Fig. 2.6-7 gives a measured BPM phase change of 2.8^o.

The horizontal dispersion and R_{56}, defined here as $\eta_x = dx/d\delta$ and $R_{56} = -dL/dp = (c/\omega)d\phi/d\delta$, where $\delta = (E[\text{MeV}] - 42)/ 42$, ω is the angular cavity frequency, and ϕ is the BPM phase change in [rad], play important roles in controlling emittance dilution and establishing energy recovery in the full CBETA design, and thus necessitated experimental verification in the FAT.

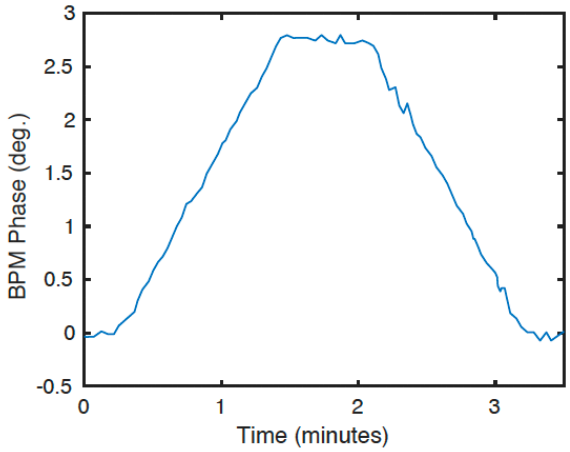

Figure 2.6-7: The beam arrival phase on S1 BPM5 during a splitter stage movement forward and back of 1 cm.

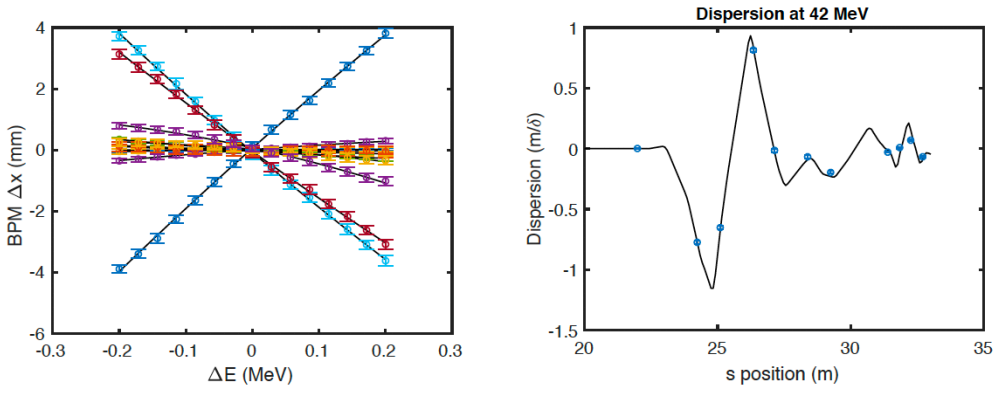

Figure 2.6-8: BPM position change with beam energy (left) and dispersion η_x along the S1 and FFA compared to the predictions.

Scanning the voltage of the last MLC cavity allows for the simultaneous determination of both the dispersion η_x and R_{56} matrix element by measuring the orbit and arrival phase response on the downstream BPMs.

2.6.4 FFA single girder energy scan

Driving betatron oscillations at various amplitudes through the FFA arc and measuring the position response on the FFA BPMs allows for determination of various lattice properties as a function of energy.

In particular, these include intrinsic properties of the FFA arc lattice cell, namely the periodic orbit position at the BPMs and the betatron phase advance per cell (i.e., the tune per cell) as shown in Fig. 2.6-9. The FFA cannot support all possible energies, and in particular there is a lowest possible stable energy.

Experimentally, the beam was found to be successfully transported from a lower bound of 38.5 MeV limited by the FFA acceptance, and an upper bound of 60 MeV, limited by the possible energy gain of the MLC. The tune in the FFA girder was measured at each energy and compared to a prediction.

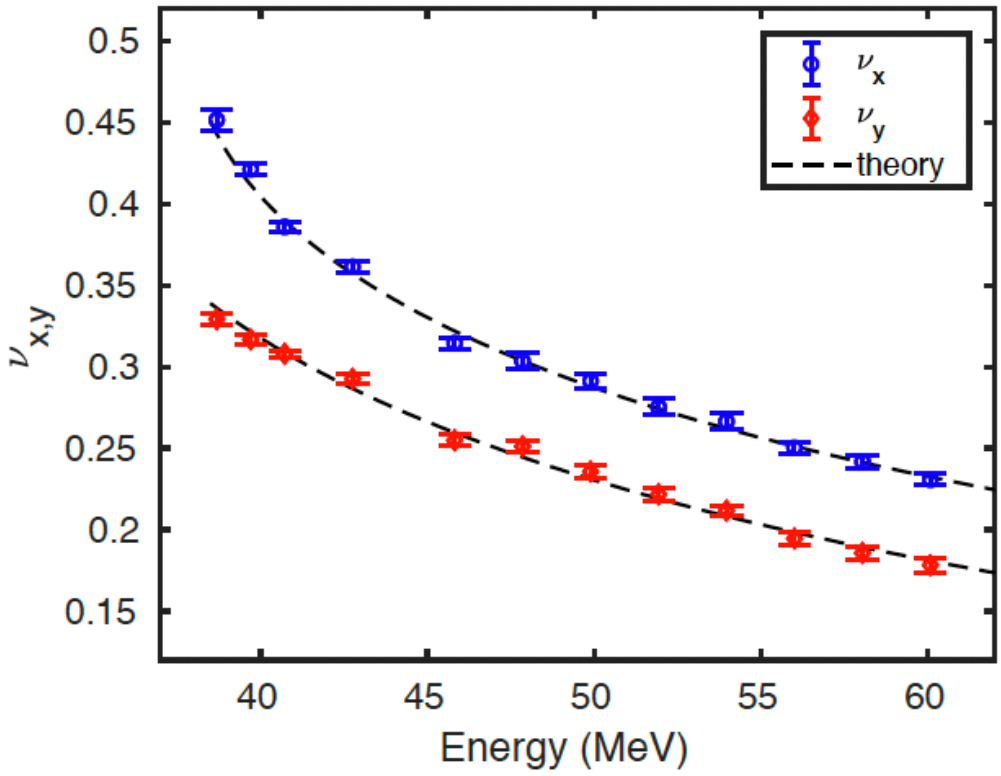

Figure 2.6-9: Measured and theoretically predicted vertical and horizontal tune dependence on energy in a single FFA girder.

2.7 Girder production run complete – Milestone #7

The risks associated with permanent magnet construction, testing, and girder assembly have been completely retired as the girder production was completed nine days before the contract milestone date.

Figure 2.7-1: The BNL CBETA team celebrating the last girder production. The girders with 220 magnets were ready to be shipped to Cornell University for installation.

The magnetic measurement and survey results from all 220 magnets have been documented and archived [83 under “Survey Plan”].

The beam pipe vacuum assemblies for each of the 27 girders were fabricated at Cornell and shipped to BNL for integration into the girder assemblies. This presented some risk as vacuum pipe assemblies are quite fragile; but with careful handling and highly qualified staff, this technique worked out very well and no damage occurred. The alternative would have been to ship the magnets to Cornell and complete the girder assemblies at Cornell. However, this was not desirable mainly because of the tools and space available at BNL to perform the tasks and because several BNL staff would have needed to spend several weeks at Cornell, which would have added significant project cost.

As part of the magnetic field tuning process for the 200+ Halbach magnets, 545 magnetic field rotating harmonic coil measurements were made.

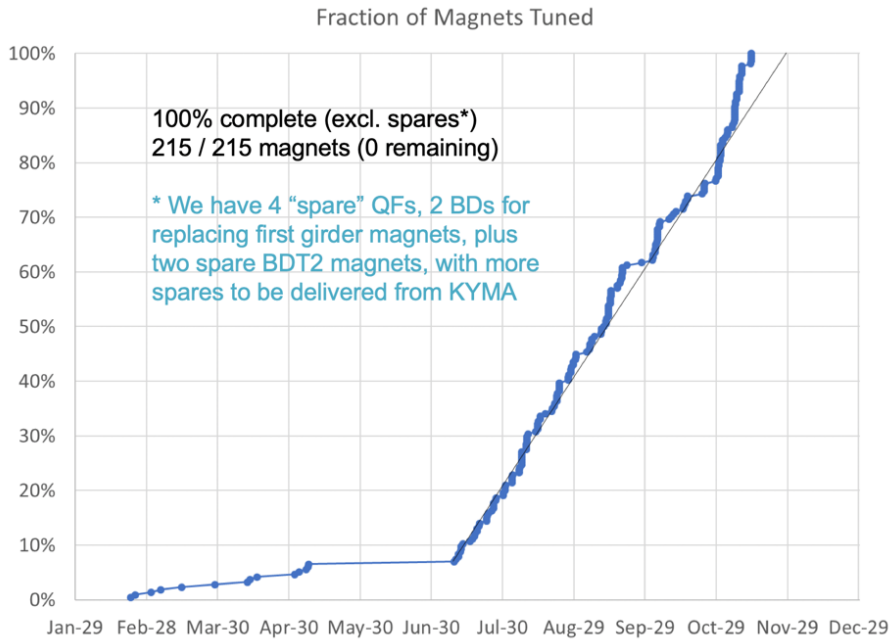

Figure 2.7-2: Production and measurement rate of the FFA magnets.

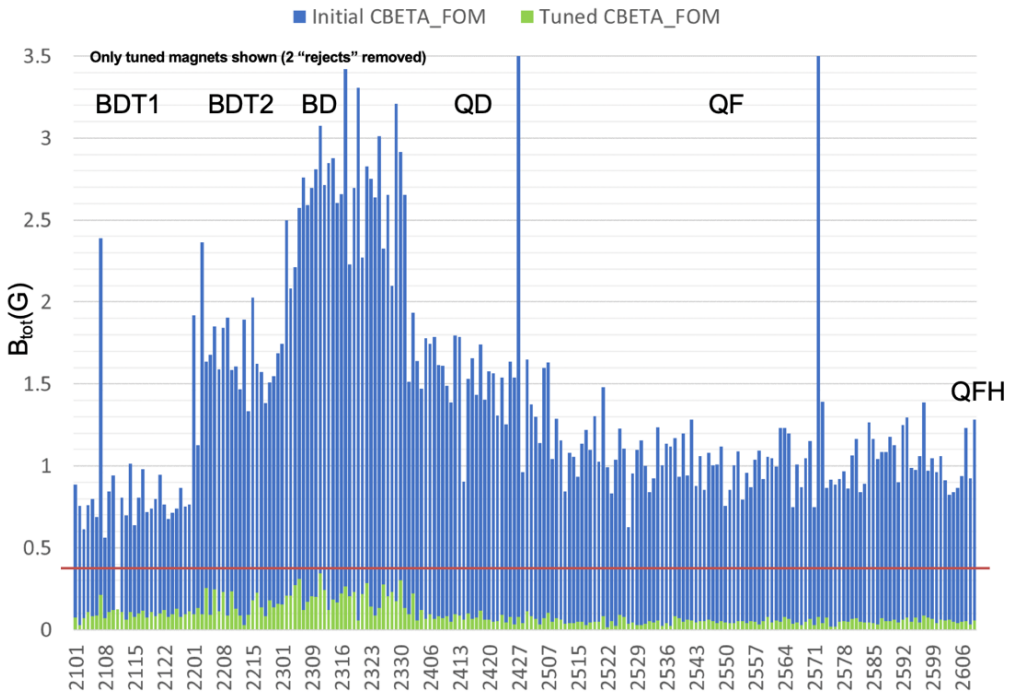

Figure 2.7-3: The quality of the "tuned" magnets (green color).

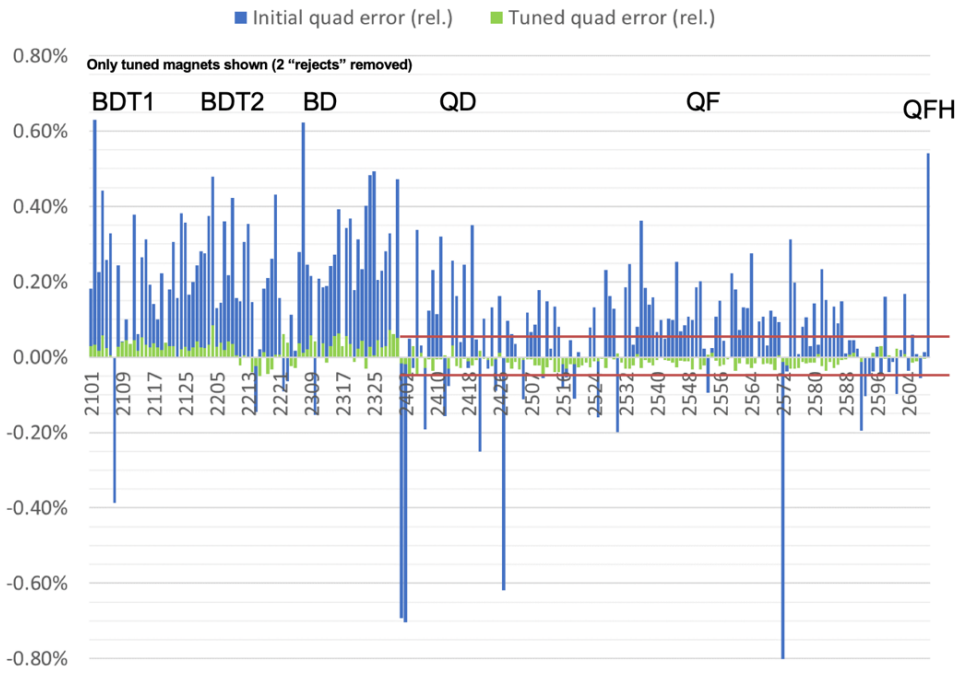

Figure 2.7-4: Integral quadrupole field requirement set to be less than 0.05%.

Custom software was used to determine specific lengths and locations for iron rods to be inserted on the inner radius of the magnets to precisely provide the required magnetic field for each magnet.

The production magnet fabrication by KYMA and magnetic field tuning at BNL included 8 magnets to replace the first girder prototype magnets, as well as several spare magnets. The successful magnet production, characterization, high level harmonic corrections was announced in a BNL newsletter [77], and included the photo shown in Fig. 2.7-1 of the team with the prototype magnet girder.

2.8 Final assembly and pre-beam commissioning complete – Milestone #8

With the girder production complete and final delivery of the BNL constructed girders with permanent magnets delivered to Cornell in December 2018, the installation assembly and alignment in the L0E hall commenced. In March 2019, the one-pass machine assembly was complete to the point that allowed beam commissioning to begin.

Many components needed to be installed, surveyed, and tested, including the vacuum system, beam instrumentation, shielding, control system, splitter magnets, power supplies, safety systems and more.

This was a major system integration task, and although the hope was to complete the majority of the final four-pass installation by February 28, 2019, a sufficient portion of the machine was complete to enable beam commissioning of the one-pass configuration by mid-March 2019. Balancing the ongoing machine installation work with the beam commissioning effort was challenging; but ultimately all beam commissioning goals were achieved on time.

Many system tests were performed prior to the start of beam operations and this certainly contributed to the success of the beam commissioning effort.

Commissioning of the CBETA machine began in mid-March 2019 after the one-pass machine configuration was available. The beam commissioning goals with the one-pass configuration were to satisfy Milestone 9 (Single pass beam energy scan) and Milestone 10 (One-pass energy recovery).

After Milestones 9 and 10 were satisfied with beam in June 2019, beam operations stopped in early July 2019 and the full four-pass machine configuration installation work began in mid-July 2019. The CBETA four-pass installation and pre-beam system tests were complete to the point that allowed four-pass beam commissioning to start on October 9, 2019.

Several pictures of the final machine assembly are shown in Figs. 2.8-1, 2.8-2, 2.8-3, and 2.8-4).

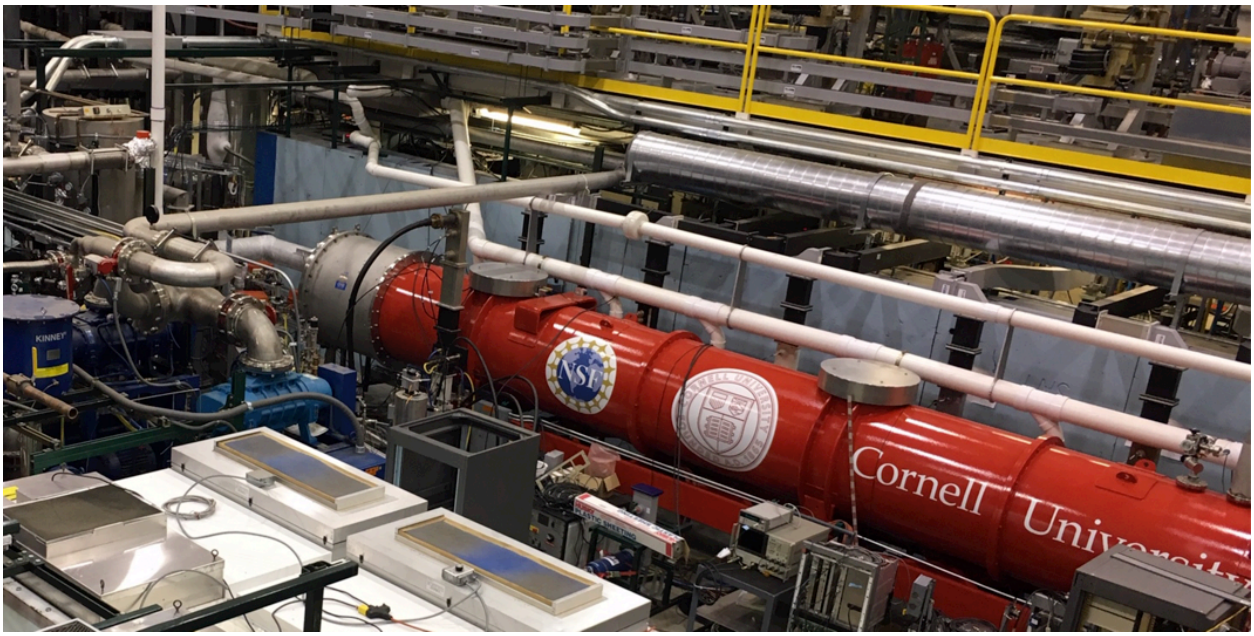

Figure 2.8-1: The Main Linac Cryo-Module.

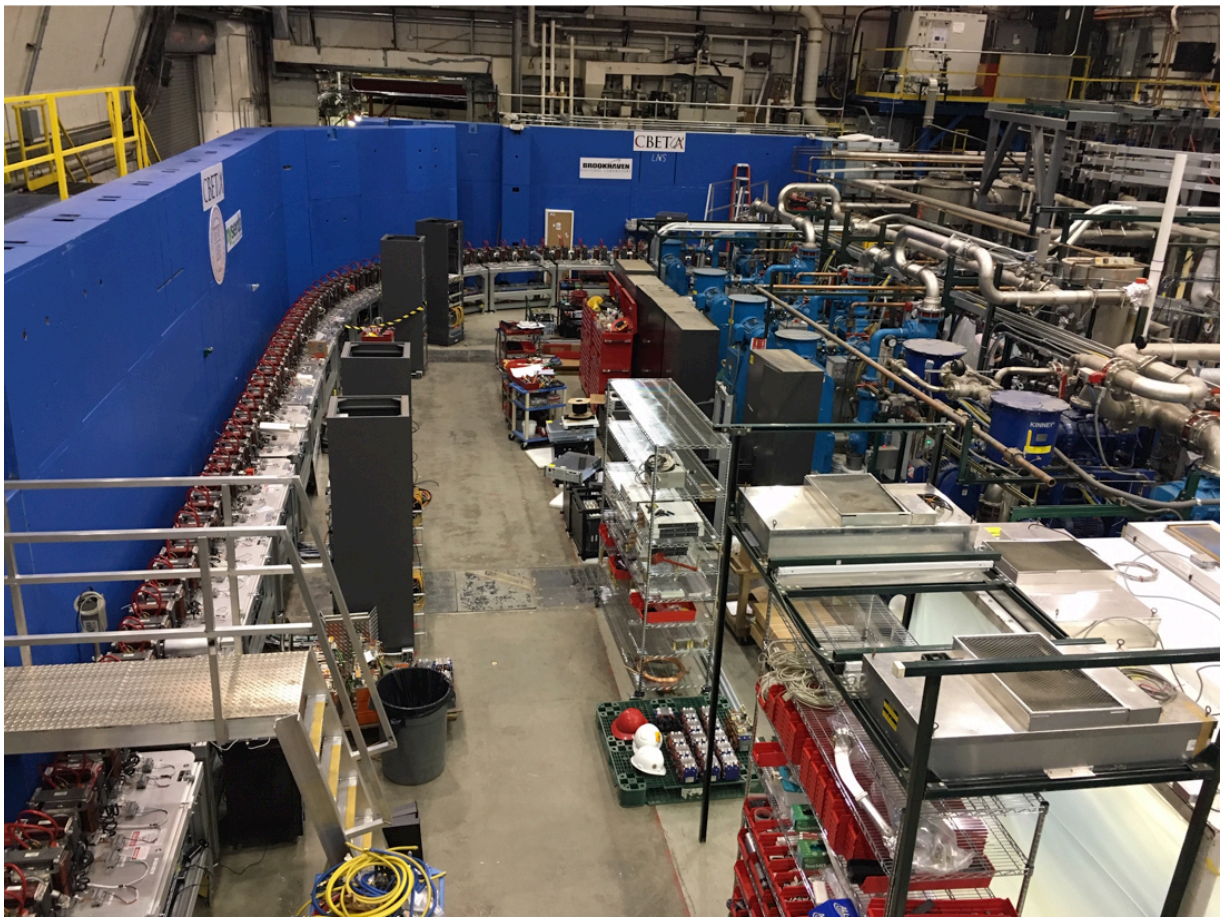

Figure 2.8-2: The Fixed Field Alternating-gradient (FFA) loop installed.

Figure 2.8-3: Photos of the FFA arcs.

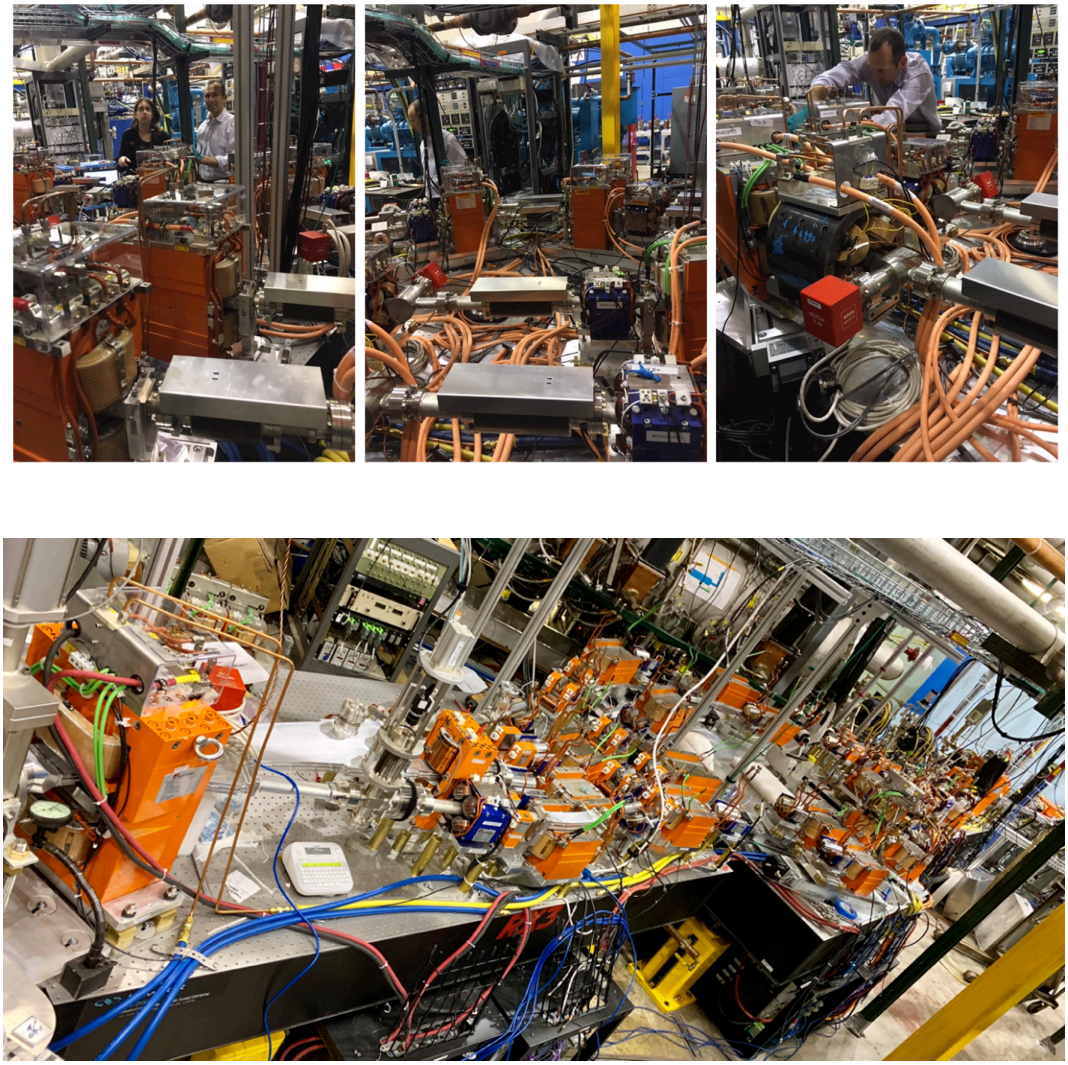

Figure 2.8-4: Photos of the splitter/combiner beamlines.

2.8.1 Electron source and Injector Cryo-Module (ICM)

Overall, the performance of the electron source and ICM (Fig. 2.8-5) were very good during the beam commissioning period [15, 23]. However, the IOT buncher was somewhat problematic during the run and the tube needed to be replaced in January 2020. Nevertheless, commissioning was able to continue when the IOT was not available due to the development of a workaround by the operations staff.

In preparation for higher beam current operation of CBETA, a new cathode must be installed in the electron source. A few unsuccessful attempts were made to complete this before February 2019. First, a high-quality cathode was delivered from BNL to Cornell, but was unfortunately damaged during the process of transferring the cathode from the BNL vacuum chamber to the Cornell vacuum chamber. Then

a new quality cathode was grown at Cornell, but unfortunately did not seat properly in the electron source and therefore could not be used.

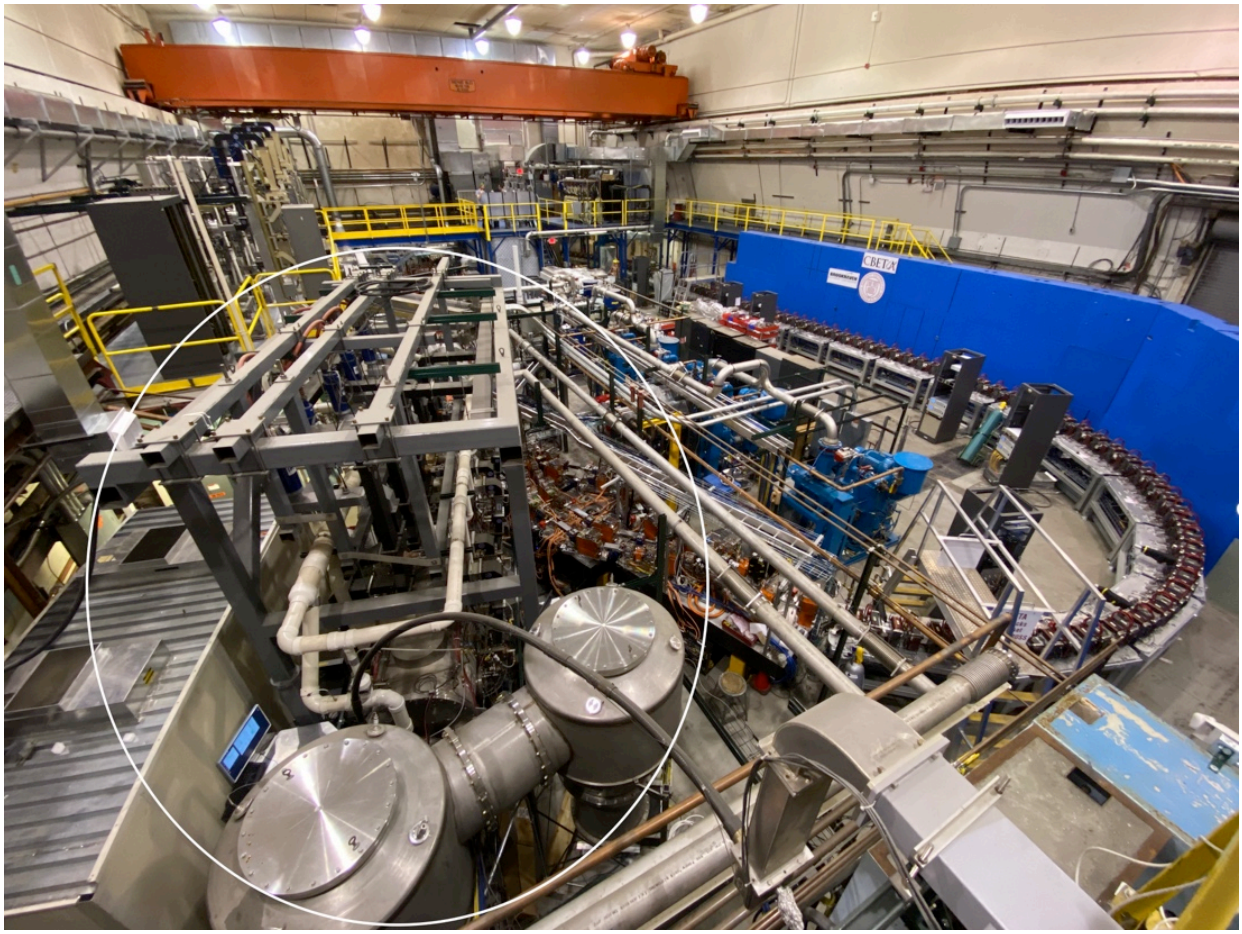

Figure 2.8-5: The CBETA accelerator with the electron source and injector cryo-module circled.

2.8.2 Main Linac Cryomodule (MLC) and related RF systems

The MLC performance was very good during the beam operational period (Fig. 2.8-6). Several improvements were made during the summer 2019 shutdown that contributed to higher reliability of the MLC. Additional bracing of the waveguides and cryogenic lines was installed to reduce cavity vibrations, which greatly improved the energy stability. However, energy stability was still somewhat problematic during the run and this is an area where future improvements would be beneficial.

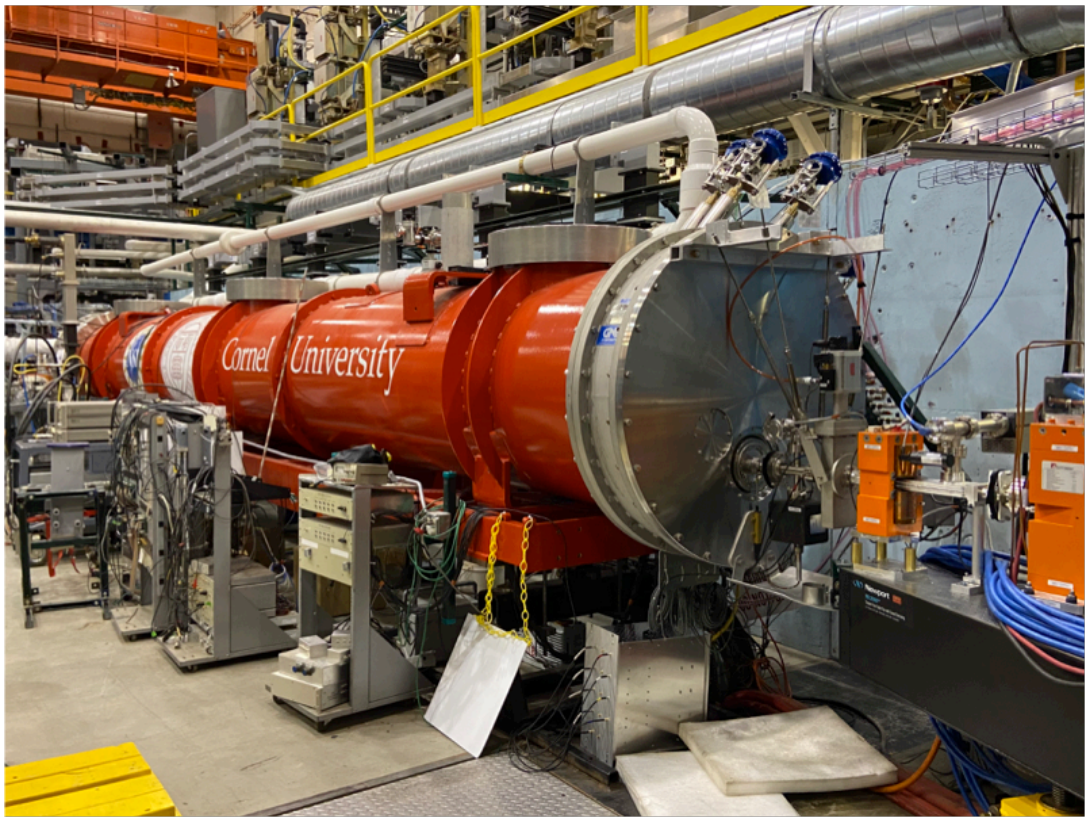

Figure 2.8-6: Downstream end of the Main Linac Cryo-module (MLC).

2.8.3 Vacuum system and beam stop

All splitter vacuum component assemblies for the final four-pass installation were completed in July 2019, several weeks earlier than anticipated (Figs. 2.8-7 and 2.8-8). This was significant as it enabled the full machine assembly to be completed quickly. The vacuum system performance was excellent during the entire operating period.

The high-power beam stop was installed and is available for high power beam operations. A lead brick shielding wall has been installed just in front of the beam stop (Fig. 2.8-8) to limit the backscattering of particles that were being detected by the personnel protection system radiation monitors and inhibiting beam operations at elevated beam currents [146].

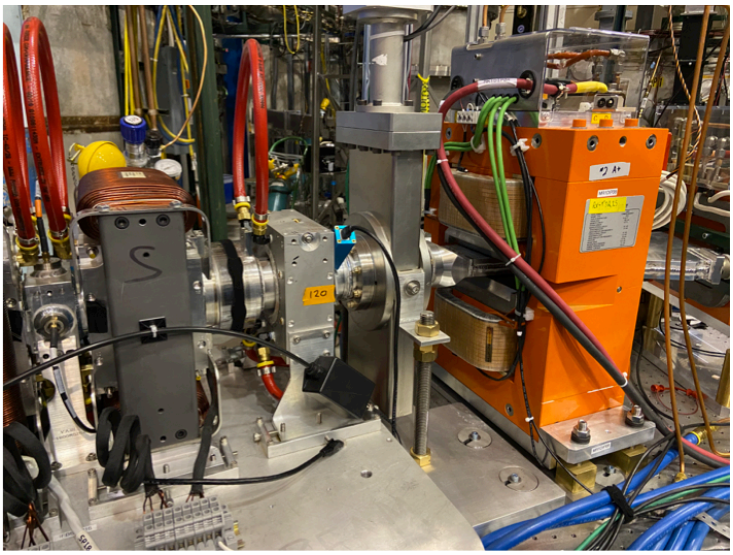

Figure 2.8-7: Portion of the vacuum system where the end of the FFA line connects to the RX line.

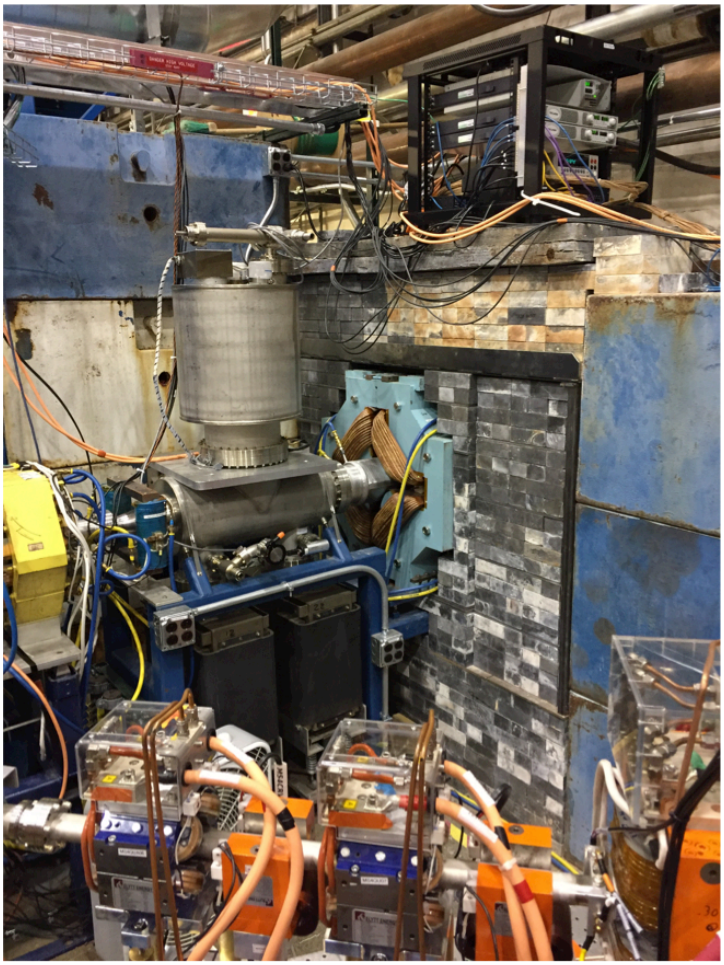

Figure 2.8-8: The beam-stop line and lead-brick shielding wall.

2.8.4 Splitter/combiner beamlines - magnets, power supplies and sliding joints

The splitter/combiner electromagnets fabricated by Elytt Energy (some visible in Fig. 2.8-9) performed very well, and all of the specialty magnets fabricated by BNL and Cornell – the four septa type 1, four septa type 2, six 10-cm-long H4 dipoles, the four 11-cm-long H5 dipoles, and the two high-gradient quadrupole magnets – also performed to specification (Fig. 2.8-10).

Figure 2.8-9: RX splitter lines.

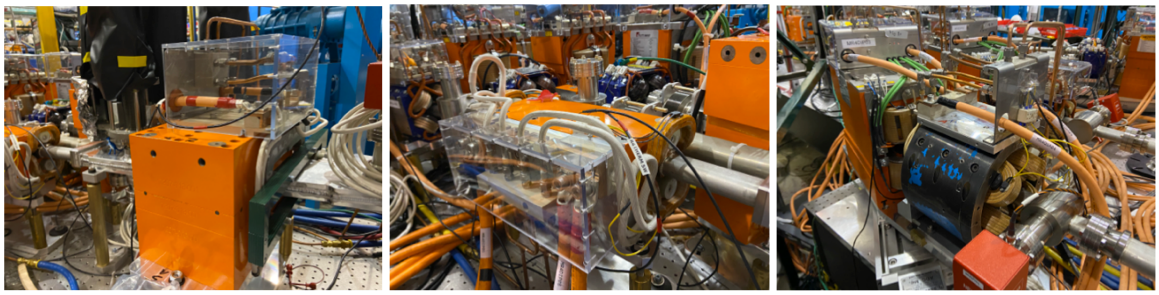

Figure 2.8-10: Septa 1 magnet (left), septa 2 magnet (center), long quadrupole magnet (right).

The power supplies for the splitter magnets were procured from Sigma-Phi [80] and TDK-Lambda [81]. Installation of the splitter magnet power supplies was a significant task and was the final major part of the installation to be completed before beginning beam operations on October 9, 2019. During initial four-pass beam operations, several power supply circuit breakers suffered occasional trips due to overloading. These issues were addressed and resolved by installing additional branch circuits and reconfiguring some of the power supply AC-power wiring.

Another issue that arose was that a few of the installed power supplies could not provide the required current because their voltage limit was reached owing to Ohmic heating of the coils as the magnets reached their equilibrium temperature. Fortunately, the issue was easily resolved by swapping power supplies with other magnets.

During the beam commissioning process, unintended beam oscillations were noted. After diagnosis the cause was determined to be oscillating power supplies. The problem was resolved by installing capacitors at the magnet connections for the offending power supplies.

During operations, one of the power supplies failed and needed to be returned to the vendor for repair. A temporary replacement was loaned to Cornell from BNL, allowing beam operations work to continue after only one day of downtime. For future operations, spare splitter power supplies should be purchased to limit downtime.

Other than the issues described above, the splitter power supplies performed well.

The operation of the sliding joints was not as smooth as expected, and movement of these was quite problematic; some were worse than others, the one in the R2 beamline being the worst case. In addition, the MLC quite often tripped off when the sliding joints were moved. This should be addressed for future operations. Despite these difficulties, seven of the eight sliding joints were successfully used remotely for the fine adjustments of path length required for accurate arrival times at the upstream end of the MLC.

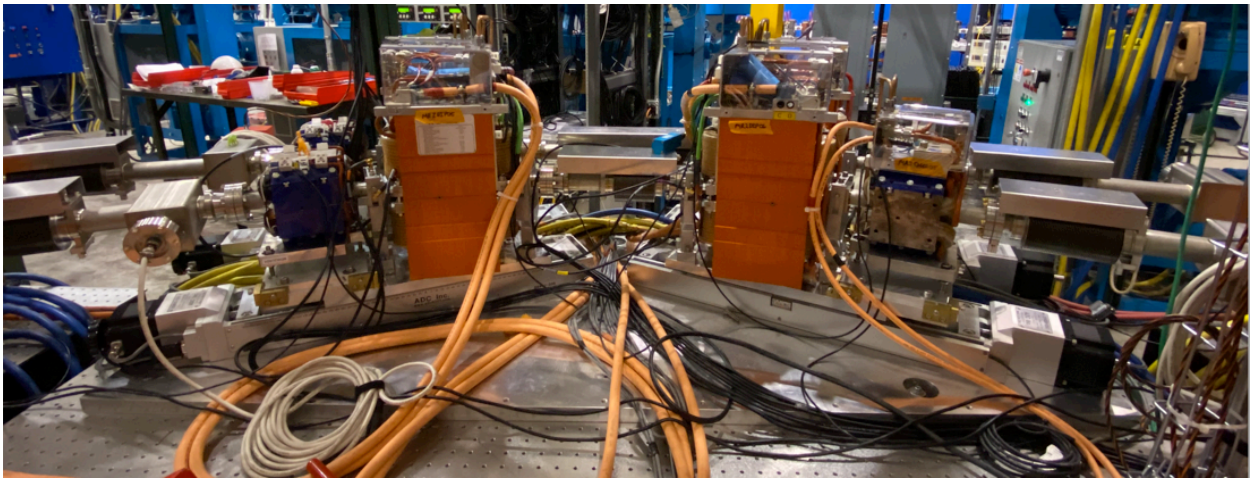

Figure 2.8-11: R2 sliding joint.

The R2 line in Fig. 2.8-11 proved to be the most difficult to tune for optimal transmission, and as of the last day of beam operations the primary contribution to beam loss was the passage of the decelerated beam through the R2 line. This is one of the major outstanding machine issues to be addressed via data analysis and modeling.

Stray fields from some of the magnets affected beams in other splitter lines. For the four septa magnets of type 1, Opera modeling for a shielding scheme combining clamp plates and mu-metal shields proved to be a successful approach. For some dipoles and vertical correctors an automated compensation technique was developed to mitigate the effects of their stray fields.

2.8.5 FFA - Halbach permanent magnets, corrector magnets and power supplies

The Halbach permanent magnets and the entire FFA section performed very well with 4 accelerated and 3 decelerated beam energies – with energy ranges from 42 MeV to 150 MeV.

The corrector magnets also operated very well. The power supplies of Fig. 2.8-13 for the corrector magnets of Fig. 2.8-12 were procured from Sigma Phi in France [80]. The Sigma Phi corrector magnet power supplies initially had a problem where the power supply would trip off when powered on. It was determined that with the inductive loads of the magnets, the power supplies would oscillate and trip on overvoltage. The workaround was to disconnect all of the magnet connections to the power supply before turning the power on, then to reconnect the magnets. This was a very time-consuming process.

Prior to the start of beam commissioning in October 2019, the vendor provided a firmware update that completely solved the problem. This update was installed in all the supplies, and there were no problems throughout the entire run.

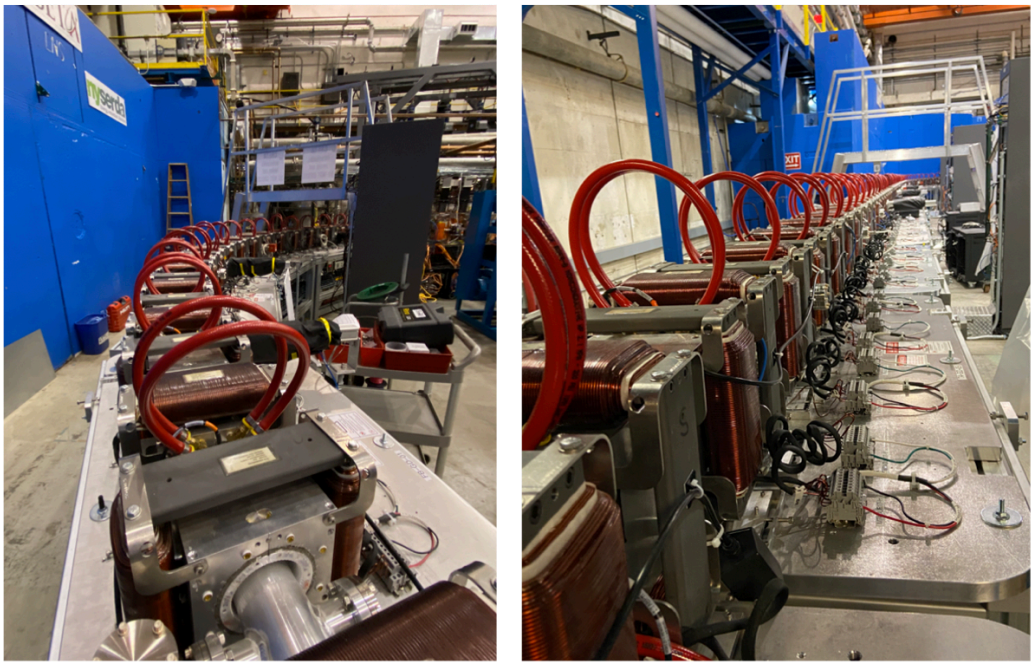

Figure 2.8-12: FFA Halbach permanent magnets and corrector coils surrounding the Halbach magnets.

Figure 2.8-13: Sigma Phi power supplies.

2.8.6 Beam instrumentation

2.8.6.1 Beam position monitor system (BPM)

The beam position monitor system [71, 122, 132, 135] (Figs. 2.8-14) was critical to the success of the CBETA project and performed extremely well during the beam-commissioning period.

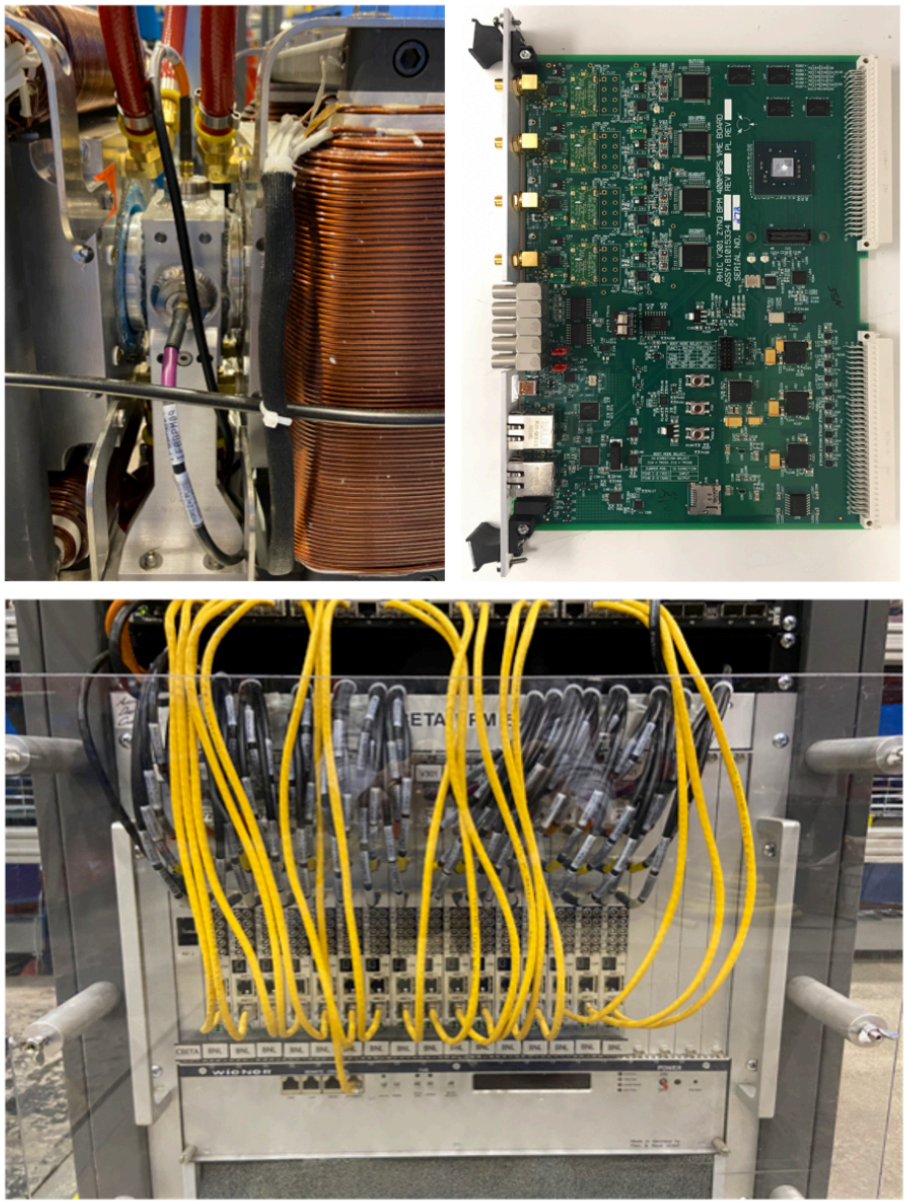

Figure 2.8-14: BPM button installed in FFA loop (top left), custom-designed BPM hardware module (top right), and 16 BPM modules installed in VME chassis (bottom).

Orbit plots from the BPM system were extensively relied upon for machine tuning. Beam position measurements for each of the 7 different FFA turns are acquired by changing the turn selection via an EPICS IOC parameter. Changing this selection reconfigures the trigger delay (in number of ADC clocks from the external trigger) for all 100+ BPMs in the FFA to the selected turn. Typical orbit plots are shown in Figs. 2.9-1 and 2.9-2 later in the report.

In addition to position measurements, the BPM system was also used as a beam intensity and transmission monitor. The raw RSS (sum of squares) signals from the 4 buttons on each BPM were summed to provide the intensity signal, which was then normalized to pC (Fig. 2.11-1).

Tune measurements in the FFA as shown in Fig 2.9-3 were also computed using BPM position data.

Raw BPM data traces are provided in Figs. 2.8-15 and 2.8-16.

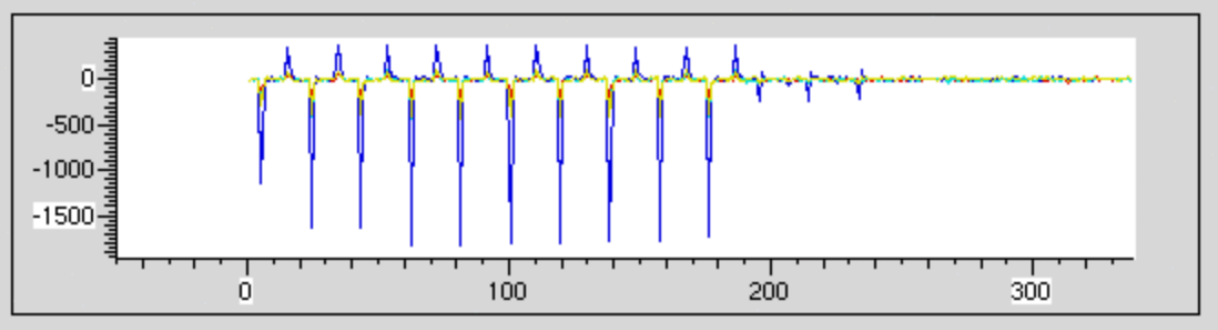

Figure 2.8-15: BPM raw data with the ADC clock at 398.387 (1300/31/2*76/4) which is synchronous with the beam and with the ADC clock timed to the peak of the bunch. The number of bunches in this train is ~20. With this ADC clock frequency and the bunch rate at 41.935 MHZ, the bunch separation is 9.5 ADC clocks. The small positive pulses here are those measured at the ½ clock period; where the time from the negative beam pulse to the small positive beam pulse is 9.5 ADC clocks.

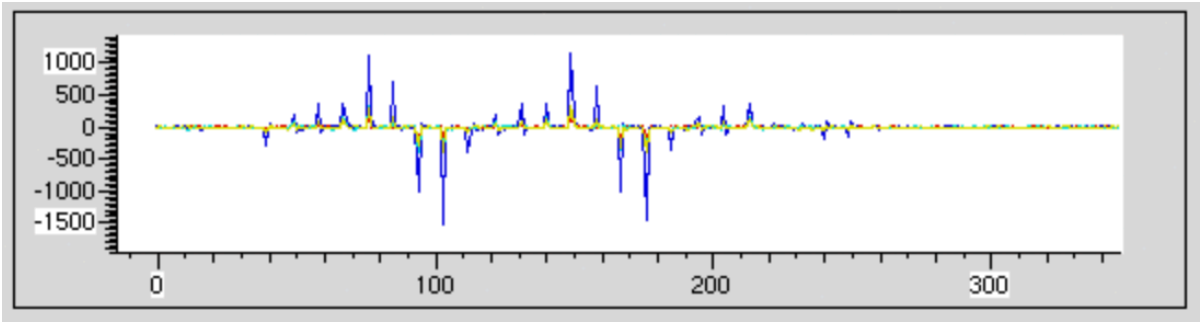

Figure 2.8-16: BPM raw data with ADC clock at a frequency of 382.66 MHz (1300/31/2*73/4), which is slightly asynchronous to the beam. The result is that with a train of bunches (~20 here), the ADC clock triggers at various amplitudes and the RSS of this data can be used to calculate position without the need to perfectly time the ADC trigger to the peak of the bunch.

2.8.6.2 Bunch arrival monitors (BAM)

The bunch arrival monitors use the same hardware as the BPM system (BPM buttons and V301 BPM hardware module), but a mixer chassis (Figs. 2.8-17) is installed between the button signals and the V301 module.

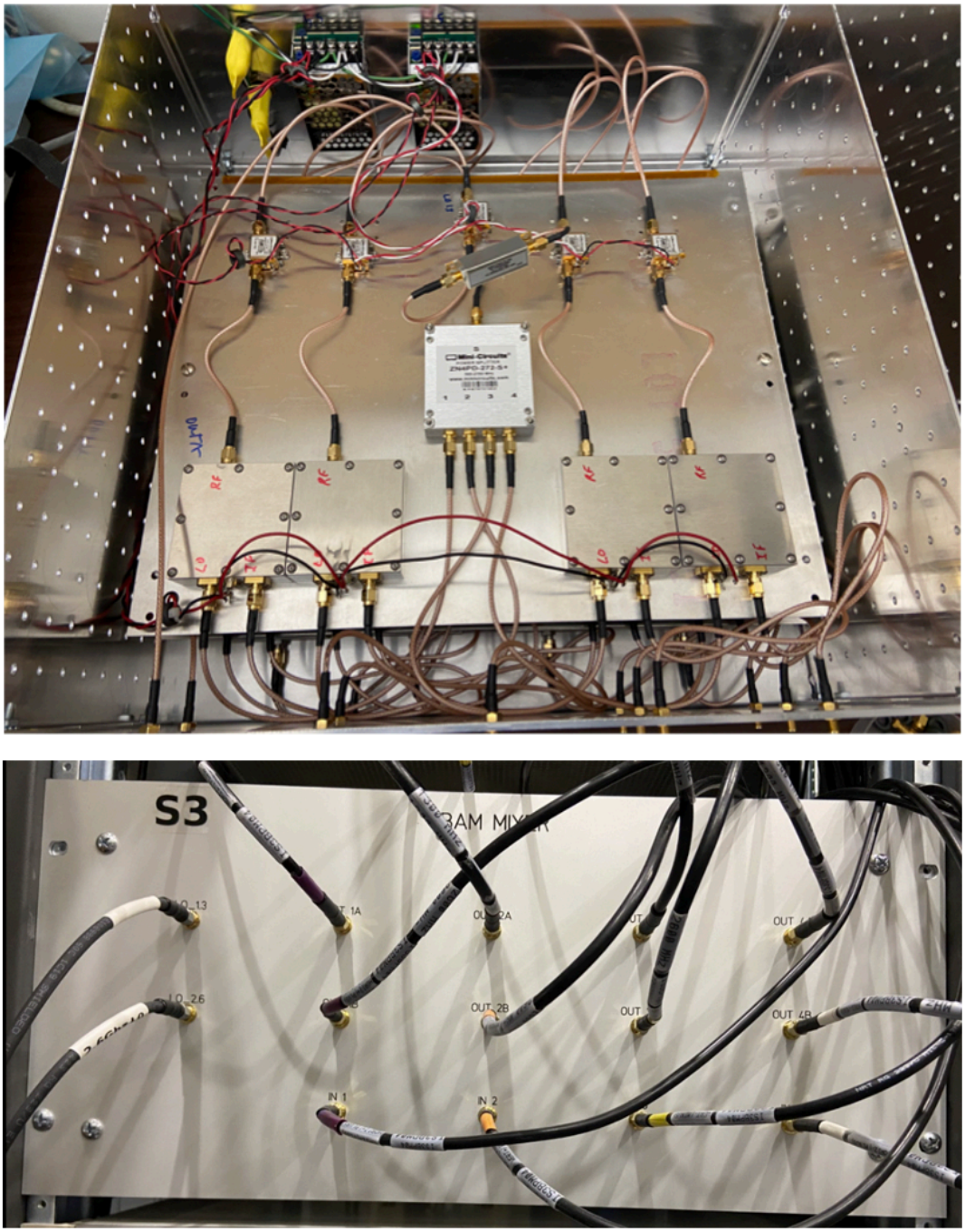

Figure 2.8-17: BAM mixer chassis.

The mixer provides 2 outputs for each button – one is the beam signal mixed with a 1279 MHz Local Oscillator clock to produce a 21 MHz signal representative of the 1300 MHz beam component (Figs. 2.8-18 and 2.8-19) and the other is the beam signal mixed with a 2579 MHz Local Oscillator clock to produce a 21 MHz signal representative of the 2600 MHz beam component as is present in the splitter lines when both accelerating and decelerating beams are present,

For the October 2019 to January 2020 beam run, only the 1300 MHz outputs were used, since the machine was not typically operated with both accelerating and decelerating beams in the splitters.

One issue exists with the BAM mixer chassis that still needs to be addressed. A 21 MHz signal is present on the 2600 MHz outputs when no beam is in the machine. It is suspected that the cause is the second harmonic of the 1279 MHz Local Oscillator clock (2558 MHz) is radiating in the chassis and mixing with the 2579 MHz Local Oscillator clock to produce an unwanted 21 MHz output. Significant time was spent diagnosing this issue, but it has unfortunately not yet been resolved.

Figures 2.8-18 and 2.8-19 show plots of the raw BAM signals. Note that the period of the oscillation is 21 MHz as generated by the mixer. One very important use of the BAM during this previous run was to measure the phase difference between each turn for BPMs at the input to the MLC and the output from the MLC. This was a critical measurement to confirm that the beam phases were matched into the MLC. A typical phase plot is provided in Fig 2.11-5.

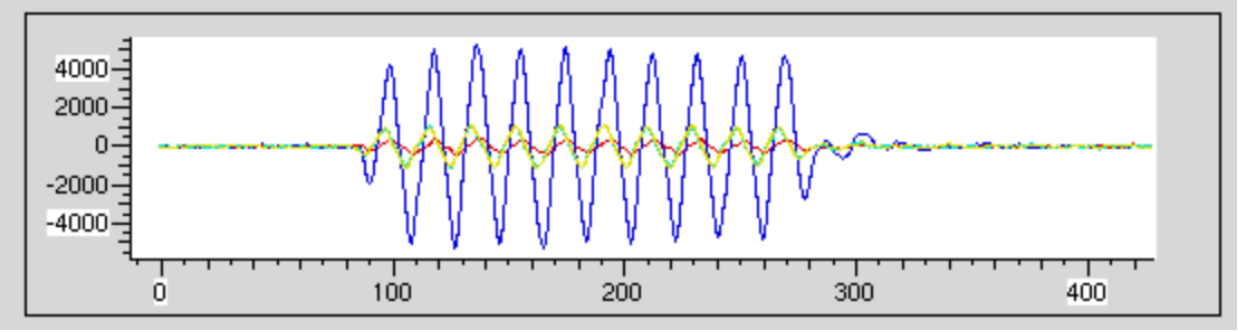

Figure 2.8-18: BPM raw data from one of the BAM mixers channels. The output frequency is 20 MHz (1279 MHz mixed with the 1300 MHz beam signal) and the number of bunches in the train is ~20.

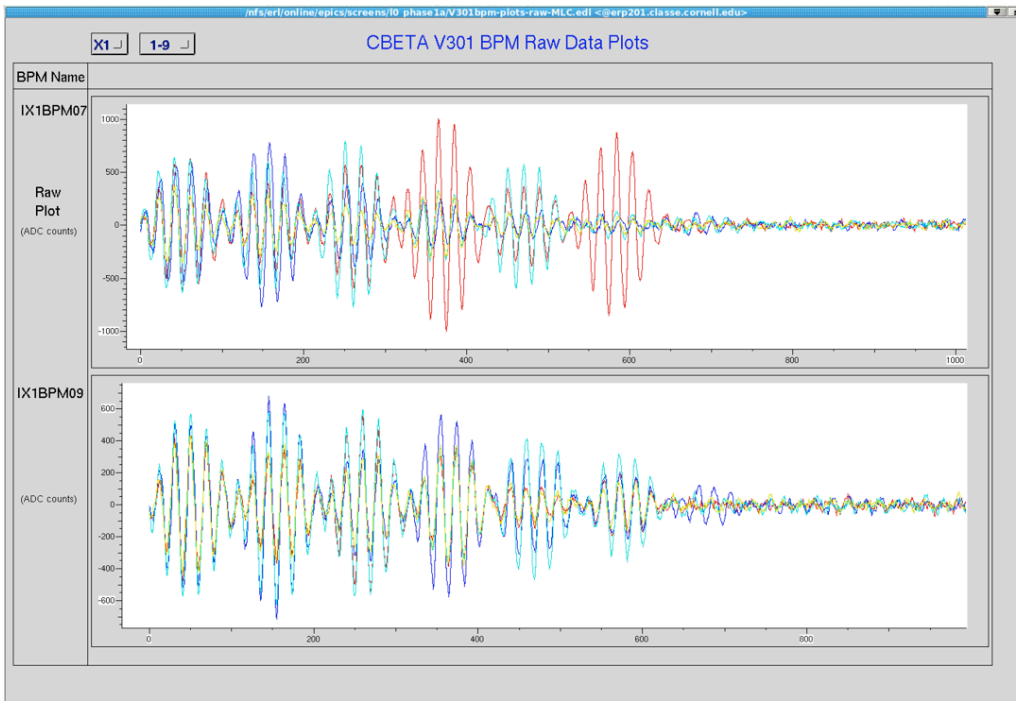

Figure 2.8-19: 12/23/2019 10:30:36pm BAM data from BPMs at input to MLC (top trace) and output from MLC (bottom trace). The bunch train length was 8. Six passes are clearly visible, and the seventh pass is visible with lower amplitude. This data was used to measure the turn-to-turn phase difference for MLC phase matching.

2.8.6.3 View screens

The view screens (Fig. 2.8-20) were another very important device used to commission the machine. This system also worked very well during the entire operating period. View screen images are shown in later sections of this report (Figs. 2.9-1, 2.10-1, and 2.11-2).

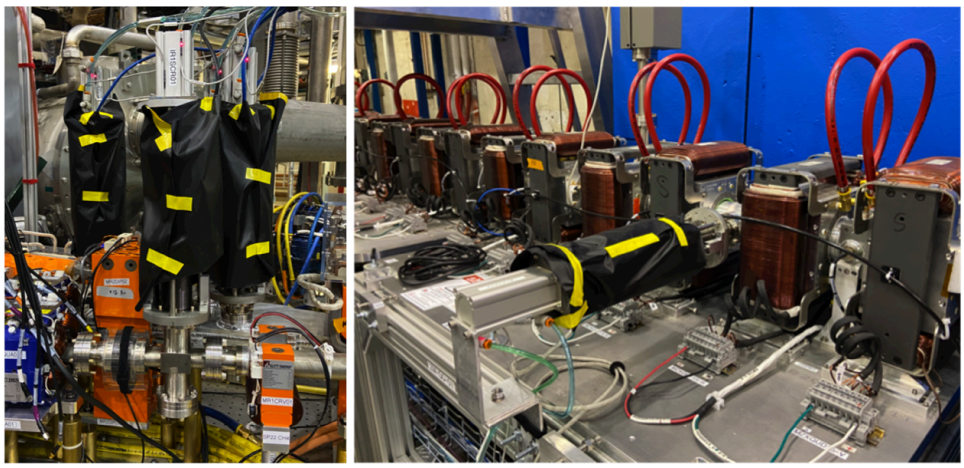

Figure 2.8-20: Three view screens at end of R1, R2, and R3 lines (left) and view screen installed in FFA loop (right).

2.8.6.4 Fast loss monitor system

The fast beam loss monitor system (BLM) was installed and tested at the end of January 2019. Figure 2.8-21 shows a plot of real beam loss data on January 29, 2020.

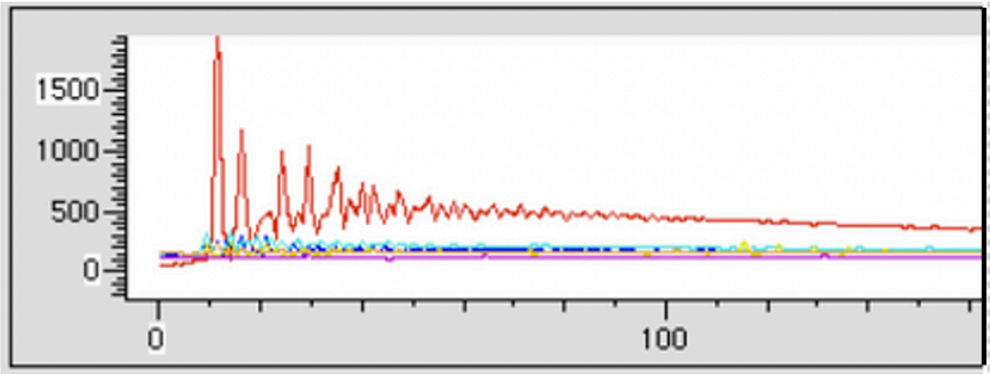

Figure 2.8-21: Fast loss monitor data in the TA section of the FFA loop. Time between ADC data samples is 50 ns. Each pulse shown represents losses in consecutive turns and the time per turn is ~250 ns.

Photos of the fast loss monitor system are provided in Figs. 2.8-22, 2.8-23 and 2.8-24). The fast loss monitor system will be very important for higher beam current operation when the beam must be quickly inhibited if beam losses exceed a programmed threshold.

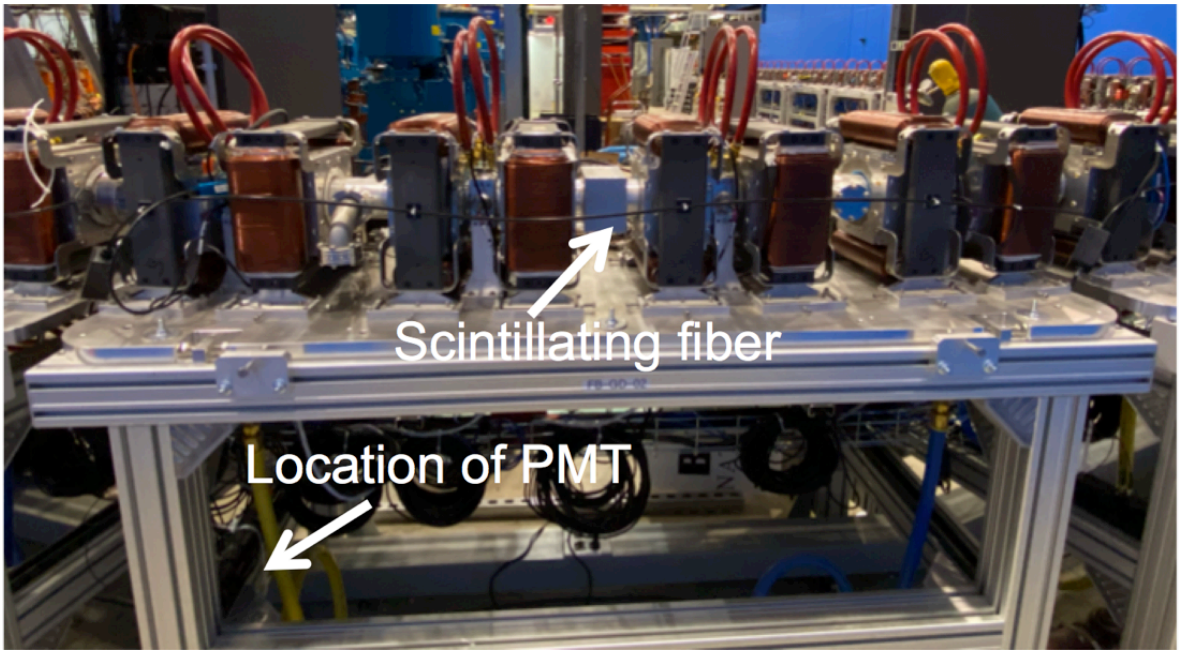

Figure 2.8-22: Fast BLM scintillating fiber installed along permanent magnets, and photo multiplier tube (PMT) installed under girder.

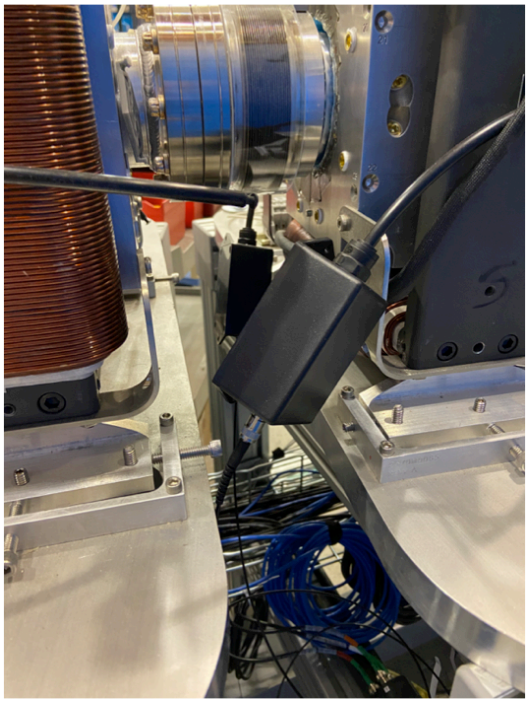

Figure 2.8-23: Fast BLM scintillating fiber to PMT interface box (top) and Photo Multiplier Tube (PMT) installed under girder.

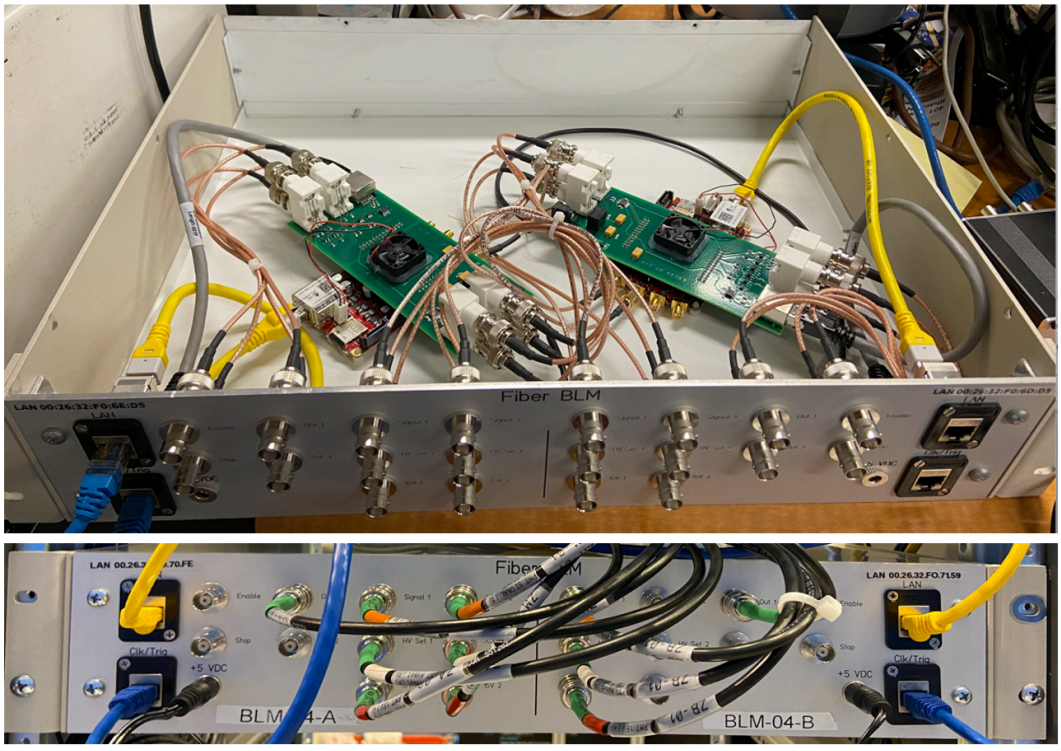

Figure 2.8-24: Fast BLM electronic chassis.

2.8.7 Bunch pattern generator

The bunch pattern generator uses custom firmware in the V301 BPM module to generate the laser triggers, BPM triggers and other instrumentation triggers. An additional machine protection component is provided by limiting the number of laser triggers to a given number over a specified period of time.

This system operated very well during the run with no issues.

2.8.8 Control system

The CBETA control system is based on EPICS. Many EPICS IOCs were developed to communicate to hardware, provide machine control, and in general control the machine. A growing set of scripts using Python and Matlab were (and continue to be) generated to assist in the automation of control system tasks.

A primary application that was used to tune the machine was the CBETA viewer (cbv), written in Matlab to display, among other important information, BPM position and intensity data for all turns. This application is capable of displaying live data or machine model data, as well as overlaying both model data and live data for comparison, as shown in Fig. 2.9-2 later in the report.

Several orbit correction programs were also developed [131, 139].

2.8.9 Equipment protection system

A detailed design document for the CBETA equipment protection system was written as a tech note [140].

For the low current operation that was used during the entire CBETA beam commissioning period, the primary equipment protection system was the slow loss monitor system. This system uses devices connected to serial links and polled via EPICS IOCs to disable the beam via software when a loss is exceeded. The response time is based on data that is updated about once per second.

The fast loss monitor system that was installed and tested at the end of January 2019 will be used to inhibit beam when a fast beam loss occurs. The response time to inhibit beam is expected to be several microseconds. This system will be required for high beam current operation. A final test of inhibiting the beam when a loss occurs still must be performed.

A dedicated hardware chassis was designed with custom firmware and software to concentrate the digital signals from the fast loss monitor system and other devices into the shutdown system that inhibits the beam (Fig. 2.8-25).

Figure 2.8-25: Fast shutdown chassis used for concentrating digital signals for inhibiting beam.

2.8.10 Personnel protection system

The personnel protection safety system (Fig. 2.8-26) operated as required for the duration of the run with no issues.

Radiation shielding analyses were performed to ensure that personnel are properly protected from radiation during operation of the machine [136, 143].

Figure 2.8-26: Personnel protection system hardware – bypass (left), light beam and bypass at stairs to mezzanine (center), and radiation monitors (right).

2.9 Single pass beam energy scan – Milestone #9

Beam commissioning of the one-pass energy recovery (ER) configuration began in March 2019. This included electron source processing, tuning the injector to the desired optics, calibrating the Main Linac Cryomodule (MLC), and fully integrating the new Beam Position Monitors (BPMs) into the system.

On May 7, 2019 the 42 MeV beam was sent through the permanent magnet arc (FFA arc), without using correctors; the orbit through the FFA arc and the beam spot on the final view screen are shown on the left and right, respectively in Fig. 2.9-1. During subsequent shifts, an orbit correction script was successfully applied. The orbit through the FFA arc is shown before and after correction in Fig. 2.9-2.

In early June, an energy scan was performed by transporting a beam of various energies through the FFA arc; the energy range went from 39 to 59 MeV.

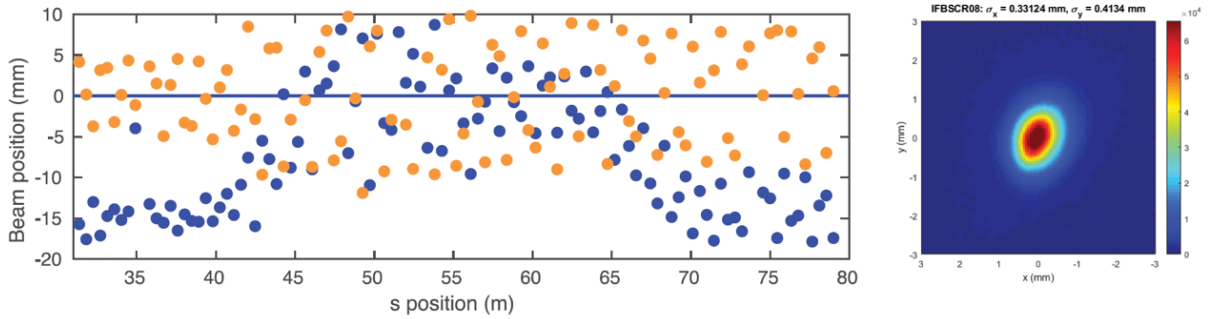

Figure 2.9-1: The orbit through the FFA arc (left) and the beam spot on the final view screen in the arc (right) while sending the 42 MeV beam through the arc for the first time, without correctors. The horizontal orbit is in blue; the vertical orbit is in orange.

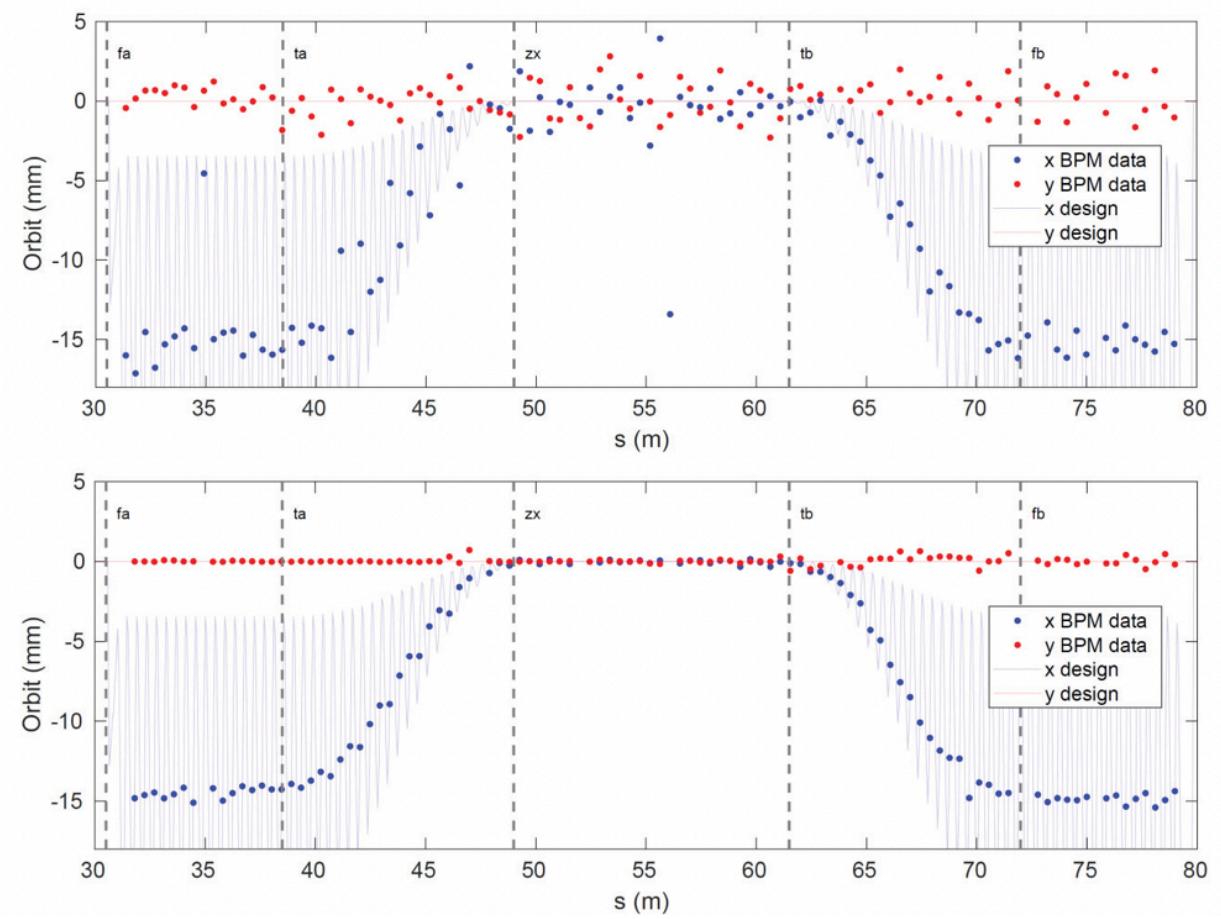

Figure 2.9-2: Orbits through the FFA arc before (top) and after (bottom) orbit correction with respect to the theoretically predicted orbit.

The tune per cell was measured in the three periodic sections of the machine – the arcs (FA and FB) and the straight (ZX). A comparison of measured tunes to the theoretical prediction is shown in Fig. 2.9-3, which shows good agreement between the measurements and predictions. The energy scan reproduced the demonstration of the energy range acceptance first demonstrated during the CBETA Fractional Arc Test (FAT) [60].

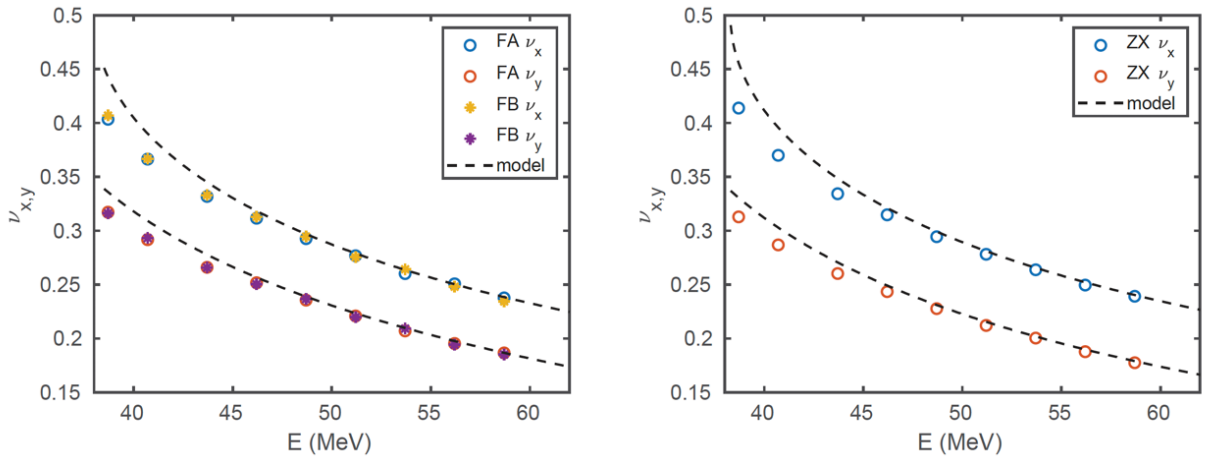

Figure 2.9-3: Measured tunes compared to theoretical predictions as a function of energy in the FA and FB arc sections (left) and the ZX straight section (right).

2.10 Single pass beam with energy recovery – Milestone #10

After successfully completing the energy scan milestone, machine commissioning continued with the goal of establishing one-pass energy recovery (ER).

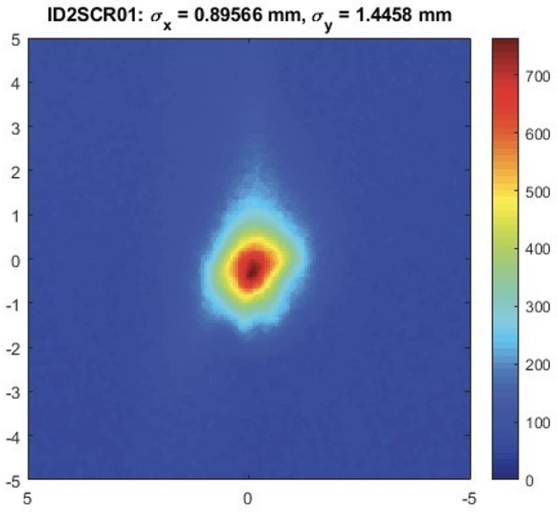

Figure 2.10-1: Beam profile of the energy recovered beam at the beam stop.

For single pass ER operation, the injected 6 MeV beam is accelerated to 42 MeV during its first pass through the Main Linac Cryomodule (MLC), sent around the FFA arc, and then decelerated back to 6 MeV during a second pass through the MLC. The resulting 6 MeV beam is then sent into a transfer line that terminates in a high-power beam stop.

The first complete recirculation occurred on June 10, 2019 [67, 69]. Figure 2.10-1 shows the image of the first beam successfully recirculated through the entire single turn setup. Of significant importance is that the centroid position of the recirculated 6 MeV beam on this screen matched the centroid of the injected 6 MeV beam sent into the same beamline with the MLC turned off. This indicates that the total energy delivered to this beam from the MLC was recovered before the beam was dumped.

The MLC has 6 cavities as shown in Fig. 2.10-2. In order to demonstrate exact energy recovery in *each* of the MLC cavities, measurements were made for both the power pumped into each cavity (forward power), as well as any power reflected back from the cavity (reflected power). The difference between these measurements (forward minus reflected) equals the power delivered to the beam (beam loading) plus any amount lost in the cavity walls. For a fixed voltage, the power lost in the walls is constant and can be computed or measured, while the power delivered to the beam is proportional to the average beam current. Thus, changing the beam current allows one to separate out the effect of the beam loading. Demonstration of energy recovery in each cavity occurs when the measured beam loading vanishes for each cavity [143].

To test this beam loading measurement procedure, the beam was accelerated from 6 MeV to 24 MeV using the first three MLC cavities set to 6 MV, and then decelerated back to 6 MeV using the last three cavities. The resulting 6 MeV beam was sent straight into the transport line to the beam stop, bypassing the FFA loop entirely. Increasing the beam current in this set up should result in linearly increasing beam loading in the first three cavities and linearly decreasing loading in the latter three cavities. Figure 2.10-3 shows the results of raising the beam current up to 1 μA. The plots on the left and right display beam loading in cavity 5, and cavity 2 respectively.

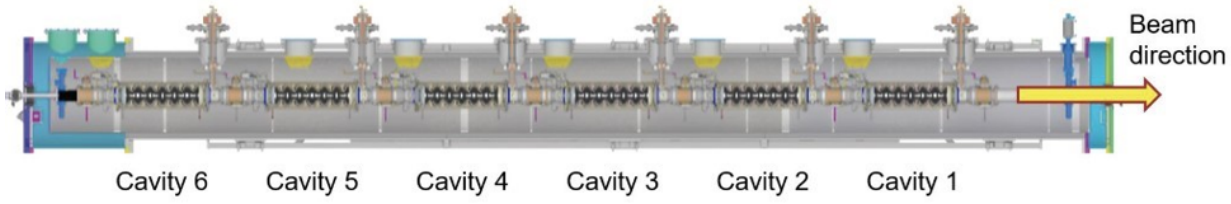

Figure 2.10-2: Layout of the superconducting cavities in the MLC with respect to the beam direction.

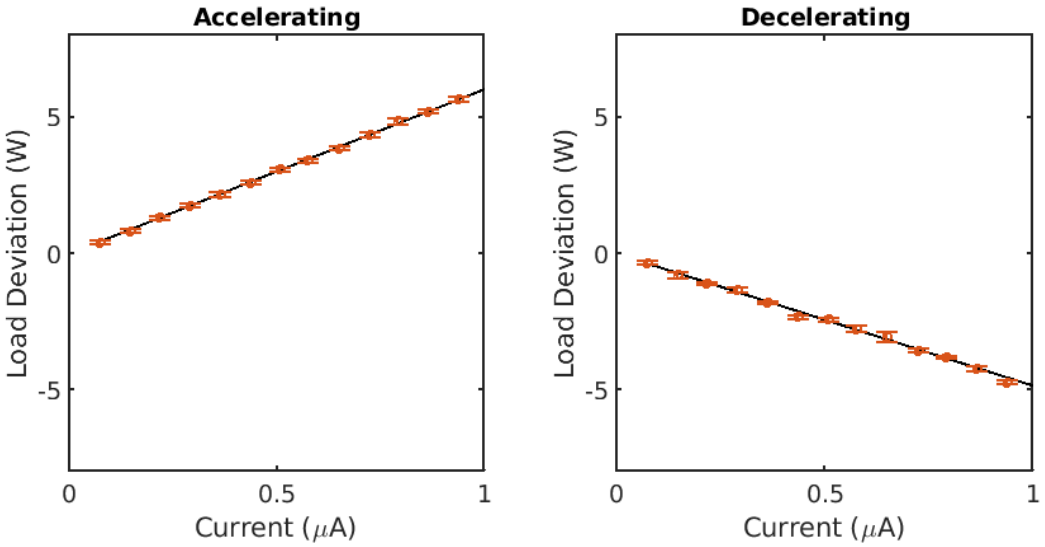

Figure 2.10-3: RF load deviation (beam loading) for an accelerating and decelerating cavity in non-ER mode as a function of average beam current. Left: loading in cavity 5, right loading in cavity 2.

With this successful test of the loading measurement procedure, data was acquired with the machine in full single pass ER mode. The first measurement of beam loading in this configuration was made on June 24, 2019.

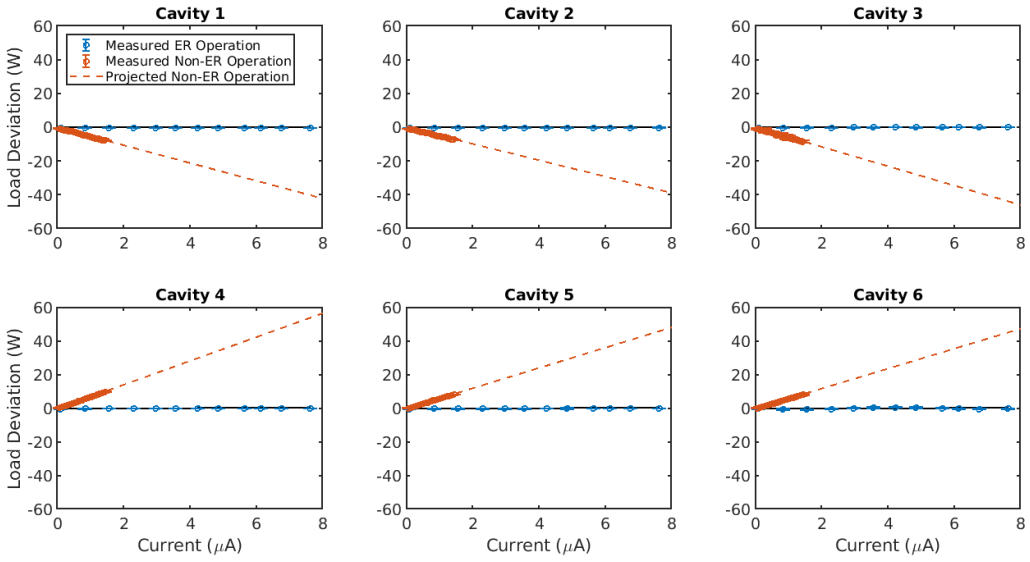

Figure 2.10-4: RF load deviation (beam loading) on each cavity in the MLC in non-ER mode measured (orange dots), non-ER mode projected (orange dashed line), and ER mode measured (blue) as a function of average beam current on July 1, 2019. This evaluation shows that 99.6+/-0.1% of the particles make it back to see the energy recovered. Each cavity recaptures at least 99.5 +/- 0.2 % of the energy of these particles.

Optimized machine settings (which included lowering the bunch charge from 5 to 2.5 pC, lead to an ER beam loading measurement demonstrating an energy recovery of 99.6 ± 0.1%. Fig. 2.10-4 shows the beam loading for each of the 6 cavities for the non-ER mode (red) and the ER mode (blue). Clearly, each cavity hardly uses any energy to accelerate beam in the ER mode. The positive slope seen here corresponds with the data taken in the non-ER test case, while the blue data points show the data taken in ER mode. These measurements represent the completion of milestone 10.

For each cavity, the ratio of the near-zero slope of the blue lines to that of the red lines is the fraction of the energy gain in a cavity that is not recovered during deceleration in that cavity. Because the sum of all accelerations adds up to the same 36 MeV as the sum of all decelerations, the average of the slopes is characteristic of the beam loss in the return loop. This evaluation shows that 99.6+/-0.1% of the particles make it back to see the energy recovered. Each cavity recaptures a large fraction of the energy of these particles. With cavity 4 having the largest blue slope, it recovers 99.5 +/- 0.2 % of the energy, all other cavities recovery an even larger percentage.

The current was increased up to 70 μA using 2.5 pC bunches., Fig. 2.10-5 displays the average current vs. time.

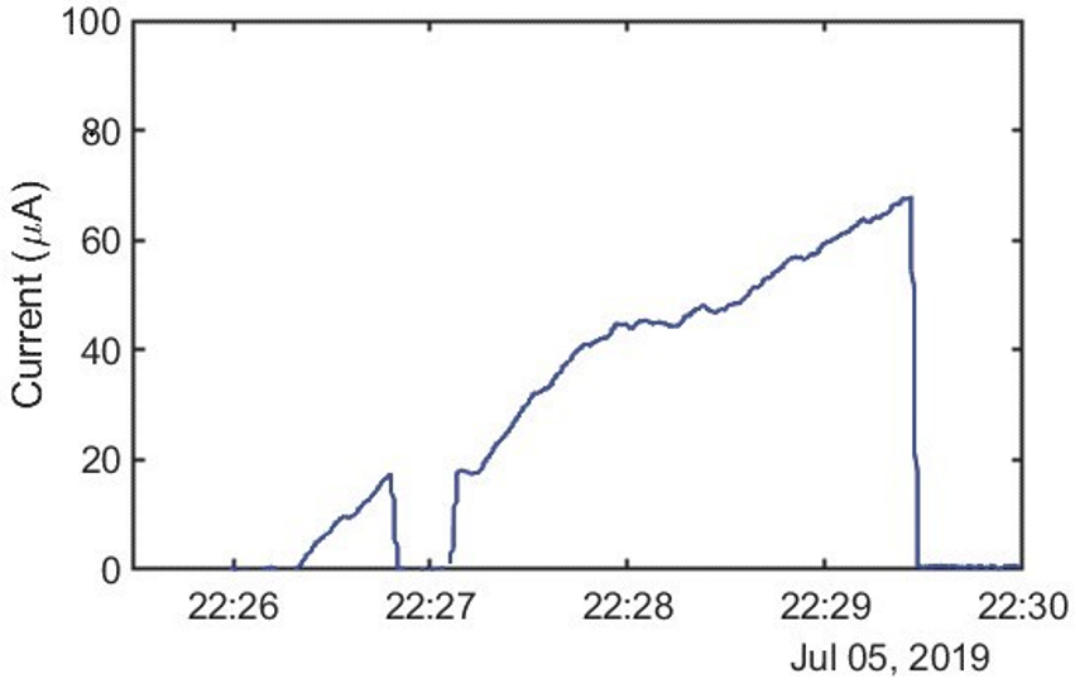

Figure 2.10-5: Plot of average beam current in the electron source during higher current push.

Two things prevented raising the current any higher: delay in the installation of a fast-internal radiation monitoring system for protecting the FFA magnets and gamma ray levels on the external Personnel Protection System (PPS) radiation monitors. The former issue has been addressed with the installation and testing of the fast monitors in January 2020, the latter was also addressed by adding more lead shielding around the beam stop area. Based on this experience, a straightforward path for reaching currents up to 1 mA in the single pass ER mode is anticipated [60, 146].

2.11 Four pass beams with energy recovery (low current) – Milestone #11

Construction of the four-pass ER configuration began in July 2019, and beam commissioning started on October 9, 2019 when the installation of all critical components was complete. Beam commissioning proceeded steadily through December and culminated with the first beam being sent through the entire four-pass ER configuration in the early hours of December 24th thus satisfying milestone 11. Commissioning continued throughout January 2020. Details regarding the beam commissioning process and the challenges incurred during the multi-pass operation are provided in this section.

The beam transmission through each of the 7 FFA transfers is shown in Fig. 2.11-1. Here the first four sets of blue data show the transmission through the FFA arc after each accelerating pass through the linac, while the last three sets show the transmission after each decelerating (or energy recovery) pass. The transmission is roughly constant as the beam is accelerated up to 150 MeV and back down to 78 MeV. Here, however, transmission suffers before the final FFA pass. Unfortunately, the cause of this beam loss is not fully understood at this time. Raising the beam's average current in future operation requires solving this problem.

Even with a remaining transmission of about 30%, the beam was still easily detected on the view screen in the transport line to the beam stop, indicating that the energy of the remaining particles had been successfully recovered. Figure 2.11-2 shows a picture of the beam on the screen in this line. With this set up it was also possible to measure both the accelerating and decelerating orbits through the FFA for all four energies. Figs. 2.11-3 and 2.11-4 show the seven horizontal and vertical FFA orbits respectively.

Establishing the correct arrival time of the beam at the entrance of the linac during each pass is critical for successful energy recovery. To accomplish this, the arrival times were measured at the entrance and the exit of the MLC for every pass of the beam. BPMs are installed just before the entrance and just after the exit of the MLC, and each pass through those BPMs creates an oscillating signal as

shown in Fig. 2.8-19. The phase of the oscillatory signal corresponding to the pass to be measured provides an accurate indication of the arrival time at the BPM.

The model provides the difference in arrival times between any given pass and the first pass for the design. The difference in phases (and therefore arrival times) between a given pass and the first pass is used to determine if the path length in the return loop is correct. Figure 2.11-5 shows the measured phases (points with error bars) and the design values (circles) near the entrance (B1) and exit (D1). The majority of these measurements are within a few degrees of the design values. Note that in Fig. 2.11-5 turns 5-8 are decelerating and the plotted phases are shifted by 180 deg.

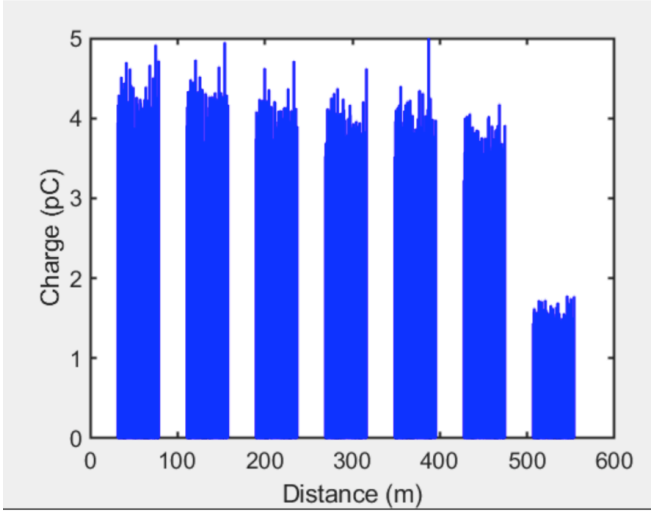

Figure 2.11-1: Transmission of the 7 transfers through the FFA (and 8 passes through the MLC).

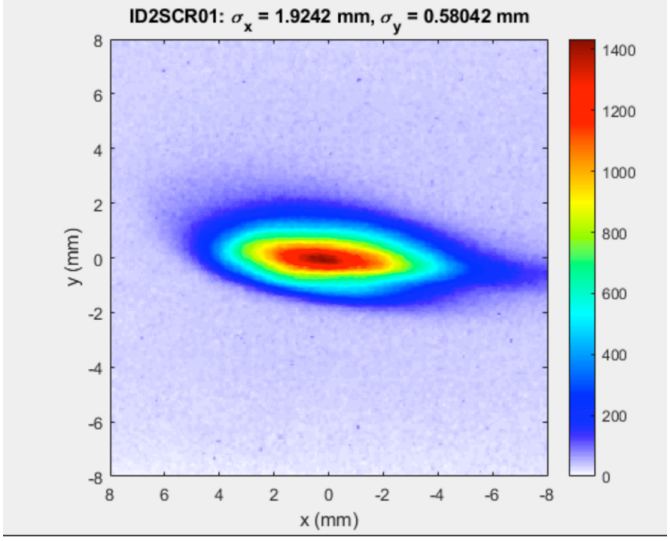

Figure 2.11-2: The final beam profile after 8 passes through the linac and full energy recovery.

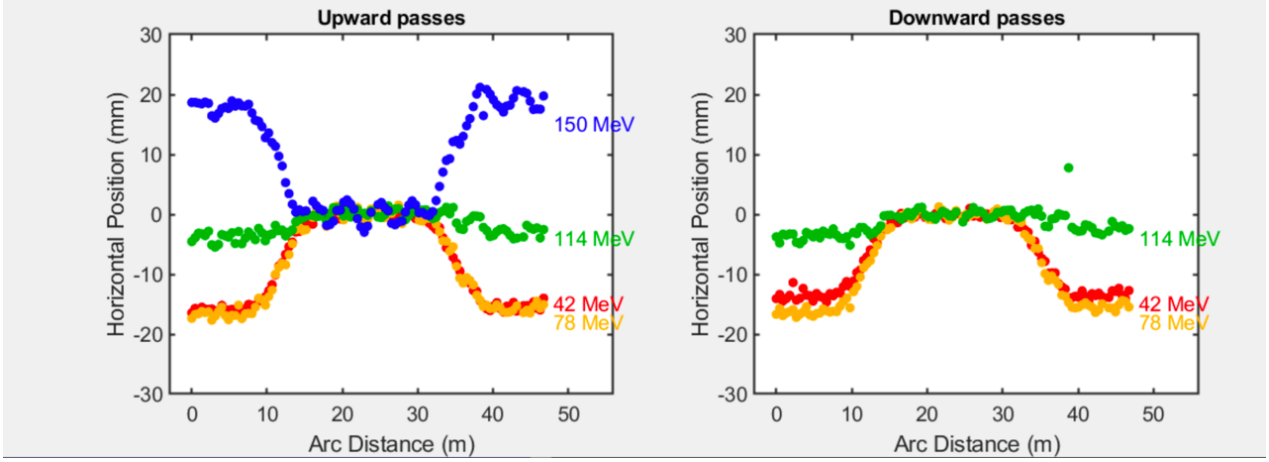

Figure 2.11-3: Horizontal orbits through the FFA beam lines during acceleration (left) and during energy recovery deceleration (right).

Finally, measurements of the beam's tune for each of the accelerating energies through the FFA straight section is shown in Fig. 2.11-6, showing excellent agreement over the beam's full energy range.

Much was learned about the new accelerator while establishing four-pass ER. Vibration suppression of MLC waveguide, for example, became important. This reduced the peak detuning in the cavities by a factor of 2 and made operating the MLC cavities significantly more stable.

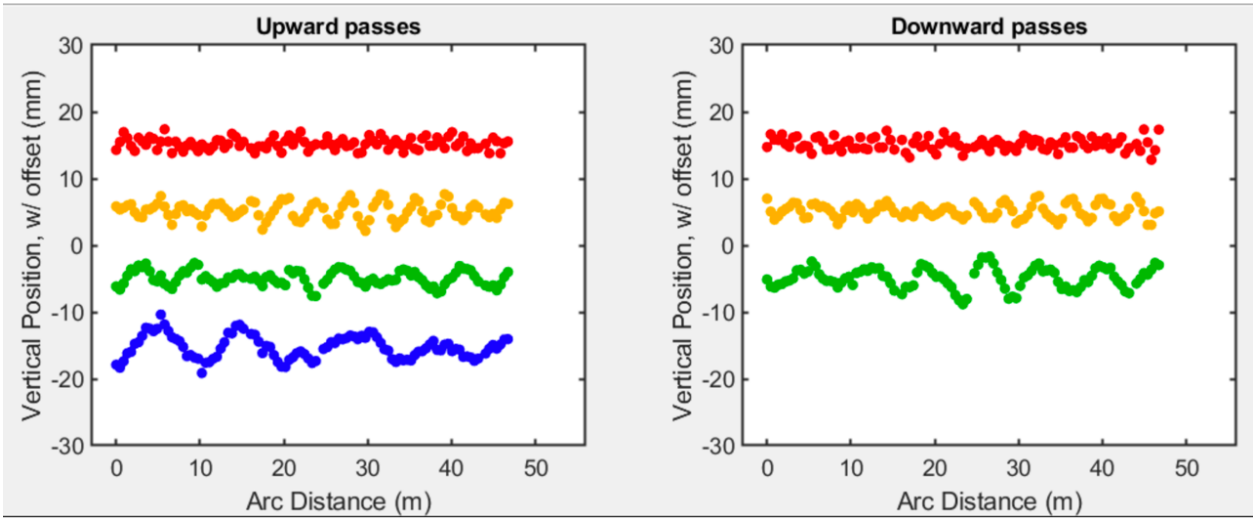

Figure 2.11-4: Vertical orbits through the FFA beam lines during acceleration (left) and during energy recovery deceleration (right).

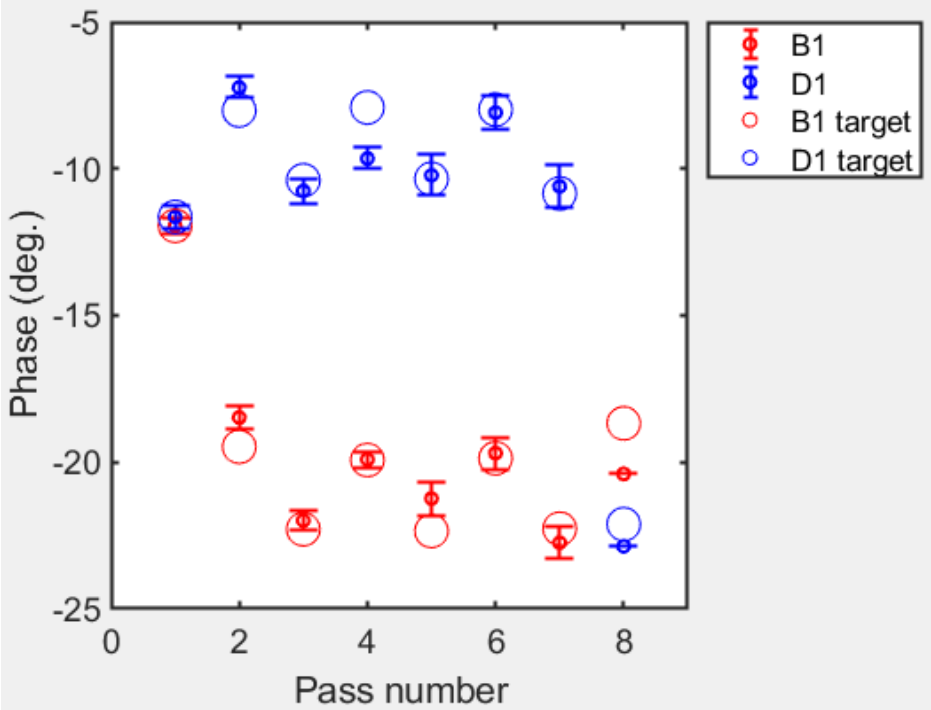

Figure 2.11-5: Arrival phases for each linac pass near the entrance (B1) and exit (D1) of the MLC. Measured values are shown along with the design values (circles).

However, two types of MLC instabilities remained during the operation period.

The energy gain from the MLC had a long-term drift; during the first 10-30 minutes of operation, after turning on the MLC, the energy would decrease by 0.5-1%. After that time, there often were slow drifts on the order of 0.1%. Measurements indicate that these were primarily due to cavities 1 and 6. As an energy-stabilization measure, the field in cavity 1 was adjusted in order to keep the orbit in a dispersion section of the S1 beamline constant. This stabilized the energy to about 0.01%.

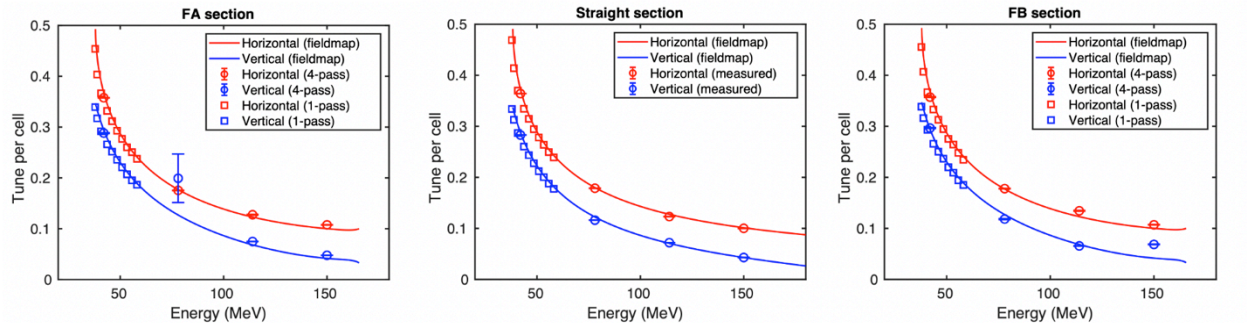

Figure 2.11-6: FFA tune measurements in the periodic machine sections (FA, ZX, FB) measured in the single-pass energy scan (squares) and the four-pass ER mode.

Prior to this operation period, the laser system for the injector had a minimum laser power; it could not provide a beam current below 300 pA. Out of a concern for radiation trips, an Acousto-Optic Modulator (AOM) was added to the laser system, decreasing this lower limit to the current by roughly a factor of 1000.

During the one-pass beam commissioning tests in Spring 2019, a simplified approach to BPM measurements was developed and tested that allows the beam position for each turn to be independently measured without using the originally planned time-consuming method of configuring the BPM timing to the peak of one bunch in the selected energy pass. This technique uses an analog-to-digital (ADC) clock that is asynchronous with the beam, and the sum-of-squares of all the samples in the bunch train for a selected energy pass are computed for each button signal instead of using a single ADC sample on the peak of one bunch in the desired energy pass. In this operation mode, the bunch train is limited to 8 bunches (at the 41.9 MHz injection rate) to ensure that the trains do not overlap from pass to pass.

Figure 2.11-7 shows a comparison of the raw BPM data using an ADC clock that is synchronous with the beam (1300MHz/31*76/2/4 = 398.4 MHz) vs. an ADC clock that is asynchronous with the beam (1300MHz/31*73/2/4 = 382.6 MHz). Note that with the synchronous ADC clock, every other 41.9 MHz bunch is nearly perfectly timed to the peak of the bunch, resulting in measurements that have similar amplitudes for each bunch. In comparison, the plot using the asynchronous clock produces data that is acquired at random parts of the bunch signal.

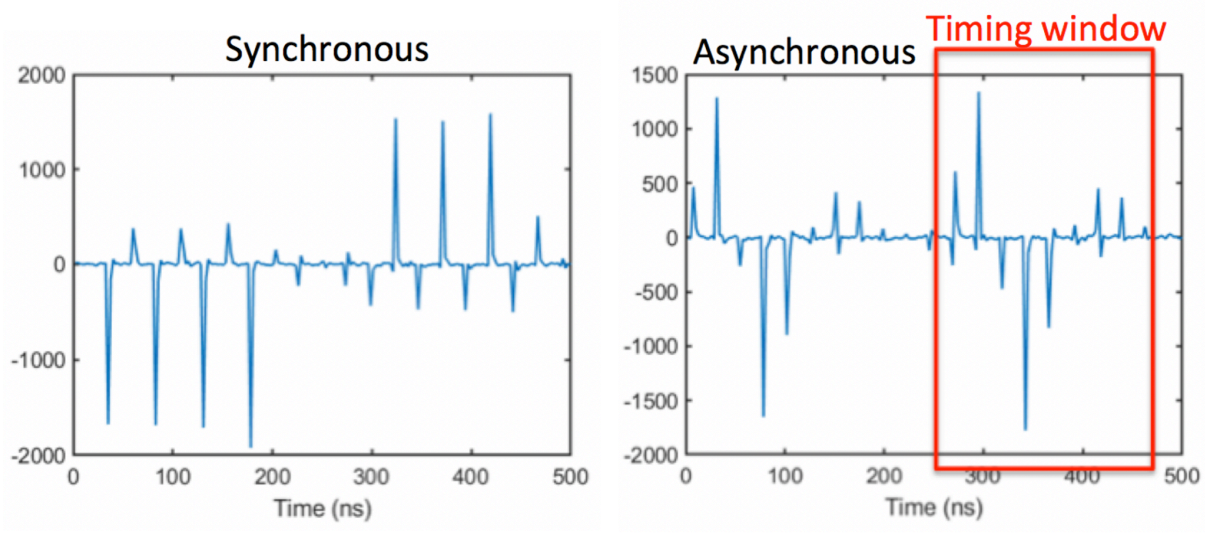

Figure 2.11-7: BPM raw plots with ADC clock synchronous with the beam (left) and asynchronous with the beam (right). ADC clock period is approx. 2.5 ns. The right plot shows the timing window for the data samples used to compute the position for turn number 2.

As a side note, with the ADC clock synchronous with the beam at 398.4 MHz, the number of ADC clock periods between 41.9 MHz bunches is exactly 9.5, which is why only every other bunch is detected. This is clearly visible in the left plot of Fig. 2.11-7. Figure 2.11-8 shows the response of a single bunch as acquired with the V301 BPM hardware.

Although limiting the bunch train to 8 bunches is not an option with high current operation, this approach provides a greatly simplified method of generating beam position measurements, and is expected to be used in the future as a setup mode prior to injecting continuous bunch trains. This technique worked very well and provided accurate and reliable beam position and phase measurements throughout the operation period.

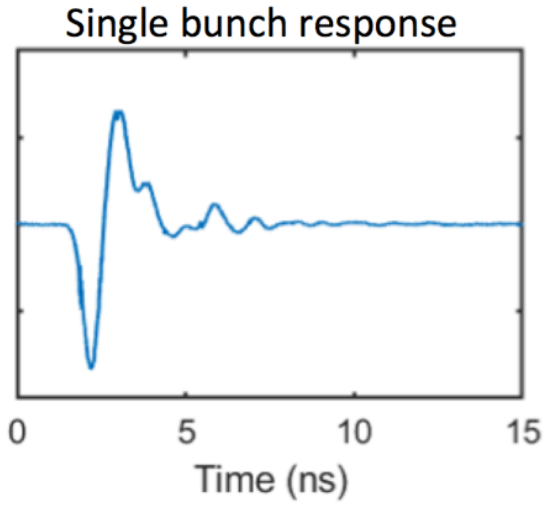

Figure 2.11-8: BPM raw bunch profile plot as acquired with the V301 BPM hardware using a sampling scope mode provided in the firmware. In this mode the ADC clock period is approx. 2.5 ns, but the ADC clock phase is varied to produce about 12 ps between samples.

Figure 2.11-9 shows an image of the EPICS control screen that is used to select a specific turn number for the BPM measurements in each section of the machine.

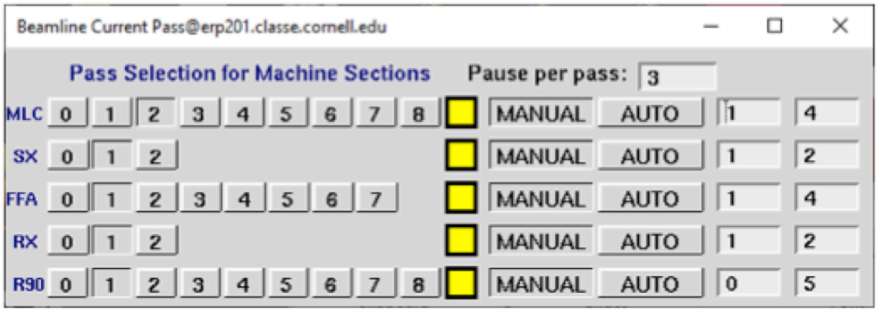

Figure 2.11-9: The EPICS control screen used to select the turn number for BPM measurements for each beam line section.

By limiting the bunch train length to avoid an overlap of the bunch trains in different passes, the phase and position data from the BPMs at the input and output of the MLC using the BAM mixers could also be easily distinguished. Note the clear signal separation of the first and second pass in Fig. 2.11-10.

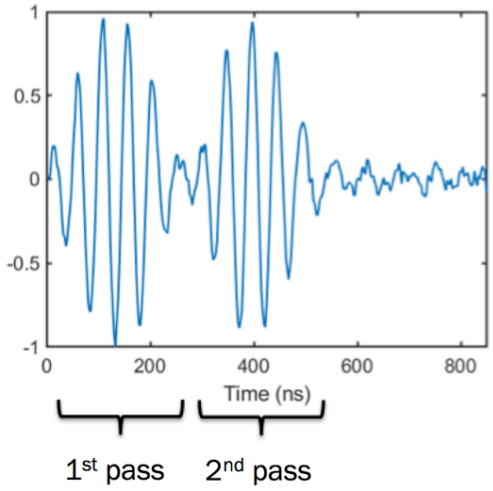

Figure 2.11-10: Raw BPM data acquired after RF mixing in the BAM chassis. This signal is used for both position and phase measurements. Note that pass 1 is easily distinguishable from pass 2 because the number of bunches in the train is limited to 8.

Machine reproducibility is key for any accelerator for which stable operation is to be established. This is especially true for an 8-pass machine where tolerances are more stringent than in one-pass transfer lines. In addition to the energy stability and reproducibility mentioned above, a reliable magnet degaussing procedure was also needed to obtain reproducible beam orbits. This procedure dramatically improved the daily reproducibility, even though it never reproduced the orbit to the precision of the BPM system. This may be due to non-optimal degauss parameter settings in the injector, because the injector magnets were less carefully tested than others. The order in which magnets were degaussed had an

influence on the orbit, indicating the effect of crosstalk from neighboring transfer lines and of stray fields of adjacent iron on magnet hysteresis. Investigating this effect was difficult due to the slow energy drift of the MLC. Stray fields were also a significant issue during orbit optimization as several magnets affect the beam in adjacent beamlines. The most severe cases stray fields were shielded by custom designed field clamps. Figure 2.11-11 shows and example of shielding installed in the R2 line. To simplify beam steering by a magnet with stray fields, select power supplies from adjacent beamlines were excited together with the magnet by control system 'knobs' so that the stray field effects on beam steering were automatically compensated. This elimination of stray-field effects on orbit steering is needed for any compact accelerator with tightly spaced magnets.

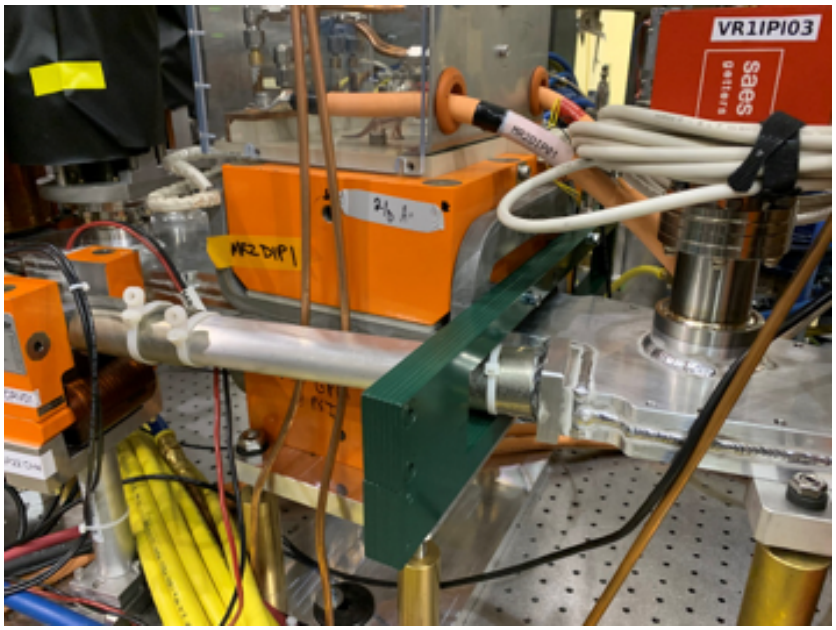

Figure 2.11-11: Image of magnets on the R2 line splitter table with magnet field shielding (green).

Controlling the effect of the orbit in the various splitter lines on the arrival times at the MLC turned out to be very important. Otherwise, orbit changes can change the arrival time at the MLC by tens of degrees. Figure 2.11-12 shows how an orbit change in a dipole can cause a significant change in the path length and thus the arrival time. While orbit steering could be used to adjust the arrival phases, this would misalign the beam in the splitter quadrupoles, which is highly undesirable.

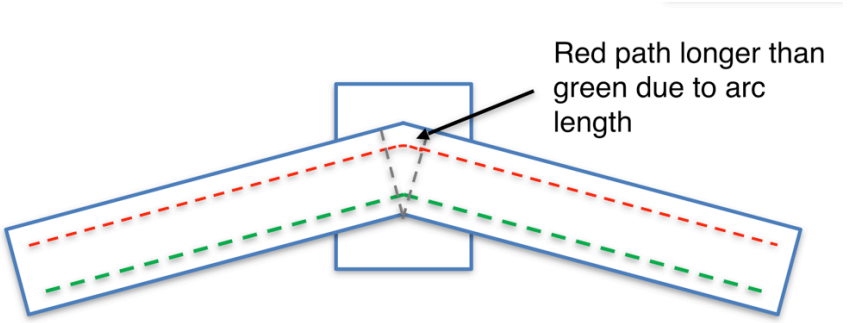

Figure 2.11-12: Schematic to show how a change in transverse orbit can change the flight time.

During the establishment of energy recovery charge-dependent microbunching structure in phase space was also observed, as in Fig. 2.11-13. This was measured on the first view screen in the S2 splitter line where there is non-zero dispersion. It is well known that CSR can cause charge-dependent microbunching, and strong CSR effects have been simulated for CBETA's beam transport. A comparison of simulation to measurement, however, remains to be done.

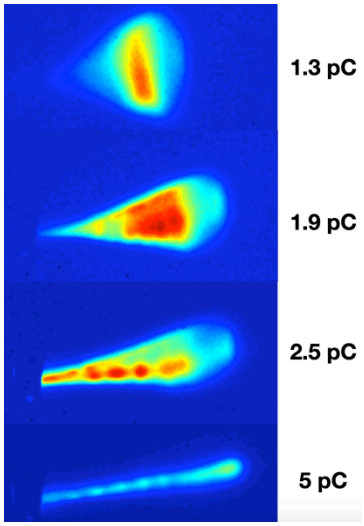

Figure 2.11-13: Evidence of charge dependent microbunching in the beam phase space on the first screen in S2.

The problem of low transmission in the R2 splitter section remains unresolved. Transmitting 100% of the beam through the R2 beamline was very difficult, especially when the quadrupole settings were near the design values. It may be no coincidence that most of the transmission losses shown in Fig. 2.11-1 occur after the second pass through that beamline. The focusing in that line is not particularly strong even compared to earlier beamlines that have good transmission. Data analysis is ongoing, and more beam time will be needed to improve the transmission efficiency.

2.12 Project complete, Milestone #12

As explained in the overview, the documentation provided in this report along with other supporting documentation, including the documents listed in the references section of this report, as well as conference papers and presentations from conferences and meetings, is intended to show that all of the NYSERDA project milestones have been satisfied.

At this point the project is considered complete. However, the accelerator is expected to continue to operate via other future funding sources.

3 Key Performance Parameters (KPP) and Ultimate Performance Parameters (UPP)

The Key Performance Parameters (KPP) and Ultimate Performance Parameters (UPP) for the CBETA accelerator as defined in the NYSERDA contract are defined in Table 3-1. The KPPs and UPPs that have been achieved as part of the NYSERDA funded project are marked as "achieved."

Table 3-1: Key Performance Parameters and Ultimate Performance Parameters. Note the parameters marked as being achieved.

Parameter	Unit	KPP	UPP (Stretch)
Electron beam energy	MeV		150 (achieved)
Electron bunch charge	pC		123
Gun current	mA	1 (achieved)	40
Bunch repetition rate (gun)	MHz		325
RF frequency	MHz	1300 (achieved)	1300 (achieved)
Injector energy	MeV		6 (achieved)
RF operation mode			CW (achieved)
Number of ERL turns		1 (achieved)	4 (achieved)
Energy aperture of arc		2 (achieved)	4 (achieved)

3.1 Achievement of the Performance Parameters

The 1 mA electron source current KPP was achieved in December 2016. In fact, the actual beam current achieved was 4 mA. Figures 3.1-1 and 3.1-2 show the machine configuration at the time when the source and ICM were connected directly to a diagnostic beam line into the high-power beam stop and Fig. 3.1-3 provides a plot of the measured beam current over several minutes.

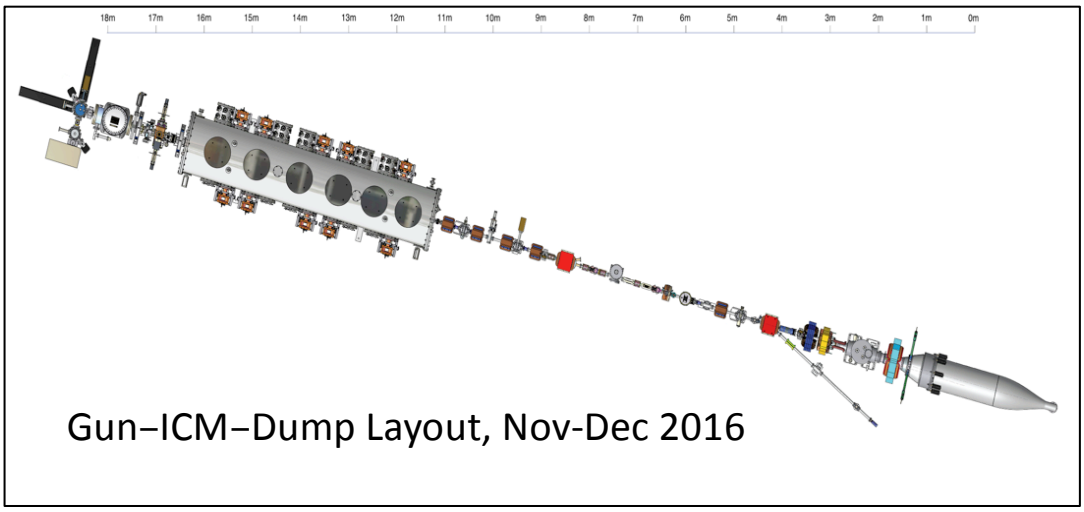

Figure 3.1-1: Machine configuration used for the 4 mA electron source test.

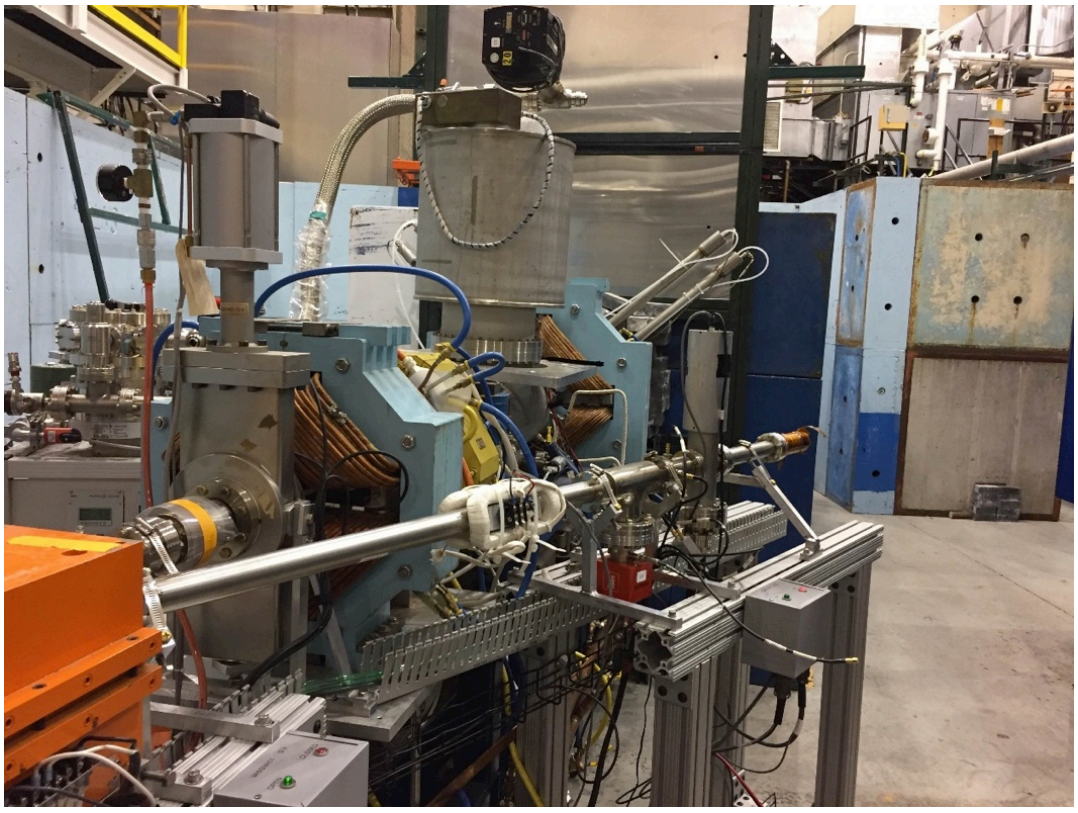

Figure 3.1-2: Photo of beam-line entrance to the beam stop during the 4 mA electron source test.

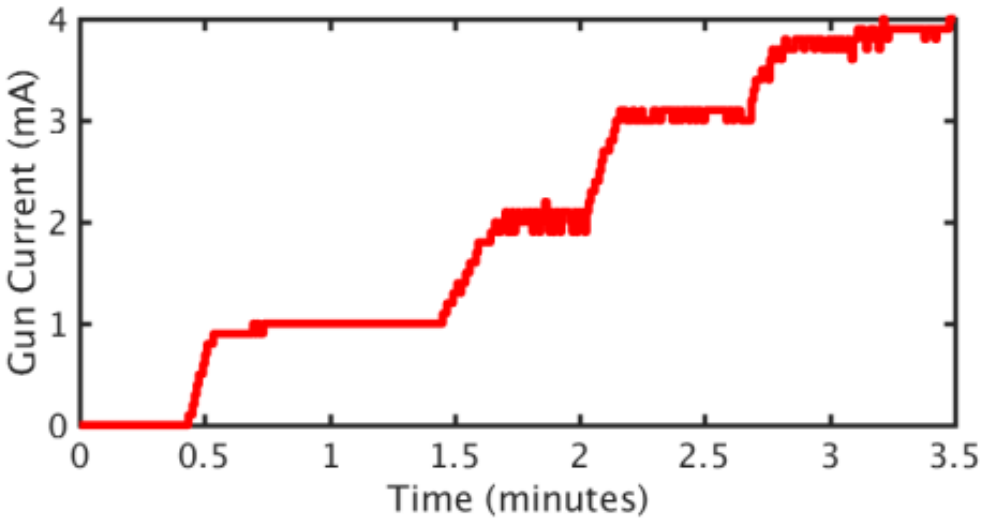

Figure 3.1-3: Plot of beam current (mA) vs. time (minutes) during the high current beam test on December 22, 2016.

The bunch repetition rate during these tests was 50 MHz and the maximum charge per bunch was 80 pC, resulting in 4 mA beam current.

The full 4-pass energy recovery was achieved on December 24, 2019, consisting of 8 total passes through the MLC, 4 accelerating and 4 decelerating. This satisfies the last 2 Ultimate Performance Parameters (UPPs) in table 3-1. In addition, the injector energy UPP of 6 MeV was achieved and regularly used throughout the beam commissioning period, and the 150 MeV electron beam energy was achieved after the fourth acceleration pass.

4 Connection to the EIC project

4.1 Need for ERLs in EIC hadron cooling

In 2016 when the CBETA project was initiated, the purpose was to test new technologies that might be used for a future electron-ion collider (EIC), the next large particle accelerator in the US. Just after CBETA satisfied the final technical milestone, DOE announced that the EIC will be built at BNL. Following is an excerpt of the press release from the DOE web page:

January 9, 2020: WASHINGTON, D.C. – *Today, the U.S. Department of Energy (DOE) announced the selection of Brookhaven National Laboratory in Upton, NY, as the site for a planned major new nuclear physics research facility. The Electron Ion Collider (EIC), to be designed and constructed over ten years at an estimated cost between $1.6 and $2.6 billion, will smash electrons into protons and heavier atomic nuclei in an effort to penetrate the mysteries of the "strong force" that binds the atomic nucleus together.* "The EIC promises to keep America in the forefront of nuclear physics research and particle accelerator technology, critical components of overall U.S. leadership in science," said U.S. Secretary of Energy Dan Brouillette. "This facility will deepen our understanding of nature and is expected to be the source of insights ultimately leading to new technology and innovation."

The US Academy of Sciences, on request from the DOE, assessed the EIC in the study "An Assessment of U.S.-Based Electron-Ion Collider Science" [3], including the following quote on the importance of the CBETA project:

'*CBETA will pioneer several energy-saving concepts in accelerator design. As an Energy Recovery Linac (ERL), of course, it will recover the energy of the beam it accelerates and reuse it to accelerate new beams. It will be the first multiturn ERL to employ superconducting radio frequency (SRF) accelerating cavities. The beam will pass four times through the single RF cryomodule. The fixed field alternating gradient arcs will be constructed from permanent magnets, requiring no electrical power, instead of conventional electromagnets. The designs advance permanent magnet technology.'*

'Besides testing numerous accelerator physics and technology concepts, CBETA also has a number of potential applications.'

By achieving all NYSERDA milestones, CBETA has realized the important developments of this quote, and is now ready to study hadron cooling for the EIC. In particular its hadron cooler will benefit from tests with CBETA. As the beam requirements of the cooler are very similar to CBETA's parameters, it is a good test bed for this important part of the EIC.

The same US Academy of Sciences study *[3] clearly describes the necessity for research in hadron cooling: "To attain the highest luminosities demanded by the science, cooling of the hadron beam is essential;" and "the full luminosity goals of eRHIC (the EIC at BNL) require the implementation of a radically new hadron cooling technology."* Also the need of ERLs for cooling is stressed: *"Energy recovery linacs (ERLs), a special type of recirculating linacs, presently offer the only credible concept for electron cooling of high-energy, colliding (hadron) beams," and "Several of these [required accelerator] advances are common to all EIC designs and include … high-current (multiturn) ERL technology."* Also, the contribution to the European Strategy Update concerning the EIC [3] states: *"An EIC will be an unprecedented collider …* Addressing the challenges of this machine requires R&D in areas *…, energy – recovery linacs (for ion beam cooling), …"*

The EIC needs hadron cooling not only to reach the highest luminosity but also to stabilize the operation of the hadron beam. Slight vibrations or instabilities in the hadron accelerator irreparably increase the emittance of the hadron beam if cooling is not available, whereas cooling stabilizes against such small operational inaccuracies.

CBETA is in an excellent position to study what it takes to make the electron beams available that are needed for an EIC hadron cooler. Additionally, CBETA allows R&D for many other accelerators with a wide range of high-current and high-brightness electron beams, including Ultrafast Electron Diffraction, hard X-ray production from Compton scattering, UEV production by an FEL for microchip lithography, and nuclear physics experiments with gas-jet targets. CBETA is therefore a national treasure, ready to study accelerator physics for the new regime of beam parameters that are enabled by its new technology.

The EIC asks for pre-cooling and for luminosity cooling. The former reduces the hadron emittance before acceleration in RHIC at about 5 MeV electron energy, while the latter maintains the small emittances during luminosity operation with 50-150 MeV electron beams. The coolers need bunch charges of about 1nC and currents of up to 100mA electron beam [85]. The electron emittances have to be small and the bunch distribution has to be smooth so that the substructure of the hadron beam can be imprinted on the electron beam, which is then used for stochastic cooling of the hadron beam.

All these required beam parameters have already been achieved in the CBETA injector individually, but not simultaneously. Achieving these parameters is the heart of the EIC-hadron-cooling research program for CBETA.

There are three fundamentally different hadron cooling techniques, all of which require ERL beams:

(1) Scattering cooling with electron beams: An electron beam with low temperature gets superimposed with a hadron beam of higher internal bunch temperature, at the same velocity. Scattering of the hadrons on the electrons reduces their temperature and therefore emittance. This technique is especially suitable for precooling hadrons at lower energies, because the required current increases with energy. Several designs of this type have been proposed for the EIC, all requiring so much beam power that an ERL seems mandatory.

(2) Stochastic cooling with electron beams, often referred to as coherent electron cooling: As in stochastic cooling with microwaves, which is used today in RHIC, the emittances of the hadron beam are reduced by measuring and correcting the properties of several slices along the hadron bunch. Using electron beams, the number of slices one can measure along the hadron bunch becomes much larger, greatly speeding up the emittance reduction. While an electron beam co-propagates with the hadron beam with equal velocity, a signal is imprinted on the electron beam that carries information about slices of the hadron bunch. A microbunching instability is then used to increase the signal on the electron beam. Once again co-propagating the electron and the hadron beam allows this signal to influence each slice of the hadron beam to make the emittances smaller. Several designs of this type have been proposed, mostly differing in the microbunching processed they use. All these designs require so much beam power that an ERL appears mandatory.

(3) Storage ring cooling: An electron storage ring is used to provide the low temperature electron beam. While superimposing it with a hadron beam to reduces the emittances, the electron beam is heated; this heating is counteracted by the radiation damping that is characteristic of high energy storage rings. Because the required electron energy is rather small, between 50-150 MeV, radiation damping is too week for sufficient cooling of the electron beam. It has been suggested to use an ERL to accelerate and later decelerate the electrons in the ring so that they have higher energy for radiation damping during part of their path around the ring.

Because all these hadron-cooling strategies rely on ERLs, CBETA can be utilized to learn how the required electron beams can be produced.

The different hadron-cooling techniques were analyzed by the "EIC Hadron Cooling Workshop," FNAL/Chicago, October 7-8, 2019. Five working groups on cooling technology and theory, led by 14 internationally recognized experts established that there is a strong collaboration in ion/proton cooling, focused on the EIC, having theoretical, computational, and experimental efforts. It established that hadron cooling with high-power electron beams will be needed for the highest luminosities of the EIC. Even

though microwave stochastic cooling may be adequate for ion beams, a hadron cooler will at least be needed from the EIC protons beam. Concluding the workshop, the experts provided this short list of essential ERL-related R&D items [86]:

Research Needs for ERLs for EICs: What research is still required?

- Need high current tests of injectors
- Still much design work to do (CSR arcs e.g.)
- Prototyping is ongoing.
- Definitely need ERL test bed facility for high current beams to test:
  - Halo
  - Beam loading
  - BBU
  - Transients
- Note: Full scale tests are expensive.

4.2 CBETA studies for EIC hadron cooling

In the hadron-cooler designs that are currently considered most promising, the required electron beam current is up to about 100mA, and the bunch charge is up to about 1nC, while the beam's transverse emittances have to be small and the beam distribution has to be smooth. The challenges for producing the required electron beams are related to these 4 parameters, current, bunch charge, emittance, and smoothness and the proposed studies address these separately.

The R&D proposed for CBETA to address electron beams for hadron cooling will progress from the DC source to the full 1-turn ERL, involving an increasing number of hardware components.

4.2.1 Injector studies without Energy Recovery

4.2.1.1 Large bunch-charge production with small emittance.

The CBETA electron source and injector linac will be used to create bunches of 1nC and to measure the phase-space distribution, minimizing the halo losses on the way to the 6-D phase-space diagnostics line. This will only use existing equipment and extends work already performed in 2016, which lead to the phase space images of fig 4.2-1 (left) [86]. The view screens that provided the measurements in Fig. 4.2-1 (right) will be used as halo monitors.

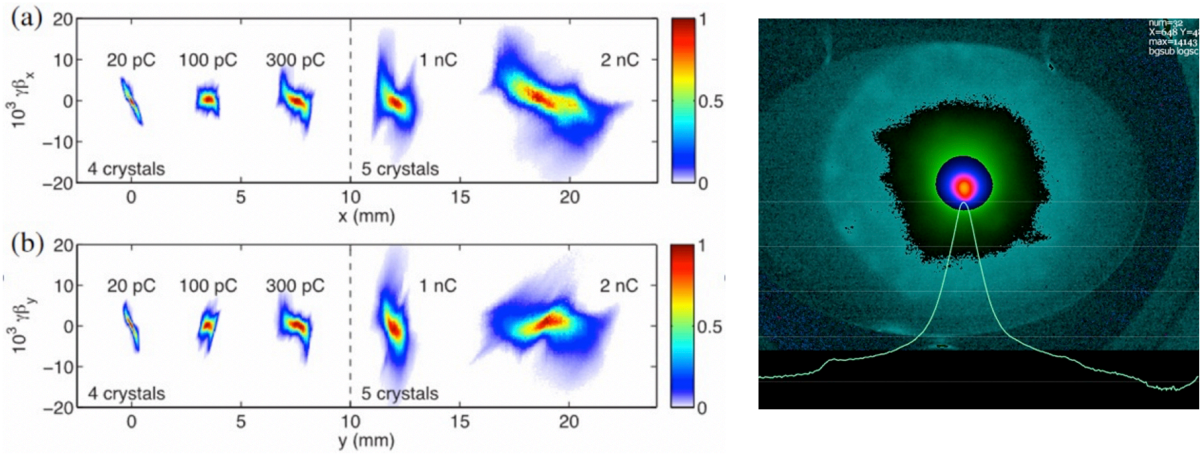

Figure 4.2-1: Left: Phase space distributions for different charges after the CBETA injector. Right: Halo in the CBETA beam down to $3x10^{-4}$ with 3% of the beam in the halo.

4.2.1.2 Large bunch-charge production with a smooth beam distribution.

A transverse mode cavity in the diagnostics line, followed by a spectrometer dipole, already allows mapping of the longitudinal phase space and often shows microstructure in the beam, as in fig 4.2-2, where structure is seen on a screen in a dispersive section. An improved resolution is desirable to study microbunching at shorter wavelength in the electron beam. It has been proposed to add a coherent transition-radiation monitor, the Happec device [87] from JLAB, to resolve microstructure in the electron bunches to show that their distribution can be sufficiently smooth for stochastic cooling with electron beams.

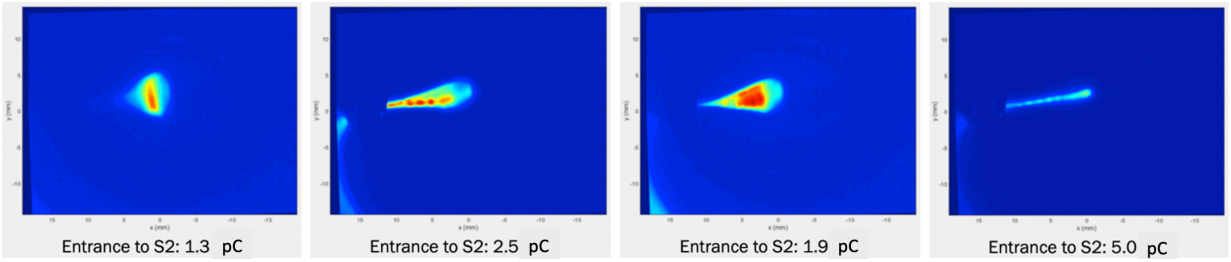

Figure 4.2-2: Beam spot in a dispersive section of CBETA as a function of bunch charge.

4.2.1.3 Large bunch-charge production with high current.

Transporting 1nC bunch charges was achieved, as shown in Fig. 4.2-1 but it produced significant halo losses, limiting the current that could be produced. In order to accelerate up to 100mA, the halo losses need to be understood and minimized. Possible sources of Halo are:

- Stray-light on the cathode.
- Out of time (ghost) pulses on the cathode, e.g. through lens reflections.
- Field emission from the cathode.
- Field emission from the SRF cavities.
- Secondary emission from lost electrons.
- Scattered electrons from Touschek scattering or rest-gas scattering.
- Nonlinear beam dynamics from
- Magnetic fields
- Space charge
- Ion accumulation around the beam

The monitor in Fig. 4.2-1 showed about 3% of the beam in the halo, even for low bunch charges. A cathode with a small, off-center active region will reduce this amount significantly. Deactivating other regions reduced the halo from stray light; the off-axis location reduced damage from ion back bombardment. A cathode of this type, as in fig 4.2-3 will be used for these studies.

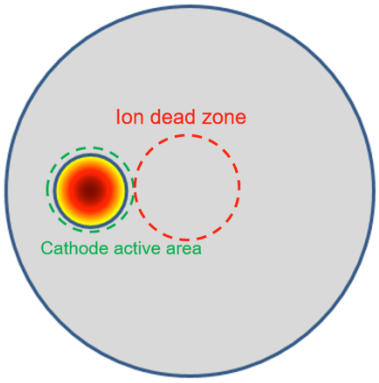

Figure 4.2-3: Cathode with small, off center active area to reduce beam halo.

These studies will only use the part of CBETA that leads from the DC electron source through the ICM and the MLC into the beam stop. Initially, low currents with 1nC bunches will be steered into the diagnostics line, where their phase space distribution can be optimized. The halo can be measured with CBETA's view screens, following the techniques established for Fig. 4.2-1. Subsequently, the mirror-imaged beam transport leads through the MLC into the beam stop. In that line, the beam current can be increased, as the beam stop is capable of absorbing 6 MeV beam up to about 100 mA.

Ion accumulation and ion elimination for high current beams is one important issue to study at this stage. A technique to inject gas into the beam pipe and measure properties of the ion column by detecting radiation from beam-ion scattering has been established [88]. Clearing electrodes and beam shaking were sufficient to eliminate ions for the several mA of current that were investigated, as shown in Fig. 4.2-4. It has to be established what ion cleaning techniques will serve for 100mA beams.

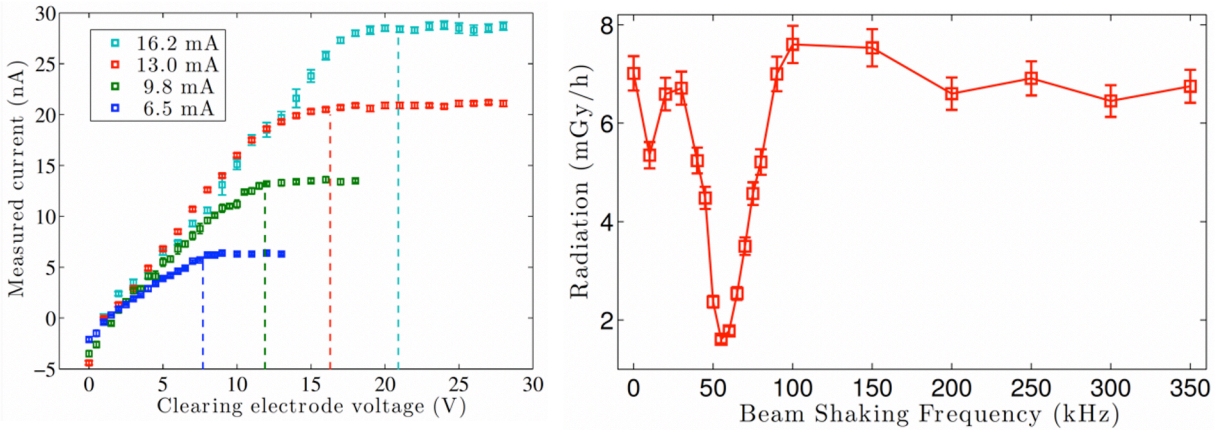

Figure 4.2-4: Left: ion current elimination as function of the voltage on the clearing electrode for different beam currents. Right: Shaking the beam at frequencies near the ion oscillation frequency eliminates the excess radiation caused by beam-ion interactions.

HOM heating is a process that can limit the beam current of an ERL. As the high current beam traverses the MLC, the heating of HOM absorbers can be studied. Before the MLC was constructed, a prototype cryomodule with one cavity was used to study heating of the HOM absorbers, showing that a 2.6 GHz bunch repetition rate in the MLC will produce tolerable HOM heating with beams below 400 mA. The bunch charge in this study was about 80 pC. Similar studies, measuring the heat load on the HOM absorbers, will have to be done for the required bunch charges and the required bunch-repetition rates of the EIC electron cooler.

4.2.2 Energy Recovering large bunch charges

Because the EIC hadron cooler is planned as a 1-turn ERL, all ERL studies in the program are concentrated on CBETA operation as a 1-turn ERL. Changing the current 4-turn configuration to 1-turn only takes about 2 weeks. All required hardware components are available. The hadron cooler ERL has been changed to a 1-turn design, from a previous 3-turn design, because studies have shown that beam transport through an ERL loop can disrupt a smooth bunch distribution for large bunch charges, in particular because of Coherent Synchrotron Radiation (CSR) and microbunching. CBETA's program for low current but high bunch-charge operation through the ERL loop therefore focuses on these effects:

- CSR and microbunching for large bunch charges.
- CSR shielding for large bunch charges.

4.2.3 Energy recovering large currents

Once large bunch charges can be transported around the ERL loop, the bunch repetition frequency is increased do use the ERL for larger currents and therefore beam powers. This allows the study of effects related to HOMs and beam loading:

- Beam Breakup instabilities.
- HOM heating.
- RF transients during start-up and during bunch gaps.

5 Conclusion

CBETA is the first four-pass superconducting ERL. It is also the first particle accelerator that uses a single FFA beam line to transport seven different accelerated and decelerated beams. Expertise from BNL was combined with expertise from Cornell University to design, construct, and successfully commission this accelerator. The success of CBETA proves not only that multi-turn ERLs can be operated but also that a single beam line can replace multiple beam lines for the ERL return loops decreasing both the installation and operating costs. CBETA was designed, constructed and commissioned by a team of scientists, engineers and technical staff from both BNL and Cornell, and included many industrial partners and input from renowned accelerator experts.

The CBETA team is reporting herein that the project milestones and KPPs have been fulfilled per the Statement of Work agreed upon in the 2016 contract with NYSERDA. The project goals and schedule were quite aggressive, and success was achieved. The result is an innovative 'green energy' machine where energy used to decelerate electrons is re-used to accelerate new electrons, thereby completely recovering the energy.

Significant achievements include:

- This is the first superconducting ERL having 8 passes through the linac (4 accelerating, 4 decelerating) to achieve full energy recovery.
- This is the first time that 7 beams spanning an energy range of nearly a factor of 4 were transported in a single beamline, made possible by FFA technology and a novel permanent magnet design
- This is the first time that multiple orbits in the FFA arcs were merged adiabatically into a single orbit in the straight section.

The accelerator technologies developed for CBETA can have applications in many areas.

Similar FFA designs with permanent magnets can be used in future applications such as:

- proton cancer therapy gantries. This would dramatically reduce the patient delivery system cost, which is the major obstacle in instituting widespread use of this new radiation method for cancer therapy. Proton cancer therapy provides what could be significant improvements over the more common X-ray radiation systems, because the X-rays propagate through the patient body while protons or heavier carbon particles deposit almost all of the energy into the tumor.
- small synchrotrons using permanent magnets for proton cancer therapy applications. Using permanent magnets prevents the need for including many costly, power hungry electro-magnet power supplies.

- isotope production machines using ERLs, where lost electron energy through isotope production targets can be accepted with the FFA beam line within $\delta p/p < \pm 60\%$.
- hadron cooling and UED. The photo-emitter electron source has already been copied for hadron cooling in RHIC and has applications in Ultra-fast Electron Diffraction.
- micro-chip and medical isotope production. The electron source and injector has already been used in designs for a radiation source for microchip lithography and for the production of medical isotopes.
- multi-turn ERL designs for hard x-ray beams and for gamma ray production in nuclear physics, both from Compton scattering.
- gas-jet collider experiments where CBETA's electrons make nuclear physics interactions with target atoms from the jet.
- technology development for future multi-turn ERL accelerators, e.g. as being discussed for the FCC-ee.

After completion of construction and commissioning, CBETA is now available for further experiments on ERL and FFA applications. Possible future studies include the limits on bunch charge, currents, and energy acceptance. It was, for example, found in numerical simulations that Coherent Synchrotron Radiation (CSR) can produce growth in energy spread and microbunching, effects that would dilute the beam density. This new facility is now available to analyze these important effects with unprecedented precision.

6 Acknowledgements

Brookhaven National Laboratory and Cornell University are very grateful to NYSERDA for funding this important and exciting project.

Thank you to the many BNL and Cornell employees that worked long hours to complete the design, construction and commissioning of CBETA, as well as the many visiting scientists from other accelerator institutions.

Thank you to the Advisory Committee for taking time away from their own accelerator work to periodically review the CBETA project performance and for making insightful recommendations.

7 References

Conference papers and reports

[1] D. Trbojevic, Brookhaven National Laboratory - Directed Research and Development Program-LDRD proposal: "Permanent magnet solution of the eRHIC with the NON-SCALING FFAG" (April 16, 2012)

[2] Georg H. Hoffstaetter, Sol M. Gruner, Maury Tigner, "Cornell Energy Recovery Linac", Cornell ERL: Project Definition Design Report (PDDR) https://www.classe.cornell.edu/Research/ERL/PDDR.html (June 5, 2013)

[3] An Assessment of U.S. Based Electron-Ion Collider Science, The National Academies Press, https://www.nap.edu/read/25171/ and F. Willeke and A. Seryi, submission to European Strategy Update, https://indico.cern.ch/event/765096/contributions/3295690/ (Aug. 2018)

[4] Ivan Bazarov, John Dobbins, Bruce Dunham, Georg Hoffstaetter, Christopher Mayes, Ritchie Patterson, David Sagan, Ilan Ben-Zvi, Scott Berg, Michael Blaskiewicz, Stephen Brooks, Kevin Brown, Wolfram Fischer, Yue Hao, Wuzheng Meng, Francois Meot, Michiko Minty, Stephen Peggs, Vadim Ptitsin, Thomas Roser, Peter Thieberger, Dejan Trbojevic, Nick Tsoupas, The Cornell-BNL FFAG-ERL Test Accelerator: White PaperarXiv:1504.00588 (2015)

[5] G.H. Hoffstaetter (PI), D. Trbojevic (PI), C. Mayes (ed.), N. Banerjee, J. Barley, I. Bazarov, A. Bartnik, J.S. Berg, S. Brooks, D. Burke, J. Crittenden, L. Cultrera, J. Dobbins, D. Douglas, B. Dunham, R. Eichhorn, S. Full, F. Furuta, C. Franck, R. Gallagher, M. Ge, C. Gulliford, B. Heltsley, D. Jusic, R. Kaplan, V. Kostroun, Y. Li, M. Liepe, C. Liu, W. Lou, G. Mahler, F. Meot, R. Michnoff, M. Minty, R. Patterson, S. Peggs, V. Ptitsyn, P. Quigley, T. Roser, D. Sabol, D. Sagan, J. Sears, C. Shore, E. Smith, K. Smolenski, P. Thieberger, S. Trabocchi, J. Tuozzolo, N. Tsoupas, V. Veshcherevich, D. Widger, G. Wang, F. Willeke, W. Xu (high resolution, low resolution, arXiv1706.04245) CBETA Design Report (2017)

[6] R.G. Eichhorn, J.V. Conway, T. Gruber, Y. He, G.H. Hoffstaetter, Y. Li, M. Liepe, T.I. O'Connel, P. Quigley, J. Sears, V.D. Shemelin, E.N. Smith, M. Tigner, Higher Order Mode Absorbers for High Current SRF Applications, SRF15 (2015)

[7] F. Furuta, B. Clasby, R.G. Eichhorn, B. Elmore, G.M. Ge, D. Gonnella, D.L. Hall, G.H. Hoffstaetter, R.P.K. Kaplan, J.J. Kaufman, M. Liepe, J.T. Maniscalco, T.I. O'Connel, S. Posen, P. Quigley, D.M. Sabol, J. Sears, E.N. Smith, V. Veshcherevich, Performance of the Cornell ERL Main Linac Prototype Cryomodule, SRF15 (2015)

[8] R.G. Eichhorn, B. Bullock, B. Clasby, J.V. Conway, B. Elmore, F. Furuta, G.M. Ge, G.H. Hoffstaetter, M. Liepe, T.I. O'Connel, P. Quigley, D.M. Sabol, J. Sears, E.N. Smith, V. Veshcherevich (Cornell), Y. He (Fermilab) Complection of the Cornell High Q CW Full Linac Cryo-module, IPAC15 (2015)

[9] R.G. Eichhorn, S.R. Markham, P. Quigley, E.N. Smith, Time Resolved Cryogenic Cooling Analysis of the Cornell Injector Cryomodule, IPAC15 (2015)

[10] R.G. Eichhorn, J.A. Robbins, V. Veshcherevich, Thermal and Mechanical Analysis of a Waveguide to Coax Symmetric Coupler for Superconducting Cavities, IPAC15 (2015)

[11] R. Eichhorn, A. Bartnik, B. Dunham, M. Ge, G. Hoffstaetter, H. Lee, M. Liepe, S. Markham, T. O'Connell, P. Quigley, D. Sabol, J. Sears, E. Smith, V. Veshcherevich, Time resolved cryogenic cooling analysis of the Cornell injector cryomodule, IPAC16 (2016)

[12] R. Eichhorn, J. Conway, F. Furuta, M. Ge, D. Gonnella, T. Gruber, G. Hoffstaetter, J. Kaufman, T. O'Connell, P. Quigley, D. Sabol, J. Sears, E. Smith, M. Liepe, V. Veshcherevich, First cool-cown of the Cornell ERL Main Linac Cryo-Module, IPAC16 (2016)

[13] F. Furuta, R. G. Eichhorn, G.M. Ge, D. Gonnella, G. H. Hoffstaetter, M. Liepe, P. Quigley, V. Veshcherevich, HOM measurements for Cornell's high-current CW ERL cryomodule, IPAC16 (2016)

[14] F. Furuta, J. Dobbins, R. G. Eichhorn, Mingqi Ge, D. Gonnella, G. H. Hoffstaetter, M. Liepe, T. O'Connell, P. Quigley, D. Sabol, J. Sears, E. Smith, V. Veshcherevich, ERL Main Linac Cryomodule cavity performance and effect of thermal cycling, IPAC16 (2016)

[15] S. Full, A. Bartnik, I.V. Bazarov, J. Dobbins, B. Dunham, G.H. Hoffstaetter, Trapped ion effects and mitigation during high current operation in the Cornell DC photoinjector, IPAC16 (2016)

[16] N. Tsoupas, S. Brooks, A. Jain, F. Meôt, V. Ptitsyn, and D. Trbojevic, Corrector magnets for the CBETA and eRHIC projects and other hadron facilities, HB16 (2016)

[17] G. H. Hoffstaetter, J. Barley, A. Bartnik, I. V. Bazarov, J. Dobbins, B. Dunham, R. G. Eichhorn, R. Gallagher, C. Gulliford, Y. Li, M. Liepe, W. Lou, C. E. Mayes, J. R. Patterson, D. Sabol, E. Smith, K. Smolenski, I. Ben-Zvi, J. S. Berg, S. Brooks, G. Mahler, F. Meot, M. Minty, S. Peggs, V. Ptitsyn, T. Roser, D. Trbojevic, N. Tsoupas, J. Tuozzolo, H. Witte, D. Douglas, CBETA: The Cornell/BNL 4-turn ERL with FFAG return arcs for eRHIC prototyping, LINAC16 (2016)

[18] S. Full, A. Bartnik, I.V. Bazarov, J. Dobbins, B. Dunham, G.H. Hoffstaetter, K. Smith, Ion effects in high brightness electron linac beams, LINAC16 (2016)

[19] M. Ge, N. Banerjee, J. Dobbins, R. Eichhorn, F. Furuta, G. Hoffstaetter, M. Liepe, P. Quigley, J. Sears, V. Veshcherevich, Measurements and analysis of cavity microphonics and frequency control in the Cornell ERL Main Linac prototype cryomodule, LINAC16 (2016)

[20] F. Furuta, J. Dobbins, R. Eichhorn, M. Ge, D. Gonnella, G. Hoffstaetter, M. Liepe, T. O'Connell, P. Quigley, D. Sabol, J. Sears, E. Smith, V. Veshcherevich, Performance of the novel Cornell ERL main linac prototype cryomodule, LINAC16 (2016)

[21] F. Furuta, R. Eichhorn, M. Ge, D. Gonnella, G. Hoffstaetter, M. Liepe, P. Quigley, V. Veshcherevich, HOM measurements for Cornell's ERL main linac cryomodule, LINAC16 (2016)

[22] R. Eichhorn, M. Ge, F. Furuta, G.H. Hoffstaetter, M. Liepe, S. Markham, T. O'Connell, P. Quigley, D. Sabol, J. Sears, E. Smith, V. Veshcherevich, D. Widger, Cool-down performance of the Cornell ERL cryomodules, LINAC16 (2016)

[23] K.W. Smolenski, B. Dunham, D.L. Barth, M. Muehlbauer, S. Wacker, J.M. Maxson, Successful Laboratory-Industrial Partnerships: THE Cornell-Friatec segmented insulator for high-voltage DC photocathode guns, NA-PAC16, (2016)

[24] J.A. Crittenden, D.C. Burke, Y.L.P. Fuentes, C.E. Mayes and K.W. Smolenski, Magnet design for the splitter/combiner regions of CBETA, the Cornell-Brookhaven Energy-Recovery-Linac Test Accelerator, NA-PAC16 (2016)

[25] D. Trbojevic, S. Bellavia, M. Blaskiewicz, S. Brooks, K. Brown, Chuyu Liu, W. Fischer, C. Franck, Y. Hao, G. Mahler, F. Meot, R. Michnoff, M. Minty, S. Peggs, V. Ptitsyn, T. Roser, S. J. Berg, P. Thieberger, N. Tsoupas, J. Tuozzolo, F. Willeke, and H. Witte, N. Banerjee, J. Barley, A. Bartnik, I. Bazarov, D. Burke, J. Crittenden, L. Cultrera, J. Dobbins, B. Dunham, R. Eichhorn(3), S. Full, F. Furuta, R. Gallagher, M. Ge, C. Gulliford, B. Heltsley, G. Hoffstaetter, D. Jusic, R. Kaplan, V. Kostroun, Yulin Li, M. Liepe, W. Lou, C. Mayes, R. Patterson, P. Quigley, E. Smith, K. Smolenski, D. Sabol, D. Sagan, J. Sears, C. Shore, V. Veshcherevich, and D. Widger, D. Douglas, CBETA - Cornell University Brookhaven National Laboratory Electron Energy recovery Test Accelerator, IPAC17 (2017)

[26] N. Banerjee, J. Dobbins, F. Furuta, D. Hall, G. H. Hoffstaetter, M. U. Liepe, P. Quigley, E. Smith, V. Veshcherevich, Microphonics Studies of the CBETA Linac Cryomodules IPAC 2017

[27] F. Furuta, N. Banerjee, J. Dobbins, R. Eichhorn, M. Ge, D. Hall, G. Hoffstaetter, M. Liepe, R. Porter, P. Quigley, D. Sabol, J. Sears, E. Smith, V. Veshcherevich, ERL Cryomodule Testing and Beam Capabilities, IPAC17 (2017)

[28] N. Tsoupas, J. S. Berg, S. Brooks, George Mahler, F. Meot, V. Ptitsyn, D. Trbojevic, S. Tygier, The Beam Optics of the FFAG Cell of the CBETA ERL Accelerator, IPAC17 (2017)

[29] W. Lou, J.A. Crittenden and G.H. Hoffstaetter, Beam-breakup Studies for the 4-pass Cornell-Brookhaven Energy-Recovery Linac Test Accelerator IPAC 2017

[30] H. Witte, J.S. Berg, B. Parker, Halbach Magnets for CBETA and eRHIC, IPAC17 (2017)

[31] D. Sagan and C. Mayes, Coherent Synchrotron Radiation Simulations for Off-axis Beams using the BMAD Toolkit, IPAC17 (2017)

[32] F. Meot, S. Brooks, D. Trbojevic, N. Tsoupas, S. Tygier, Numerical Beam Dynamics Studies Regarding CBETA Cornell-BNL ERL, IPAC17 (2017)

[33] H. Witte, N. Tsoupas, G. Mahler, J. Cintorino, J.S. Berg, P. Wanderer, A permanent Magnet Quadrupole Magnet for CBETA, IPAC17 (2017)

[34] S. Tygier, F. Meot, N. Tsoupas, C. Mayes, PyZgoubi Simulations of the CBETA Lattice, IPAC17 (2017)

[35] S.J. Brooks, G. Mahler, J. Cintorino, A.K. Jain, Production of Low Cost, High Field Quality Halbach Magnets, IPAC17 (2017)

[36] Dejan Trbojevic, Stephen Brooks, William Lou, Brett Parker, and Nicholaos Tsoupas, Permanent Halbach magnet Proton and Superconducting Carbon Cancer Therapy Gantries, IPAC17 (2017)

[37] N.Tsoupas, S.Brooks, A.Jain, G.Mahler, F.Meot, V.Ptitsyn and D.Trbojevic, Main Magnets and Correctors for the CBETA and eRHIC Projects, and Hadron Facilities Physics Procedia, Volume 90, 143-150 (2017)

[38] F. Furuta, N. Banerjee, A. Bartnik, J. Dobbins, R. Eichhorn, M. Ge, G. Hoffstaetter, M. Liepe, P. Quigley, D. Sabol, J. Sears, E. Smith, V. Veshcherevich, High-Efficiency, High-Current Optimized Main-Linac Cryomodule, SRF17 (2017)

[39] W. Lou, G.H. Hoffstaetter, Beam break-up current limit in multi-turn ERLs and CBETAarXiv:1812.09356 [physics.acc-ph] (2018)

[40] C. Gulliford, D. Sagan, A. Bartnik, S. Berg, J. Dobbins, A. Nunez-delPrado, Experience with online modeling tools during the CBETA fractional arc test and single pass commissioning, IPAC18, Barcelona (2018)

[41] F. Méot, N. Tsoupas, S. Brooks, D. Trbojevic, Beam dynamics validation of the Halbach Technology FFAG Cell for Cornell-BNL Energy Recovery Linac Nucl. Instrum. Methods A, Vol: 896, 60-67 (July 2018)

[42] G.H. Hoffstaetter, N. Banerjee, J. Barley, A. Bartnik, I. . Bazarov, D.C. Burke, J.A. Crittenden, L. Cultrera, J. Dobbins, S. Full, F. Furuta, R. Gallagher, M. Ge, C. Gulliford, B. Heltsley, D. Jusic, R. Kaplan, V. Otakar Kostroun, Y. Li, M. Liepe, W. Lou, C. Mayes, J.R. Patterson, P. Quigley, D. Sabol, D. Sagan, J. Sears, C.H. Shore, E. Smith, K.W. Smolenski, V. Veshcherevich, D. Widger, J. Scott Berg, S. Brooks, C. Liu, G. Mahler, F. Meot, R. Michnoff, M. Minty, S. Peggs, V. Ptitsyn, T. Roser, P. Thieberger, D. Trbojevic, N. Tsoupas, J. Tuozzolo, F.J. Willeke, H. Witte, D. Douglas, B. Kuske, M. McAteer, J. Völker, J. Jones, D. Kelliher, CBETA, the 4-turn ERL with SRF and single return loop, IPAC18, Barcelona (2018)

[43] W. Lou, A.C. Bartnik, J.A. Crittenden, C.M. Gulliford, G.H. Hoffstaetter, D. Sagan, J.S. Berg, S.J. Brooks, F. Méot, D. Trbojevic, N. Tsoupas, C.E. Mayes The Beam Optics of the FFAG Cell of the CBETA ERL Accelerator, IPAC18, Barcelona (2018)

[44] W. Lou, A.C. Bartnik, J.A. Crittenden, C.M. Gulliford, G.H. Hoffstaetter, D. Sagan, J.S. Berg, S.J. Brooks, F. Méot, D. Trbojevic, N. Tsoupas, C.E. Mayes Start to End Simulation of the CBETA Energy Recovery Linac, IPAC18, Barcelona (2018)

[45] F. Méot, S.J. Brooks, D. Trbojevic, N. Tsoupas Validation of the Halbach FFAG Cell of Cornell-BNL Energy Recovery Linac, IPAC18, Barcelona (2018)

[46] W. Lou, G.H. Hoffstaetter Beam Breakup Studies for the 4-Pass Cornell-Brookhaven Energy Recovery Linac Test Accelerator, IPAC18, Barcelona (2018)

[47] N. Banerjee, J. Dobbins, F. Furuta, G.H. Hoffstaetter, R.P. Kaplan, M. Liepe, P. Quigley, E.N. Smith, V. Veshcherevich Microphonics Suppression in the CBETA Linac Cryomodules, IPAC18, Barcelona (2018)

[48] J. A. Crittenden, A. Bartnik, R. Bass, D.C. Burke, J. Dobbins, C. Gulliford, Y. Li, D. Sagan, K. W. Smolenski, J. Turco, J.S. Berg, D. Jusic, Initial Performance of the Magnet System in the Splitter/Combiner Section of the Cornell-Brookhaven Energy-Recovery Linac Test Accelerator, IPAC18, Barcelona (2018)

[49] W. Lou, G. H. Hoffstaetter, Beam breakup current limit in multiturn energy recovery linear accelerators PRAB 22, 112801, Nov 2019

[50] F. Meot, An overview of Zgoubi Workshop 2019, Boulder, CO, Aug. 26-30, 2019, FFA 2019, Switzerland (Nov. 2019)

[51] S. Brooks, CBETA: a 4-pass superconducting ERL with permanent FFA magnet return arc, FFA19, Switzerland (Nov. 2019)

[52] S. Brooks Permanent Magnet VFFA for 18GeV Electron Acceleration, FFA19, Switzerland (Nov. 2019)

[53] N. Tsoupas, F. Meot, The CBETA project: arXiv:1706.04245, FFA19, Switzerland (Nov. 2019)

[54] G. Hoffstaetter , CBETA, a 4-turn ERL Based on SRF Linacs: construction and commissioning, ERL19, Berlin (Sept. 2019)

[55] D. Trbojevic, ERL with Fixed Field Altrernating Gradient Linear Gradient Role in EIC, ERL 2019, Sept. 2019, Berlin

[56] W. Lou, CSR phase space dilution in ERLs, ERL19, Berlin (Sept. 2019)

[57] N. Banerjee, Passive and active control of microphonics at CBETA and elsewhere, ERL19, Berline (Sept. 2019)

[58] N. Banerjee, Essential instrumentation for the characterization of ERL beams, ERL19, Berlin (Sept. 2019)

[59] Rosalyn Koscica, Beam timing and cavity phasing, ERL19, Berline (Sept. 2019)

[60] K.E. Deitrick, N. Banerjee, A.C. Bartnik, J.A. Crittenden, L. Cultrera, J. Dobbins, C.M. Gulliford, G.H. Hoffstaetter, W. Lou, P. Quigley, D. Sagan, K.W. Smolenski, D. Widger, J.S. Berg, S.J. Brooks, R.L. Hulsart, R.J. Michnoff, S. Peggs, D. Trbojevic,, Status of the CBETA Cornell-BNL ERL Prototype, NAPAC19, THYBA1 (2019)

[61] W. Lou, G.H. Hoffstaetter, D. Sagan, C.E. Mayes CSR Phase Space Dilution in CBETA, NAPAC19, WEXBA3 (2019)

[62] R. Koscica, N. Banerjee, G. H. Hoffstaetter, W. Lou, and G. Premawardhana, Energy and rf cavity phase symmetry enforcement in multiturn energy recovery linac models, PRAB 22, 091602 (Sep 2019)

[63] S.J. Brooks, G.J. Mahler, R.J. Michnoff, J.E. Tuozzolo, CBETA Permanent Magnet Production Run, IPAC19, THPTS088 (2019)

[64] N. Banerjee, K.E. Deitrick, J. Dobbins, G.H. Hoffstaetter, R.P.K. Kaplan, M. Liepe, C.W. Miller, P. Quigley, E.N. Smith, V. Veshcherevich, RF Commissioning and Performance in the CBETA ERL, IPAC19, WEPRB078 (2019)

[65] C.M. Gulliford, A.C. Bartnik, J.A. Crittenden, P. Quigley, J.S. Berg, Beam Based Measurements of the CBeta Main Linac Cavity Alignment, IPAC19, MOPRB078 (2019)

[66] C.M. Gulliford, N. Banerjee, A.C. Bartnik, J.A. Crittenden, P. Quigley, J.S., Berg Results From the CBETA Fractional Arc Test, IPAC19, MOPRB077 (2019)

[67] C.M. Gulliford, N. Banerjee, A.C. Bartnik, I.V. Bazarov, J.A. Crittenden, K.E. Deitrick, A. Galdi, G.H. Hoffstaetter, P. Quigley, K.W. Smolenski, J.S. Berg, S.J. Brooks, R.J. Michnoff, D. Trbojevic, CBETA Beam Commissioning Results, IPAC19, MOPRB076 (2019)

[68] V.O. Kostroun, C.M. Gulliford, Radiation Limits on Permanent Magnets in CBETA, IPAC19, MOPRB075 (2019)

[69] C.M. Gulliford, N. Banerjee, A.C. Bartnik, J.A. Crittenden, P. Quigley, J.S. Berg, Using an Energy Scan to Determine the Tunes and Orbit in the First FFA Girder of CBETA IPAC 2019 MOPRB074

[70] W. Lou, C.M. Gulliford, G.H. Hoffstaetter, D. Sagan, C.E. Mayes, N. Tsoupas, Coherent Synchrotron Radiation Simulation for CBETA, IPAC19, MOPGW124 (2019)

[71] R.J. Michnoff, R.L. Hulsart, J. Dobbins, The CBETA Beam Position Monitor (BPM) System Design and Strategy for Measuring Multiple Simultaneous Beams in the Common Beam Pipe, IPAC19, WEPGW104 (2019)

[72] R.J. Michnoff, J.S. Berg, S.J. Brooks, J. Cintorino, Y. Hao, C. Liu, G.J. Mahler, F. Méot, S. Peggs, V. Ptitsyn, T. Roser, P. Thieberger, S. Trabocchi, D. Trbojevic, N. Tsoupas, J.E. Tuozzolo, F.J. Willeke, H. Witte, N. Banerjee, J. Barley, A.C. Bartnik, I.V. Bazarov, D.C. Burke, J.A. Crittenden, L. Cultrera, J. Dobbins, S.J. Full, F. Furuta, R.E. Gallagher, M. Ge, C.M. Gulliford, B.K. Heltsley, G.H. Hoffstaetter, D. Jusic, R.P.K. Kaplan, V.O. Kostroun, Y. Li, M. Liepe, W. Lou, J.R. Patterson, P. Quigley, D.M. Sabol, D. Sagan, J. Sears, C.H. Shore, E.N. Smith, K.W. Smolenski, V. Veshcherevich, D. Widger, D. Douglas, M. Dunham, C.E. Mayes, CBETA - Novel Superconducting ERL, IPAC19, TUPGW102 (2019)

[73] R.M. Koscica, N. Banerjee, C.M. Gulliford, G.H. Hoffstaetter, W. Lou Energy and RF Cavity Phase Symmetry Enforcement in Multi-Turn ERL Models, IPAC19, TUPGW086 (2019)

[74] K.E. Deitrick, C. Franck, G.H. Hoffstaetter, V.O. Kostroun, K.W. Smolenski, J. Crone, H.L. Owen, B.D. Muratori, A Hard X-Ray Compact Compton Source at CBETA, IPAC19, TUPGW085 (2019)

[75] C. Gulliford, N. Banerjee, A. Bartnik, J. S. Berg, J. Crittenden, J. Dobbins, R. Hulsart, J. Jones, D. J. Kelliher, B. Kuske, W. Lou, M. McAteer, R. Michnoff, S. Peggs, P. Quigley, D. Sagan, K.

Smolenski, V. Vesherevich, D. Widger, G. H. Hoffstaetter, D. Trbojevic, Beam Commissioning Results from the CBETA Fractional Arc Test arXiv:1902.03370 [physics.acc-ph] (2019)

[76] N. Banerjee, G. Hoffstaetter, M. Liepe, P. Quigley, Z. Zhou, Active Suppression of Microphonics Detuning in high QL Cavities arXiv:1902.05122 [physics.acc-ph] (2019)

Other References

[77] Karen McNulty Walsh, BNL news, "Brookhaven Delivers Innovative Magnets for New Energy-Recovery Accelerator", https://www.bnl.gov/newsroom/news.php?a=213259 (2020)

[78] KYMA Undulators, www.kyma-undulators.eu

[79] Elytt Energy, www.elytt.com

[80] Sigma Phi, www.sigmaphi.fr

[81] TDK Lambda, www.us.tdk-lambda.com

[82] Sag Harbor Industries, www.sagharborind.com

[83] CBETA Supporting Documents web page, https://wiki.classe.cornell.edu/CBETA/CBETA-Supporting-Documents

[84] BNL news, Transformative 'Green' Accelerator Achieves World's First 8-pass Full Energy Recovery", https://www.bnl.gov/newsroom/news.php?a=216982 (2020)

[85] Electron Ion Collider at Brookhaven National Laboratory Pre-Conceptual Design Report 2019, BNL Formal Report, BNL-211943-2019-FORE (Aug 9, 2019)

[86] S. Nagaitsev, Workshop Summary (presentation), EIC Hadron Cooling Workshop, FNAL/Chicago (October 7-8, 2019)

[86] Colwyn Gulliford, Adam Bartnik, Ivan Bazarov, Bruce Dunham, and Luca Cultrera, Demonstration of cathode emittance dominated high bunch charge beams in a DC gun-based photoinjector, Appl. Phys. Lett. 106, 094101 (2015) and Adam Bartnik,Colwyn Gulliford,Ivan Bazarov, Luca Cultera, Bruce Dunham, Operational experience with nanocoulomb bunch charges in the Cornell photoinjector, Phys. Rev. ST-AB 18, 083401 (2015)

[87] G. A. Krafft, P. Piot, K. Jordan, and J. Song, U. Happek and M. James, "Measuring and characterizing ultrashort bunches in the Jefferson Lab Free Electron Laser", Proceedings of the EPAC98, http://accelconf.web.cern.ch/AccelConf/e98/PAPERS/WEP24G.PDF (1998) and P. Evtushenko, J. Coleman, K. Jordan, J. Michael Klopf, G. Neil, G. P. Williams, "Bunch Length Measurements at JLAB FEL", Proceedings of the FEL 2006 meeting, Berlin, Germany. http://accelconf.web.cern.ch/AccelConf/f06/PAPERS/THPPH064.PDF (2006)

[88] S. Full,* A. Bartnik, I. V. Bazarov, J. Dobbins, B. Dunham, and G. H. Hoffstaetter, Detection and clearing of trapped ions in the high current Cornell photoinjector, Phys. Rev. AB 19, 034201 (2016)

[89] Melanie Lefkowitz, Energy-saving particle accelerator achieves breakthrough, Cornell Chronicle, https://news.cornell.edu/stories/2020/01/energy-saving-particle-accelerator-achieves-breakthrough (January 21, 2020)

[90] EurekaAlert!, Transformative 'green' accelerator achieves world's first 8-pass full energy recovery, https://www.eurekalert.org/pub_releases/2020-01/dnl-ta012120.php (January 21, 2020)

[91] Interactions.com, Transformative 'green' accelerator achieves world's first 8-pass full energy recovery, https://www.interactions.org/press-release/transformative-green-accelerator-achieves-worlds-first-8 (Janaruy 21, 2020)

[92] PHYS.ORG, Transformative 'green' accelerator achieves world's first 8-pass full energy recovery, https://phys.org/news/2020-01-green-world-pass-full-energy.html (Janaruy 21, 2020)

[93] newswise, Transformative 'green' accelerator achieves world's first 8-pass full energy recovery, https://www.newswise.com/doescience/?article_id=725422&returnurl=aHR0cHM6Ly93d3cubmV3c3dpc2UuY29tL2FydGljbGVzL2xpc3Q (January 21, 2020)

[94] News Break, Energy-saving particle accelerator achieves breakthrough, https://www.newsbreak.com/new-york/ithaca/news/0NuO4Crz/energy-saving-particle-accelerator-achieves-breakthrough (January 21, 2020)

[95] The Lansing Star, 'Miracle' breakthrough to shape future of particle accelerators, https://lansingstar.com/around-town/16940-miracle-breakthrough-to-shape-future-of-particle-accelerators (January 24, 2020)

[96] Anna Powers, New 'green' particle accelerator has implications across virtually all industries relying on electronics, https://www.forbes.com/sites/annapowers/2020/01/25/new-green-particle-accelerator-has-implications-across-virtually-all-industries-relying-on-electronics/#2353f23359a6 (January 25, 2020)

[97] reddit.com, New 'green' particle accelerator has implications across virtually all industries relying on electronics, https://www.reddit.com/r/Futurology/comments/etx0kh/new_green_particle_accelerator_has_implications/ (January 25, 2020)

[98] Earth Mystery News (EMN), New 'green' particle accelerator has implications across virtually all industries relying on electronics, https://earthmysterynews.com/2020/01/28/new-green-particle-accelerator-has-implications-across-virtually-all-industries-relying-on-electronics/ (January 28, 2020)

[99] Dan Garisto, Cornell's Prototype Low-Energy Particle Accelerator Completes Key Test, IEEE Spectrum, https://spectrum.ieee.org/green-tech/conservation/cornells-prototype-lowenergy-particle-accelerator-completes-key-test (February 27,2020)

[100] Daniel Dunaief, BNL, Cornell's 'green' accelerator design now a reality, https://tbrnewsmedia.com/bnl-cornells-green-accelerator-design-now-a-reality/ (February 29, 2020)

CBETA internal tech notes

[101] Stephen Brooks, Magnet & lattice specifications for the CBETA first girder, Internal Report CBETA-1 (12/29/2016)

[102] Stephen Brooks, Halbach magnets risks & challenges, Internal Report CBETA-2 (12/15/2016)

[103] Stephen Brooks, Dejan Trbojevic, Nick Tsoupas, George Mahler, Halbach magnets outline construction method, Internal Report CBETA-3 (10/28/2016)

[104] J.A. Crittenden, D.C. Burke, Y.L.P. Fuentes, C.E. Mayes and K.W. Smolenski, Magnet design for the splitter/combiner regions of CBETA, the Cornell-BNL ERL Test Accelerator, Internal Report CBETA-4 and Proceedings NAPAC'16 (01/06/2017)

[105] Dejan Trbojevic for the Halbach-magnet design team, Halbach magnets for CBETA, Internal Report CBETA-5 (12/30/2016)

[106] Frank Karl and Dejan Trbojevic, Survey DRAFT, Internal Report CBETA-6 (01/12/2017)

[107] Francois Meot, Large amplitude motion in "BD_x/ QF_x" cell, Internal Report CBETA-7 (01/17/2017)

[108] Dejan Trbojevic for the Halbach-magnet design team, Halbach magnets for CBETA, Internal Report CBETA-8 (01/19/2017)

[109] Stephen Brooks, Halbach cell candidate February 2017, Internal Report CBETA-9 (02/23/2017)

[110] Stephen Brooks, Error studies of Halbach magnets, Internal Report CBETA-10 (03/02/2017)

[111] Stephen Brooks, Transverse forces in the first girder magnets, Internal Report CBETA-11 (04/14/2017)

[112] Stephen Brooks, Steve Peggs, Dejan Trbojevic, Joe Tuozzolo, TM2: assemble prototype girder, Internal Report CBETA-12 (04/30/2017)

[113] Scott Berg, The Halbach return loop for the CBETA ERL, Internal Report CBETA-13 (04/30/2017)

[114] Scott Berg, Summary of April 10, 2017 lattice, Internal Report CBETA-14 (04/30/2017)

[115] G.H. Hoffstaetter (PI), D. Trbojevic (PI), C. Mayes (Ed.), N. Banerjee, J. Barley, I. Bazarov, A. Bartnik, J. S. Berg, S. Brooks, D. Burke, J. Crittenden, L. Cultrera, J. Dobbins, D. Douglas, B. Dunham, R. Eichhorn, S. Full, F. Furuta, C. Franck, R. Gallagher, M. Ge, C. Gulliford, B. Heltsley, D. Jusic, R. Kaplan, V. Kostroun, Y. Li, M. Liepe, C. Liu, W. Lou, G. Mahler, F. M´eot, R. Michnoff, M. Minty, R. Patterson, S. Peggs, V. Ptitsyn, P. Quigley, T. Roser, D. Sabol, D. Sagan, J. Sears, C. Shore, E. Smith, K. Smolenski, P. Thieberger, S. Trabocchi, J. Tuozzolo, N. Tsoupas, V. Veshcherevich, D. Widger, G. Wang, F. Willeke, W. Xu, CBETA Design Report , Internal Report CBETA-15 (06/08/2017)

[116] Adam Bartnik for the CBETA team, TM4: Beam through the MLC, Internal Report CBETA-16 (06/15/2017)

[117] Stephen Brooks, Transverse forces in the CBETA v6/v6.5 magnets, Internal Report CBETA-17 (06/16/2017)

[118] Stephen Brooks, Description of CBETA magnet tuning wire holders, Internal Report CBETA-18 (11/14/2017)

[119] Stephen Brooks, Measurement Procedure for CBETA Halbach Magnets, Internal Report CBETA-19 (11/08/2017)

[120] J.A. Crittenden, R.M. Bass, D.A. Burke, and K.W. Smolenski, Status of the CBETA splitter common magnet design, Internal Report CBETA-20 (09/08/2017)

[121] R.M. Bass, J.A. Crittenden, Comprehensive Tracking Study for the H-Dipoles and Common Magnets in the Splitter Sections of the Cornell-BNL ERL Test Accelerator, Internal Report CBETA-21 (08/10/2017)

[122] R. Michnoff, J. Dobbins, R. Hulsart, D. Jusic, Y. Li, CBETA contributions to Beam Position Measurement Errors and a Plan to Provide Measurements with Sufficient Accuracy, Internal Report CBETA-22 (10/20/2017)

[123] Stephen Brooks, Measurement of first magnet made with production material, Internal Report CBETA-23 (12/21/2017)

[124] Nick Tsoupas for the Halbach-magnet design team, Design of a modified Halbach magnet for the CBETA project, Internal Report CBETA-23A (01/08/2018)

[125] Francois Meot, Dejan Tsoupas, Stephen Brooks, Dejan Trbojevic, Beam dynamics validation of the Halbach technology FFAG cell for Cornell-BNL ERL Test Accelerator, Internal Report CBETA-23B (01/29/2018)

[126] Stephen Brooks, Data directory for Halbach magnets, Internal Report CBETA-24 (03/02/2018)

[127] Adam Bartnik for the CBETA team, TM6: Fractional Arc Test - beam through MLC & girder, Internal Report CBETA-25 (04/20/2018)

[128] J. A. Crittenden, A. Bartnik, R.M. Bass, D. Burke, J. Dobbins, C. Gulliford, Y. Li, D. Jusic, D. Sagan, K. Smolenski, J. Turco, Internal performance of the magnet system in the splitter/combiner section of the Cornell-BNL ERL Test Accelerator, Internal Report CBETA-26 (06/03/2018)

[129] A. Morris, Review of various methods of detecting & measuring beam halos, Internal Report CBETA-27 (08/21/2018)

[130] Eric Biddulph-West, James Crittenden, First test of electron beam transport in the CBETA S1 splitter line, Internal Report CBETA-28 (09/06/2018)

[131] Antonett Nunez-delPrado, Colwyn Gulliford, Online simulation tools for orbit correction in the CBETA machine, Internal Report CBETA-29 (09/27/2018)

[132] R. Michnoff, J. Dobbins, R. Hulsart, CBETA Beam Position Monitor System Design And Plan for Measurement of Different Energy Bunches, Internal Report CBETA-30 (10/02/2018)

[133] D. Trbojevic (PI), G. Hoffstaetter (PI), S. Brooks, C. Gulliford, A. Bartnik, J. S. Berg, G. Mahler, J. Tuozzolo, N. Tsoupas, S. Trabocci, W Lou, N. Banerjee, J. Barley, I. Bazarov, I. Ben-Zvi, D. Burke, J. Crittenden, J. Dobbins, R. Gallagher, B. Heltsley, R. Hulsart, J. Jones, D. Jusic, R. Kaplan, D. Kelliher, V. Kostroun, B. Kuske, Y. Li, M. Liepe, W. Lou, G. Mahler, M. Mcateer, F. Meot, R. Michnoff, ´ M. Minty, R. Patterson, S. Peggs, V. Ptitsyn, P. Quigley, T. Roser, D. Sabol, D. Sagan, J. Sears, K. Smolenski, E. Smith, V. Veshcherevich, J. Voelker, D. Widger, CBETA technical report, Internal Report CBETA-31 (09/27/2018)

[134] G. Hoffstaetter (PI), D. Trbojevic (PI), C. Gulliford (Ed.), N. Banerjee, J. Barley, A. Bartnik, I. Bazarov, I. Ben-Zvi, J. S. Berg, S. Brooks, D. Burke, J. Crittenden, J. Dobbins, R. Gallagher, B. Heltsley, R. Hulsart, J. Jones, D. Jusic, R. Kaplan, D. Kelliher, V. Kostroun, B. Kuske, Y. Li, M. Liepe, W. Lou, G. Mahler, M. Mcateer, F. M´eot, R. Michnoff, M. Minty, R. Patterson, S. Peggs, V. Ptitsyn, P. Quigley, T. Roser, D. Sabol, D. Sagan, J. Sears, K. Smolenski, E. Smith, S. Trabocchi, J. Tuozzolo, N. Tsoupas, V. Veshcherevich, J. V¨oelker, D. Widger, The CBETA Fractional Arc Test, Internal Report CBETA-32 (09/28/2018)

[135] Adam Bartnik, Nonlinear BPM positions using Poisson, Internal Report CBETA-33 (09/28/2018)

[136] Nathaniel Macfadden, Colwyn Gulliford1, Development and Validation of a Geant4 Radiation Shielding Simulation Framework, Internal Report CBETA-34 (11/01/2018)

[137] Stephen Brooks, CBETA Halbach magnet production run, Internal Report CBETA-35 (11/28/2018)

[138] Stephen Brooks, Radiation limits for CBETA Halbach magnets, Internal Report CBETA-36 (07/06/2018)

[139] William Lou, CBETA 4-pass orbit correction and tolerance study, Internal Report CBETA-37 (11/29/2018)

[140] Nilanjan Banerjee et al., Equipment Protection System for CBETA, Internal Report CBETA-38 (03/28/2019)

[141] Colwyn Gulliford et al, Beam Commissioning Results from the CBETA Fractional Arc Test, Internal Report CBETA-39 (04/10/2019)

[142] Petrullo, Nilanjan Banerjee, Radiation dosages for NdFeB magnets in CBETA, Internal Report CBETA-40 (05/07/2019)

[143] Vaclav Kostroun, Notes on CBETA dump shield, Internal Report CBETA-41 (03/05/2019)

[144] Cheng-Ying Tsai and Rui Li, Preliminary study of microbunching for CBETA arc, Internal Report CBETA-42 and JLAB-TN-16-028 (08/30/2016)

[145] Rosalyn Koscica, ERL Timing and Optimized CBETA Models, Internal Report CBETA-43 (05/23/2019)

[146] V.O. Kostroun, Shielding of the CBETA Electron Dump, Internal Report CBETA-44 (07/13/2019)

[147] G.H. Hoffstaetter (PI), D. Trbojevic (PI), N. Banerjee, J. Barley, A. Bartnik, I. Bazarov, J.S. Berg, L. Borak, S. Brooks, D. Burke, J. Crittenden, J. Crone, L. Cultrera, K. Deitrick, J. Dobbins, C. Franck, R. Gallagher, C. Gulliford, B. Heltsley, R. Hulsart, J. Jones, D. Jusic, R. Kaplan, D. J. Kelliher, G. Mahler, F. Meot, V. Kostroun, B. Kuske, Y. Li, M. Liepe, W. Lou, G. Mahler, M. Mcateer, F. Meot, R. Michnoff, K. Ming, B. Muratori, S. Peggs, P. Quigley, T. Roser, D. Sabol, D. Sagan, J. Sears, C. Shore, E. Smith, K. Smolenski, C. Stoll, S. Thomas, S. Trabocchi, N. Tsoupas, J. Tuozzollo, V. Vesherevich, J. Völker, D. Widger, H. Witte, Energy recovery achieved in CBETA, the Cornell-BNL ERL Test Accelerator, Internal Report CBETA-45 (06/24/2019)

[148] M. Fabus, Hysteresis and Degaussing of H1 Dipole Magnets, CBETA Magnetic Measurements, Internal Report CBETA-45 (July 30, 2019)

[149] CBETA Magnetic Measurements V20190809, Elytt Energy internal technical note (August 2019)